

الجمهورية الجزائرية الديمقراطية الشعبية
People's Democratic Republic of Algeria
Ministry of Higher Education and Scientific Research
University of Ferhat Abbas Setif -1-



Thesis

Presented to the Faculty of Sciences
Computer Science department
to obtain the title of

PhD of Science

Specialty: Computer Science

Defended by
Hafida CHELLAKH

Theme

**Expert-guided extraction of relevant
informations: Application to medical pathology
detection**

Defended on 12 /06 /2025

Jury:

Dr. TOUMI Lyazid	University of Setif	President
Pr. MOUSSAOUI Abdelouahab	University of Setif	Advisor
Pr. ZAOUICHE Djaafar	University of Bordj Bou Arreridj	Examinator
Pr. LABRAOUI Nabila	University of Tlemcen	Examinator
Dr. LAKHFIF Abdelaziz	University of Setif	Examinator
Pr. ATTIA Abdelouahab	University of Bordj Bou Arreridj	Invited

2024 - 2025

الجمهورية الجزائرية الديمقراطية الشعبية
République Algérienne Démocratique et Populaire
Ministère de l'Enseignement Supérieur et de la
Recherche Scientifique
Université Ferhat Abbas de Sétif -1-



Université Ferhat Abbas Sétif 1

Thèse

Présentée à la Faculté des Sciences
Département d'Informatique
En vue de l'obtention du diplôme de

Doctorat en Sciences

Option : INFORMATIQUE

Par

Hafida CHELLAKH

Thème

Extraction d'informations pertinentes guidées
par expertise : Application à la détection de
pathologies médicales

Soutenu le: **12/06 /2025**
devant le jury composé de :

Dr. TOUMI Lyazid	Université Setif	Président
Pr. MOUSSAOUI Abdelouahab	Université Setif	<i>Rapporteur</i>
Pr. ZAOUACHE Djaafar	Université Bordj Bou Arreridj	<i>Examineur</i>
Pr. LABRAOUI Nabila	Université Tlemcen	Examineur
Dr. LAKHFIF Abdelaziz	Université Setif	Examineur
Pr. ATTIA Abdelouahab	Université Bordj Bou Arreridj	Invité

2024 - 2025

بِسْمِ اللَّهِ الرَّحْمَنِ الرَّحِيمِ

﴿وَمَا رَمَيْتَ إِذْ رَمَيْتَ وَلَكِنَّ اللَّهَ رَمَى﴾ ﴿سورة الأنفال، الآية 17﴾

﴿وما توفيقى إلا بالله عليه توكلت وإليه أنيب﴾ ﴿سورة هود، الآية 88﴾

Acknowledgements

*First and foremost, I would like to thank **ALLAH** Almighty, " الحمد لله " , for granting me the strength and patience to complete this work. My success is only from **ALLAH**. Upon Him I have relied, and to Him I return.*

I would like to express my deepest gratitude to my thesis supervisor, Pr. Moussaoui Abdelouahab, from Ferhat Abbas University of Setif, for proposing this topic. I am grateful for his patience, support, availability, attentiveness, and encouragement throughout these years. May he find in this thesis my profound gratitude and great respect.

I would like, also, to thank Pr. Attia Abdelouahab from university of Bordj Bou Arreridj, whose ideas, suggestions, and ongoing discussions had a significant impact on this thesis.

I especially wish to express my gratitude to Dr. Toumi Lyazid, from university of Setif, for honoring me by presiding over the jury. My thanks also go to Pr. Labraoui Nabila from university of Tlemcen, Dr. Iakhfif Abdelaziz from university of Setif, Pr. Zouache Djaafar from university of Bordj Bou Arreridj, the jury members for agreeing to evaluate this thesis and for taking time to read and review it. Your recommendations will be carefully considered and will undoubtedly contribute to the improvement of the final version.

I would like to thank all the members of the LMSE laboratory, especially Pr. Mostefai Messaoud, Pr. Gharbi, and Dr. Laadoui Ibtissem, for their warm welcome, support, and encouragement during difficult times.

I also extend my thanks to all my colleagues at the MI faculty who supported and encouraged me, as well as everyone who contributed, directly or indirectly, to the completion of this thesis.

A special thank you to Dr. Nora Lakhlef from the University of Bordj Bou Arreridj. Her encouraging words kept me motivated throughout this work.

Last but not least, I cannot forget to acknowledge those whose contributions are beyond words. I am deeply grateful to my husband and children for their unwavering support throughout the years of this thesis journey. Their steadfast encouragement, continuous support, and immense patience were crucial for the completion of this work. Without them, this project would never have come to fruition.

Dedicates

I dedicate this achievement

- ***To my beloved parents**, whose unwavering strength and faith have inspired me. They taught me the importance of patience, perseverance, and trust in God.*
- ***To my husband**, whom words truly fail to thank.*
- *To the apple of my eye, **my children** Oussama, Abdel Jalil, Kaouthar and Hako.*
- ***To my family.***
- ***To everyone aiming high.***

Hafida

Abstract

Magnetic Resonance Imaging (MRI) brain tumor identification and classification are costly and time-consuming due to tumor complexity and reliance on radiologist expertise. To overcome these challenges, automating the process is essential. This thesis leverages the power of deep learning for brain tumor analysis, presenting two key contributions.

In the first contribution, we introduce an efficient model titled "Deep Rule-Based Classifier using Bank of Binarized Statistical Image Features (DRB-BBSIF)". This approach addresses the limitations of conventional MRI brain tumor diagnosis by offering a model that improves classification performance while reducing the complexity of the diagnostic process. The model explores the BSIF image descriptor for the feature extraction phase. Furthermore, to enhance its performance, we have constructed a Bank-BSIF, which is founded by the best parameters of BSIF filters. For the classification phase, we employed a deep rule-based (DRB) classifier. The DRB classifier functions through a self-organized set of IF-THEN fuzzy rules, guided by prototypes. These fuzzy rules, generated by the DRB classifier, serve as the classifier's core decision-making mechanism. **The second contribution** titled "MRI Brain Tumor Identification and Classification using Deep Learning Techniques" focuses on the synergistic integration of deep learning and rule-based classification. We propose a novel, simple, and automatic DRB-based scheme for MRI brain tumor classification. This model leverages the power of deep learning for feature extraction and combines it with the effectiveness of DRB for classification. The framework consists of three stages: preprocessing, feature extraction, and classification. Feature extraction utilizes deep learning networks like AlexNet, VGG-16, ResNet-50, and ResNet-18 to extract features from the MRI images. A DRB classifier then utilizes these deep features for classification.

Both methods are evaluated on publicly available datasets and demonstrate significant performance in classifying brain tumors (presence or absence) and even tumor types (multiclass). They outperform traditional techniques, highlighting their effectiveness in MRI brain tumor analysis. The thesis provides significant advancements in MRI brain tumor identification and classification using deep learning techniques, presenting promising tools for computer-aided diagnosis. It also contributes to enhancing early disease detection and improving the efficiency and outcomes of treatment.

Keywords: MRI; brain tumor; Deep Learning; feature extraction; BSIF descriptor; DRB classifier.

Résumé

L'identification et la classification des tumeurs cérébrales sur l'Imagerie par Résonance Magnétique (IRM) sont des tâches délicates, fortement dépendantes de l'expertise des radiologues et souvent coûteuses en temps. Pour alléger leur charge de travail et améliorer la précision des diagnostics, cette thèse propose d'automatiser une partie de ce processus grâce à l'apprentissage profond. Deux contributions majeures sont présentées.

Dans la première contribution, nous introduisons un modèle efficace intitulé « Classificateur Basé sur des Règles profondes utilisant une Banque de Descripteurs d'images Statistiques Binarisées (DRB-BBSIF) ». Cette approche permet de remédier aux limites du diagnostic conventionnel des tumeurs cérébrales sur IRM en proposant un modèle qui améliore les performances de classification tout en réduisant la complexité du processus de diagnostic. Le modèle explore le descripteur d'image BSIF pour la phase d'extraction de caractéristiques. De plus, pour améliorer ses performances, nous avons construit une Banque-BSIF, basée sur les meilleurs paramètres des filtres BSIF. Pour la phase de classification, nous avons utilisé un classificateur basé sur des règles profondes (DRB). Le classificateur DRB fonctionne à travers un ensemble autoorganisé de règles floues de type SI-ALORS, guidé par des prototypes. Ces règles floues, générées par le classificateur DRB, constituent le mécanisme central de prise de décision du classificateur.

La deuxième contribution, intitulée « Identification et classification des tumeurs cérébrales par IRM à l'aide de techniques d'apprentissage profond » se concentre sur l'intégration synergique de l'apprentissage profond et de la classification basée sur des règles. Nous proposons un schéma novateur, simple et automatique basé sur DRB pour la classification des tumeurs cérébrales sur IRM. Ce modèle exploite la puissance de l'apprentissage profond pour l'extraction de caractéristiques et la combine avec l'efficacité du DRB pour la classification. Le cadre proposé se compose de trois étapes : prétraitement, extraction de caractéristiques et classification. L'extraction de caractéristiques utilise des réseaux d'apprentissage profond tels qu'AlexNet, VGG-16, ResNet-50 et ResNet-18 pour extraire des caractéristiques à partir des images IRM. Un classificateur DRB utilise ensuite ces caractéristiques profondes pour la classification.

Les deux méthodes sont évaluées sur des ensembles de données disponibles publiquement et démontrent des performances significatives dans la classification des tumeurs cérébrales (présence ou absence) ainsi que des types de tumeurs (multi classe). Elles surpassent les techniques traditionnelles, soulignant leur efficacité dans l'analyse des tumeurs cérébrales par IRM. La thèse apporte des avancées significatives dans l'identification et la classification des tumeurs cérébrales par IRM à l'aide de techniques d'apprentissage profond, offrant des outils prometteurs pour le diagnostic assisté par ordinateur. Elle contribue également à renforcer la détection précoce des maladies et à améliorer l'efficacité et les résultats des traitements.

Mots-clés : tumeur cérébrale ; IRM ; apprentissage profond ; extraction de caractéristiques ; descripteur BSIF ; classificateur DRB.

يعد تحديد وتصنيف أورام الدماغ باستخدام التصوير بالرنين المغناطيسي (MRI) عملية مكلفة وتستغرق وقتًا طويلاً بسبب صعوبة وتعقيد الأورام. تتأثر هذه العملية بشكل كبير بخبرة ومعرفة أطباء الأشعة والأعصاب. لذلك، أصبحت أوتوماتيكية هذه العملية ضرورية لتجاوز هذه التحديات. تعتمد هذه الأطروحة على قوة التعلم العميق لتحليل أورام الدماغ، وتقديم مساهمتين رئيسيتين.

في المساهمة الأولى، نقدم نموذجًا فعالاً بعنوان "المُصنّف العميق المعتمد على القواعد باستخدام مجموعة من الميزات الإحصائية المُرَمَّزة للصور". (DRB-BBSIF) يهدف هذا النهج إلى معالجة القيود التي يواجهها التشخيص التقليدي لأورام الدماغ باستخدام الرنين المغناطيسي، من خلال تقديم نموذج يُحسن أداء التصنيف ويقلل من تعقيد عملية التشخيص. يستكشف النموذج موصّف الصور BSIF لمرحلة استخراج الخصائص، وعلاوة على ذلك، لتحسين الأداء، قمنا ببناء بنك BSIF-يعتمد على أفضل معايير فلاتر BSIF. أما في مرحلة التصنيف، استخدمنا مصنعًا يعتمد على القواعد العميقة (DRB) يعمل المصنف DRB من خلال مجموعة ذاتية التنظيم من القواعد الضبابية من نوع إذا-اذن تقودها النماذج. هذه القواعد الضبابية، التي يولدها مصنف DRB، تشكل آلية اتخاذ القرار الأساسية للمصنف. أما **المساهمة الثانية،** التي تحمل عنوان "استخراج الميزات العميقة باستخدام مصنف DRB"، فتركز على التكامل التآزري بين التعلم العميق والتصنيف المعتمد على القواعد. نقترح مخططًا مبتكرًا وبسيطًا وآليًا يعتمد على DRB لتصنيف أورام الدماغ باستخدام الرنين المغناطيسي. يستفيد هذا النموذج من قوة التعلم العميق لاستخراج الميزات، ويجمع بينه وبين فعالية DRB للتصنيف. يتكون الإطار المقترح من ثلاث مراحل: المعالجة المسبقة، استخراج الميزات، والتصنيف. تستخدم عملية استخراج الميزات شبكات التعلم العميق مثل AlexNet و VGG-16 و ResNet-50 و ResNet-18 لاستخراج الميزات من صور الرنين المغناطيسي. بعد ذلك، يستخدم مصنف DRB هذه الميزات العميقة للتصنيف.

تم تقييم الطريقتين على مجموعات بيانات متاحة للجمهور، وأظهرتا أداءً مميزًا في تصنيف أورام الدماغ (وجود أو عدم وجود) وحتى أنواع الأورام (متعددة الفئات). تفوقت على التقنيات التقليدية، مما أبرز فعاليتها في تحليل أورام الدماغ باستخدام التصوير بالرنين المغناطيسي.

تقدم الأطروحة تقدمًا كبيرًا في تحديد وتصنيف أورام الدماغ باستخدام تقنيات التعلم العميق، مقدمة أدوات واعدة للتشخيص بمساعدة الحاسوب. كما تسهم في تعزيز القدرة على الكشف المبكر عن الأمراض وتحسين فعالية العلاج ونتائجه.

الكلمات المفتاحية: ورم الدماغ؛ الرنين المغناطيسي؛ التعلم العميق؛ استخراج الميزات؛ موصّف BSIF؛ المصنف DRB.

List of Publications

International Journal

H. Chellakh, A. Moussaoui, A. Attia, and Z. Akhtar, “MRI Brain Tumor Identification and Classification Using Deep Learning Techniques.,” *Ingénierie des Systèmes d’Information*, vol. 28, no. 1, 2023.

<https://www.iieta.org/journals/isi/paper/10.18280/isi.280102>

DOI: <https://doi.org/10.18280/isi.280102>

International Conferences

1. **H. Chellakh**, A. Moussaoui and A. Attia, “Rule Based Classifier for MRI Brain Tumor Identification and Classification”, Second International Conference and School on Radiation Imaging and Nuclear Medicine (ICSRI-2023), June 11-15, Setif Algeria.

<https://ocs.univ-setif.dz/ICSRI/ICSRI>

icsri@univ-setif.dz

2. **H. Chellakh**, A. Moussaoui and A. Attia, “Improved Binarized Statistical Image Features for MRI Brain Tumor Identification and Classification” 2024 International Conference on Information and Communication Technologies for Disaster Management (ICT-DM) November 19-21, 2024, Setif Algeria.

<https://ieeexplore.ieee.org/document/10798938>

DOI: [10.1109/ICT-DM62768.2024.10798938](https://doi.org/10.1109/ICT-DM62768.2024.10798938)

Contents

ACKNOWLEDGEMENTS	I
ABSTRACT	I
RESUME	II
ملخص	III
LIST OF PUBLICATIONS	IV
CONTENTS	V
LIST OF TABLES	X
LIST OF FIGURES	XI
LIST OF ABBREVIATIONS.....	XIII
GENERAL INTRODUCTION	1
1. CONTEXT AND MOTIVATION.....	1
2. PROBLEM STATEMENT.....	1
3. THESIS OBJECTIVES	3
4. THESIS CONTRIBUTIONS.....	3
5. THESIS ORGANIZATION.....	5
I CHAPTER I MRI FOR BRAIN TUMOR DIAGNOSIS	6
I.1 INTRODUCTION.....	6
I.2 BRAIN TUMORS	6
I.2.1 WHAT IS BRAIN TUMOR?	6
I.2.2 TYPES OF BRAIN TUMORS.....	6
I.2.3 IMPACT OF BRAIN TUMOR ON THE HEALTH.....	8

I.2.3.1	Benign Tumors.....	8
I.2.3.2	Malignant Tumors.....	8
I.2.3.3	Metastatic Tumors.....	9
I.3	MAGNETIC RESONANCE IMAGING – MRI – AN OVERVIEW.....	10
I.3.1	INTRODUCTION.....	10
I.3.2	OVERVIEW OF VARIOUS IMAGING METHODS	10
I.3.2.1	X-ray.....	11
I.3.2.2	Tomographic Imaging.....	11
I.3.3	MAGNETIC RESONANCE IMAGING (MRI)	13
I.3.3.1	Advantages of MRI.....	14
I.3.3.2	Disadvantages of MRI.....	14
I.3.3.3	Basic Principles of MRI	15
I.4	CONCLUSION.....	18
II.	CHAPTER II MATERIALS AND METHODS.....	19
II.1	INTRODUCTION.....	19
II.2	ARTIFICIAL INTELLIGENCE, MACHINE LEARNING AND DEEP LEARNING PARADIGM	19
II.3	MACHINE LEARNING (ML):.....	20
II.3.1	DEFINITION	20
II.3.2	TYPES OF MACHINE LEARNING.....	20
II.3.2.1	Supervised Learning:.....	20
II.3.2.2	Unsupervised Learning.....	20
II.3.2.3	Reinforcement Learning.....	21
II.3.3	CONCEPTS OF MACHINE LEARNING MODELS.....	21
II.4	DEEP LEARNING (DL)	22
II.4.1	DEFINITION	22
II.4.2	HISTORY OF DEEP LEARNING	22
II.4.3	CONCEPTS OF DEEP LEARNING MODELS.....	24
II.4.3.1	Neurons.....	24
II.4.3.2	Activation Functions: The Decision Maker	25
II.4.3.3	Artificial Neural Network.....	29
II.4.4	TYPES OF ARTIFICIAL NEURAL NETWORK	30
II.4.4.1	Perceptron.....	30
II.4.4.2	Multilayer Perceptron (MLP)	30
II.4.4.3	Convolutional Neural Network (CNN).....	30
II.4.4.4	Recurrent Neural Network (RNN).....	31
II.4.4.5	Long Short-Term Memory (LSTM)	32
II.4.4.6	Generative Adversarial Networks (GANs)	32

II.4.4.7	Sequence to Sequence Models (Seq2Seq)	33
II.5	DEEP LEARNING IN MEDICAL IMAGE ANALYSIS:	34
II.5.1	THE IMPACT OF DEEP LEARNING ON MEDICAL IMAGE ANALYSIS	34
II.5.2	APPLICATIONS IN MEDICAL IMAGING	34
II.5.3	DL TECHNIQUES FOR MEDICAL IMAGE ANALYSIS	35
II.5.4	ADVANTAGES OF DEEP LEARNING IN MEDICAL IMAGING	37
II.5.5	CHALLENGES AND LIMITATIONS	37
II.5.6	FUTURE DIRECTIONS	37
II.5.7	CNNs FOR MRI BRAIN TUMOR CLASSIFICATION	38
II.5.7.1	Input layer	39
II.5.7.2	Convolutional Layer	39
II.5.7.3	Pooling Layer	40
II.5.7.4	Fully Connected Layer	41
II.5.7.5	Logistic or Softmax Layer (LOSS)	41
II.5.7.6	Output Layer: The Final Decision Maker	41
II.6	PERFORMANCE EVALUATION MEASUREMENTS	42
II.6.1	CONFUSION MATRIX	42
II.6.2	ACCURACY	42
II.6.3	SENSITIVITY	42
II.6.4	SPECIFICITY	43
II.6.5	F1-SCORE	43
II.6.6	ROC CURVE	43
II.7	CONCLUSION	44
III.	CHAPTER III BRAIN TUMOR CLASSIFICATION	45
III.1	INTRODUCTION	45
III.2	TAXONOMY OF MRI BRAIN IMAGE CLASSIFICATION ALGORITHMS	45
III.3	CLASSIFICATION PROCESS	48
III.3.1	PRE-PROCESSING STEP	49
III.3.2	FEATURE EXTRACTION STEP	49
III.3.2.1	Binarized Statistical Image Features (BSIF)	50
III.3.2.2	Histogram of Oriented Gradients (HOG)	51
III.3.2.3	GIST Descriptor: A Low-Dimensional Image Representation	51
III.3.2.4	AlexNet	52
III.3.2.5	VGG-16	52
III.3.2.6	Residual Network (ResNet-50 and ResNet-18)	53
III.3.3	CLASSIFICATION STEP:	53
III.3.3.1	Naive Bayes	54

III.3.3.2	K-Nearest Neighbor.....	54
III.3.3.3	Support Vector Machine (SVM).....	55
III.3.3.4	Decision Trees.....	57
III.4	OVERVIEW OF BRAIN TUMOR CLASSIFICATION.....	58
III.4.1	MACHINE LEARNING TECHNIQUES.....	58
III.4.2	DEEP LEARNING TECHNIQUES.....	59
III.5	DEEP RULE BASED CLASSIFIER FOR MRI BRAIN TUMOR CLASSIFICATION.....	60
III.5.1	GENERAL ARCHITECTURE OF THE DRB CLASSIFIER.....	60
III.5.2	MASSIVELY PARALLEL FRB.....	62
III.5.2.1	Training process of the DRB system.....	63
III.5.2.2	Validation process of the DRB system.....	65
III.5.2.3	Decision Maker.....	65
III.6	CONCLUSION.....	67
IV.	CHAPTER IV: DRB-BBSIF FOR BRAIN TUMOR CLASSIFICATION.....	68
IV.1	INTRODUCTION.....	68
IV.2	THE ARCHITECTURE OF PROPOSED DRB-BBSIF CLASSIFIER.....	68
IV.2.1	EXTRACTION OF THE REGION OF INTEREST (ROI).....	69
IV.2.2	EXPLORING BINARIZED STATISTICAL IMAGE FEATURES (BSIF).....	69
IV.2.3	DEEP RULE-BASED CLASSIFIER FOR MRI BRAIN TUMOR CLASSIFICATION.....	71
IV.3	EXPERIMENTS AND RESULTS.....	72
IV.3.1	DATABASE.....	72
IV.3.2	EXPERIMENT 1 – CONSTRUCTION OF BANK OF BSIF FILTERS.....	73
IV.3.2.1	Objectives and Methodology.....	73
IV.3.2.2	Analysis of Results.....	74
IV.3.2.3	Interpretation of Results.....	76
IV.3.2.4	Key findings.....	78
IV.3.3	EXPERIMENT 2: IMPACT OF FEATURE EXTRACTOR METHODS.....	78
IV.3.3.1	Objective of Experiment 2.....	78
IV.3.3.2	Analysis of results.....	78
IV.3.3.3	Interpretation of results.....	79
IV.3.3.4	Key findings.....	80
IV.3.4	EXPERIMENT 3: EVALUATION OF THE DRB-BBSIF MODEL.....	80
IV.3.4.1	Objective of Experiment 3.....	80
IV.3.4.2	Analysis of Results.....	80
IV.3.4.3	Interpretation of Results.....	82
IV.3.4.4	Key Finding.....	83
IV.4	CONCLUSION.....	83

V. CHAPTER V: DRB WITH DEEP FEATURE EXTRACTION	85
V.1 INTRODUCTION.....	85
V.2 PROPOSED METHODOLOGY	85
V.2.1 PRE-PROCESSING STEP	86
V.2.2 FEATURE EXTRACTION STEP	86
V.2.3 CLASSIFICATION STEP	86
V.3 DATABASE	86
V.4 EXPERIMENTS AND RESULTS	87
V.4.1 EXPERIMENT 1: ALEXNET WITH 4 DIFFERENT CLASSIFIERS	88
V.4.1.1 Analysis of Results.....	89
V.4.1.2 Key Finding	91
V.4.2 EXPERIMENT 2: VGG-16 WITH 4 DIFFERENT CLASSIFIERS.....	92
V.4.2.1 Analysis of results	93
V.4.2.2 Key Findings.....	94
V.4.3 EXPERIMENT 3: RESNET-50 WITH 4 DIFFERENT CLASSIFIERS	96
V.4.3.1 Analysis of Results.....	97
V.4.3.2 Key Findings.....	98
V.4.4 EXPERIMENT 4: RESNET-18 WITH 4 DIFFERENT CLASSIFIERS	100
V.4.4.1 Analysis of Results.....	100
V.4.4.2 Key findings	103
V.4.5 COMPREHENSIVE ANALYSIS OF RESULTS.....	103
V.4.5.1 Classifiers: Strengths and Challenges.....	104
V.4.5.2 Deep Learning Features	105
V.5 COMPARISON BETWEEN THE TWO CONTRIBUTIONS	108
V.6 HIGH PERFORMANCE OF THE DRB CLASSIFIER.....	109
V.6.1 CHARACTERISTICS OF DRB CLASSIFIER	109
V.6.2 PERFORMANCE METRICS OF THE DRB CLASSIFIER	110
V.6.3 COMPARISON WITH OTHER CLASSIFIERS.....	110
V.7 CONCLUSION.....	111
CONCLUSION AND PERSPECTIVES	112
VI. REFERENCES.....	114

List of Tables

Table I.1	: Types of Brain Tumors [14][15][16]	7
Table I.2	: Comparison of different imaging techniques [22]	11
Table II.1	: Timeline of the main contributions in the field of ANN [36]	23
Table II.2	: Confusion matrix	42
Table III.1	: MRI Brain Tumor Classification Techniques	47
Table III.2	: Summary of prior works on MRI brain tumor and classification system	58
Table III.3	: Key Notation Descriptions of the DRB Classifier	62
Table III.4	: Samples of AnYa-type fuzzy rules derived from the brain tumor dataset	65
Table IV.1	: All parameters of BSIF applied on the MRI brain tumor	74
Table IV.2	: Best BSIF filters	75
Table IV.3	: Comparison between BSIF descriptor and Bank BSIF	76
Table IV.4	: Performance of feature descriptor methods with the DRB classifier	78
Table IV.5	: Performance of the DRB-BBSIF for each class	81
Table IV.6	: Comparison of the DRB-BSIF with KNN	81
Table IV.7	: Fuzzy rules generated through the training process	82
Table V.1	: Summary of CNN's models	86
Table V.2	: Datasets descriptions	87
Table V.3	: Details of AlexNet layers	88
Table V.4	: Comparative performance of AlexNet with 4 different classifiers	89
Table V.5	: Architecture of VGG-16 layers	92
Table V.6	: Comparative performance of VGG-16 with 4 different classifiers	93
Table V.7	: Architecture of ResNet-50	96
Table V.8	: Comparative performance of ResNet 50 with 4 different classifiers	97
Table V.9	: Details of ResNet-18 layers	100
Table V.10	: Comparative performance of ResNet18 with 4 different classifiers	101
Table V.11	: Comparison of different classifiers	105
Table V.12	: Performance Comparison of DRB with Different Deep Features	107
Table V.13	: Comparison of Feature Extractors	108

List of Figures

Figure I-1	: Example of Brain Tumor [14]	8
Figure I-2	: The Most Common Brain Tumors [16]	9
Figure I-3	: Medical Imaging Techniques [19].....	10
Figure I-4	: Magnetic Resonance Imaging [25]	13
Figure I-5	: The spin movement [22]	16
Figure I-6	: Splitting of the magnetic moment M. [22]	16
Figure I-7	: The FID and signal detection to generate MR images. [27].....	17
Figure I-8	: Various MRI images sequences [29].....	18
Figure II-1	: AI, machine learning and deep learning paradigm [31]	19
Figure II-2	: Types of Machine Learning [33]	20
Figure II-3	: The typical process of ML [30]	21
Figure II-4	: Difference between ML and DL [30]	22
Figure II-5	: Trade of representation power and computation complexity [36]	24
Figure II-6	: Structure of a neuron [30]	24
Figure II-7	: Binary Step Function [39]	26
Figure II-8	: Linear Activation Function [38]	26
Figure II-9	: Sigmoid Activation Function [38]	27
Figure II-10	: Tanh Activation Function [38].....	28
Figure II-11	: ReLu Activation Function [38].....	28
Figure II-12	: Deep Neural Network [30].....	29
Figure II-13	: Perceptron, Simple Neural Network [43]	30
Figure II-14	: Convolutional Neural Network Architecture [42]	31
Figure II-15	: RNN Architecture [43]	31
Figure II-16	: LSTM Architecture [46].....	32
Figure II-17	: GAN Architecture [47]	33
Figure II-18	: Sequence to Sequence Model [48]	33
Figure II-19	: Representation of Convolutional Networks [54]	38
Figure II-20	: Convolution Operation [37]	39
Figure II-21	: Convolutional Layer [55].....	40
Figure II-22	: Example of the Pooling Principle [56].....	40
Figure II-23	: Fully Connected Layers [30].....	41
Figure II-24	: Roc Curve [60]	43
Figure III-1	: Taxonomy of MRI Brain Tumor Classification Techniques	46
Figure III-2	: Classification Process.....	48
Figure III-3	: Taxonomy of feature extraction used in MRI Brain Tumor Detection	50
Figure III-4	: HOG descriptor [64]	51
Figure III-5	: VGG and Alexnet Architecture [71]	53
Figure III-6	: VGG-16 CNN Architecture [69]	53
Figure III-7	: The Naive Bayes classifier [75]	54
Figure III-8	: Example of classification with KNN [77]	55
Figure III-9	: Hyper plan of SVM classifier [80]	55
Figure III-10	: Example of a non-linearly separable problem.[80].....	56

Figure III-11 : Example of Decision Tree [82]	57
Figure III-12 : General Architecture of the DRB Classifier.....	61
Figure III-13 : Flowchart of the training process of the FRB subsystem	66
Figure IV-1 : DRB-BBSIF Classifier Architecture	69
Figure IV-2 : An example of an MRI image processed with BSIF filters	71
Figure IV-3 : Illustrations of three typical brain tumors [5].....	73
Figure IV-4 : The model of the B-BSIF descriptor	73
Figure V-1 : Block diagram of the proposed method.	85
Figure V-2 : Experimental evaluation of the proposed system.	87
Figure V-3 : Architecture of experiment1	88
Figure V-4 : Confusion matrix of DRB with data 1 and Data 2.....	90
Figure V-5 : ROC curves of dataset 1 and dataset 2.....	91
Figure V-6 : VGG-16 with the classifiers.....	92
Figure V-7 : Confusion matrix of DRB with data 1 and Data 2.	95
Figure V-8 : ROC curves of dataset 1 and dataset	95
Figure V-9 : Confusion matrix of DRB with data 1 and Data 2.....	99
Figure V-10 : ROC curves of dataset 1 and dataset 2	99
Figure V-11 : Confusion matrix of DRB with data 1 and Data 2.	102
Figure V-12 : ROC curves of dataset 1 and dataset 2.	102

List of Abbreviations

AI	: Artificial Intelligence
ANN	: Artificial Neural Network
AUC	: Area Under Curve
BSIF	: Binarized Statistical Image Features
BWT	: Berkeley Wavelet Transformation
CAD	: Computer Aided Diagnosis
CNN	: Convolutional Neural Network
CT	: Computed Tomography
DCNN	: Deep Convolutional Neural Network
DL	: Deep Learning
DRB	: Deep Rule Based
DWT	: Discrete Wavelet Transformation
EL-LRF	: Extreme Learning Machine Local Receptive Field
FC	: Fully Connected
FCM	: Fuzzy Clustering Means
FID	: Fee Induction Decay
fMRI	: Functional Magnetic Resonance Imaging
FN	: False Negative
FP	: False Positive
GAN	: Generative Adversarial Network
GLCM	: Gray Level Co-occurrence Matrix
HOG	: Histogram of Oriented Gradients
KNN	: K Nearest Neighborhood
KSVM	: Kernel Support Vector Machine
LBP	: Local Binary Pattern
LPQ	: Local Phase Quantization
LSTM	: Long Short-Term Memory
ML	: Machine Learning
M_L	: Longitudinal Magnetization
MLP	: Multi-Layer Perceptron
MRI	: Magnetic Resonance Imaging
M_T	: Transverse Magnetization
NMR	: Nuclear Magnetic Resonance
PCA	: Principal Component Analysis
PBD	: Pathological Brain Detection
PET	: Positron Emission Tomography
RF	: Radiofrequency
RNN	: Recurrent Neural Network
ROI	: Region of Interest
ROC	: Receiver Operating Characteristic
SPECT	: Single Photon Emission Computed Tomography
SVM	: Support Vector Machine
TN	: True Negative
TP	: True Positive
US	: Ultrasound
WHO	: World Health Organization
WLD	: Weber Local Descriptor
WPTE	: Wavelet Packet Tsallis Entropy

General Introduction

1. Context and Motivation

According to the World Health Organization (WHO), cancer is one of the leading causes of death worldwide [1] [2]. Unlike cancer, a tumor can be either benign or malignant. Benign tumors have uniform structures and non-active cancer cells, while malignant tumors have non-uniform structures and active cancer cells that can spread to other parts of the body. Early and accurate detection of brain tumors are crucial for determining the most suitable treatment, such as therapy, radiation, surgery, or chemotherapy, to prevent further complications. This can significantly increase the chances of survival for patients with tumors [3]. In this context Magnetic Resonance Imaging (MRI) is the most effective technique for diagnosing brain tumors due to its high contrast in soft tissues, high spatial resolution, and non-invasive nature.

Today, automatic classification of tissue types in MRI is crucial for computer-aided diagnosis, but it remains challenging and time-consuming due to the complexity of brain tumors. Manual evaluation of results and images deeply depends on the radiologist's experience and knowledge. Additionally, traditional methods are impractical for handling large amounts of data, are not reproducible, and are prone to human error. This is why computer-aided diagnosis (CAD) systems are essential to overcome these limitations.

2. Problem Statement

Over the years, automated machine learning methods have been developed for medical image analysis, but traditional approaches face significant limitations when applied to MRI images, particularly due to the large volume of data and complex anatomical structures. Recent advancements in Artificial Intelligence (AI) and deep learning (DL) have demonstrated their ability to efficiently process big data, offering promising solutions in various domains, including healthcare, autonomous systems, speech recognition, and image classification. In medical diagnosis, deep learning frameworks can automatically extract meaningful features from MRI images, surpassing classical approaches that rely on manually designed features. This has contributed to improve accuracy in brain tumor classification, a critical task for early detection and effective treatment planning.[4]

Brain tumor classification is generally categorized into two main types: (i) **binary classification**, which differentiates between normal and abnormal brain tissues, and (ii) **multi-class classification**, which distinguishes between specific tumor types such as Glioma, Meningioma, Pituitary, and Metastatic tumors [5]. Despite advances in machine learning and deep learning for MRI-based brain tumor classification, several challenges persist, impacting performance and clinical adoption: [6] [7] [8]

1. Data-Related Challenges

MRI data often contain noise, artifacts, or low resolution, which can hinder the extraction of relevant features. Anatomical variability among patients further complicates analysis, while the rarity of certain tumor types results in limited training data, increasing the risk of biased classification. Additionally, the creation of high-quality, annotated MRI datasets is both costly and time-consuming, requiring specialized medical expertise.

2. Challenges Related to Classification Methods

Effective classification depends on extracting meaningful features, which is not always straightforward. While deep learning models can learn complex patterns, they require large amounts of data to generalize well and avoid overfitting. Furthermore, many deep learning architectures, particularly convolutional neural networks (CNNs), are often considered "black boxes" making it difficult to interpret their decision-making process.

3. Challenges in Medical Interpretation and Clinical Adoption

The integration of AI-based tumor classification into clinical practice faces hurdles related to interpretability, reliability, and validation. Radiologists and clinicians must be able to trust and explain the model's predictions to ensure patient safety. Misclassifications can lead to severe diagnostic consequences, highlighting the need for robust, transparent, and clinically validated models before they can be widely adopted in healthcare settings.

Addressing these challenges is essential for enhancing the accuracy, reliability, and interpretability of brain tumor classification models, ultimately improving diagnostic support and patient outcomes.

3. Thesis Objectives

This thesis proposes a novel automated MRI brain tumor classification framework based on deep learning techniques. The framework aims to address the limitations mentioned previously and enhance the accuracy and efficiency of brain tumor classification.

The specific objectives of this research are:

- To Improve the classification efficiency through enhanced feature extractors.
- To develop a deep learning-based framework for automated MRI brain tumor classification.
- To investigate the effectiveness of deep learning for feature extraction in the context of brain tumor classification.
- To integrate explainability into the classification process by leveraging interpretable models, thereby supporting clinical decision-making and ensuring transparency in medical diagnoses.
- To explore the use of Deep Rule-Based (DRB) classifiers for brain tumor classification with deep features.
- To evaluate the performance of the proposed framework on publicly available MRI brain tumor datasets, including both binary and multi-class classification tasks.
- To compare the performance of the proposed framework with state-of-the-art methods, including traditional machine learning algorithms and other deep learning approaches.

By achieving these objectives, this research seeks to contribute to the development of more accurate, efficient, and reliable automated brain tumor classification systems, ultimately improving patient care and outcomes.

4. Thesis Contributions

The expected contributions of this doctoral thesis are as follows:

- **First contribution: Construction of Bank of BSIF descriptor [9]**

The first contribution presents an innovative model, DRB-BBSIF (Deep Rule-Based Classifier using Bank of Binarized Statistical Image Features), designed to overcome the limitations of traditional brain tumor classification methods. It focuses on two key improvements:

1. **Enhanced Feature Extraction:** BSIF is a valuable tool for extracting texture information from images due to its balance of simplicity and effectiveness. However, its reliance on hand-crafted features can hinder its ability to capture complex patterns. To overcome this limitation, we have developed Bank-BSIF, a refined version of BSIF that leverages the optimal parameter settings.
2. **Automated Classification with Deep Rules:** The model incorporates a Deep Rule-Based (DRB) classifier that automates the classification process. This classifier utilizes a self-organizing system of fuzzy rules based on data prototypes, enabling an efficient and accurate approach to tumor classification.

Through these enhancements, DRB-BBSIF provides a more robust and effective solution for brain tumor identification and classification, addressing key challenges in medical image analysis. The model's effectiveness was validated on a large T1-weighted CE-MRI brain tumor dataset, highlighting the critical role of advanced feature extraction techniques in achieving accurate classification results.

- **Second Contribution: MRI Brain Tumor Identification and Classification using Deep Learning Techniques** [\[10\]](#)

The second contribution emphasizes the powerful combination of deep learning and rule-based classification. We introduce an innovative, straightforward, and fully automated DRB-based framework for MRI brain tumor classification. This approach utilizes deep learning for feature extraction, while leveraging DRB's strength in classification.

1. **Deep Feature Extraction:** The framework employs pre-trained deep learning models such as AlexNet, VGG-16, ResNet-50, and ResNet-18 to extract deep features from MRI images. These features capture intricate patterns and relationships within the data, leading to enhanced classification accuracy.
2. **DRB for Classification:** As in the first contribution, the model uses DRB for classification. DRB processes the deep features to automatically generate fuzzy rules, enabling precise tumor detection and classification.

The framework was evaluated on two MRI brain tumor datasets from Kaggle: a binary classification dataset (tumor vs. no tumor) and a multiclass dataset (Meningioma, Glioma, and Pituitary tumor). Experimental results demonstrate that this novel DRB-based scheme is robust, simple, and effective, achieving high performance across both datasets. By automatically generating a set of fuzzy rules from the extracted deep features, the DRB

classifier accurately identifies tumors, showcasing its ability to synergize deep learning's feature extraction capabilities with rule-based decision-making for reliable MRI brain tumor classification.

By addressing the challenges of traditional methods and utilizing the power of deep learning, this research contributes to the development of more accurate, efficient, and reliable automated brain tumor classification systems, ultimately improving patient care and outcomes.

5. Thesis Organization

This thesis is organized to provide a comprehensive understanding of brain tumor identification and classification using deep learning techniques applied to MRI data.

- **Chapter 1** establishes the context and background by discussing the challenges of brain tumors and the significance of MRI in their diagnosis.
- **Chapter 2** delves into the theoretical foundation, exploring machine learning and deep learning concepts relevant to medical image analysis.
- **Chapter 3** presents a critical review of existing literature on deep learning approaches for brain tumor classification using MRI.
- **Chapter 4** presents our first contribution called DRB-BBSIF (Deep Rule-Based Classifier using Bank of Binarized Statistical Image Features) designed to address the shortcomings of conventional methods.
- **Chapter 5** presents our second contribution, DRB-based scheme for MRI brain tumor classification, that leverage deep learning and rule-based techniques for improved tumor identification and classification.
- **Finally, Conclusion** summarizes the key findings, discusses limitations and future directions, and concludes by highlighting the importance of this research while outlining promising areas for further investigation and development.

Chapter I MRI for Brain Tumor Diagnosis

I.1 INTRODUCTION	6
I.2 BRAIN TUMORS.....	6
I.2.1 WHAT IS BRAIN TUMOR?.....	6
I.2.2 TYPES OF BRAIN TUMORS.....	6
I.2.3 IMPACT OF BRAIN TUMOR ON THE HEALTH.....	8
I.3 MAGNETIC RESONANCE IMAGING – MRI – AN OVERVIEW	10
I.3.1 INTRODUCTION.....	10
I.3.2 OVERVIEW OF VARIOUS IMAGING METHODS	10
I.3.3 MAGNETIC RESONANCE IMAGING – MRI	13
I.4 CONCLUSION.....	18

Chapter I: MRI for Brain Tumor Diagnosis

I.1 Introduction

Brain tumors are a serious health concern that require precise identification and classification for optimal treatment. MRI has become the gold standard in the medical field for the diagnosis and evaluation of brain tumors due to its non-invasive nature, superior soft tissue contrast, and ability to provide detailed anatomical and functional information. MRI offers a comprehensive view of the brain, allowing clinicians to visualize the tumor's location, size, and morphology with great precision. These qualities make it an indispensable tool for guiding diagnosis.[\[11\]](#)[\[12\]](#)

This chapter provides a comprehensive overview of brain tumors and MRI, laying the foundation for subsequent chapters that delve into the application of deep learning techniques for brain tumor identification and classification using MRI images.

I.2 Brain Tumors

I.2.1 What is brain tumor?

A brain tumor is an abnormal growth of mass of cells in the brain or near it, as illustrated in **Figure I-1**. This growing is uncontrolled, unchecked by the mechanisms that control normal cells. Brain tumors can be classified as a primary tumors, which originates and starts inside the brain, and secondary tumors, also known as a metastatic brain tumor, which begin as cancer somewhere else in the body and spread to the brain. Brain tumors can be cancerous (malignant), which tend to be fast-growing, or noncancerous (benign), which tend to be slow-growing. [\[11\]](#)[\[13\]](#)

I.2.2 Types of brain tumors

Understanding the diverse types of brain tumors is crucial for effective diagnosis and treatment planning. Brain tumors encompass a wide spectrum of neoplastic growths that arise within the brain or its surrounding tissues. Each type varies significantly in terms of location, growth pattern, and potential impact on neurological function. **Table I.1** aims to explore the classification and characteristics of different types of brain tumors. The most common brain tumors are presented in **Figure I-2**. [\[14\]](#)[\[15\]](#)

Table I.1 Types of Brain Tumors [14][15][16]

Tumors	Location	Types	Benign or Malignant
• Gliomas And related brain tumors	The glial cells surround and support nerve cells in the brain tissue.	astrocytoma, glioblastoma, oligodendroglioma ependymoma.	Gliomas can be benign, but most are malignant.
• Choroid plexus tumors	located in the fluid-filled cavities in the brain, called the ventricles.	Choroid plexus carcinoma	Choroid plexus tumors can be benign or malignant.
• Embryonal tumors	Begin in embryonal cells that are left over from fetal development.	medulloblastoma.	Embryonal tumors are malignant brain tumors
• Germ cell tumors	they're often located near the pineal gland or the pituitary gland. But sometimes they're in other parts of the body.	Germ cell tumors	Germ cell tumors are mostly benign. They're more common in children.
• Pineal tumors	Pineal tumors start in and around the brain's pineal gland, located in the center of the brain.	Pineoblastoma	Pineal tumors can be benign or malignant.
• Meningiomas	start in the membranes around the brain and spinal cord.	Meningiomas	are usually benign, but sometimes they can be malignant.
• Nerve tumors	located on the main nerve that connects the inner ear to the brain.	acoustic neuroma, also called schwannoma.	Benign
• Pituitary tumors	begin in and around the pituitary gland. This small gland is located near the base of the brain.	Craniopharyngioma	Benign
• Other brain tumors	Tumors can start in the muscles, blood vessels and connective tissue around the brain. Tumors can form in the bones of the skull. Malignant brain tumors can start from the germ-fighting immune system cells in the brain.		

I.2.3 Impact of brain tumor on the health

Whether a brain tumor is benign, malignant, or metastatic, all are potentially life-threatening conditions. The seriousness of a brain tumor stems from its ability to interfere with the intricate and vital functions of the brain.[12]

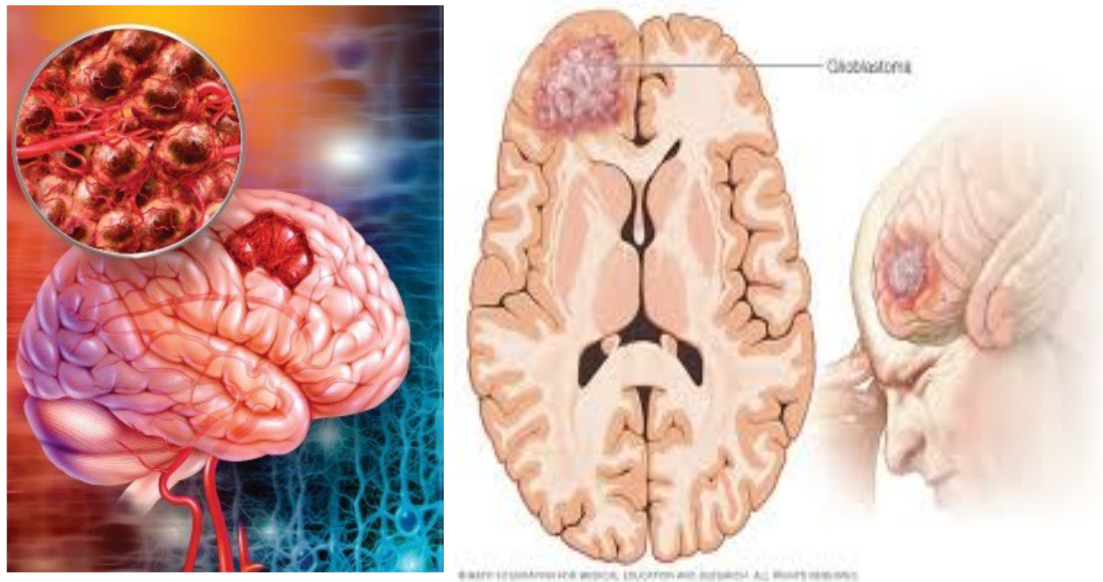


Figure I-1: Example of Brain Tumor [14]

I.2.3.1 Benign Tumors

While benign tumors are non-cancerous and typically grow slowly, they can still pose significant health risks depending on their size and location. Benign tumors may cause complications by exerting pressure on surrounding brain tissue, leading to neurological symptoms and impairments. In some cases, even a benign tumor can become life-threatening if it compresses critical structures or causes increased intracranial pressure.[14]

I.2.3.2 Malignant Tumors

Malignant brain tumors, on the other hand, are cancerous and often grow rapidly. They can infiltrate and invade surrounding healthy brain tissue, making complete surgical removal challenging. The aggressive nature of malignant tumors contributes to their potential to spread to other parts of the brain and spinal cord, further complicating treatment and prognosis.[14]

I.2.3.3 Metastatic Tumors

Metastatic brain tumors, originating from cancer in other parts of the body, represent another life-threatening category. These tumors reach the brain through the bloodstream or the lymphatic system, forming secondary tumors. The presence of metastatic tumors in the brain indicates advanced cancer elsewhere in the body, and their impact on health can be severe. In all cases, the location of the tumor is a critical factor. Tumors in certain areas of the brain may affect vital functions such as breathing, heart rate, or consciousness, intensifying the potential for life-threatening complications. [14][15]

Timely and appropriate medical intervention, including surgery, radiation therapy, chemotherapy, and other targeted treatments, is essential to manage and potentially mitigate the life-threatening aspects of brain tumors. Regular monitoring and follow-up care are crucial to assess the effectiveness of treatment and address any recurrence or new developments.

The impact of a brain tumor on an individual's health underscores the importance of early detection, accurate diagnosis, and comprehensive treatment planning to maximize the chances of a favorable outcome. Additionally, the multidimensional nature of care for individuals with brain tumors often includes addressing emotional, psychological, and supportive aspects to enhance overall well-being during the treatment and recovery process.

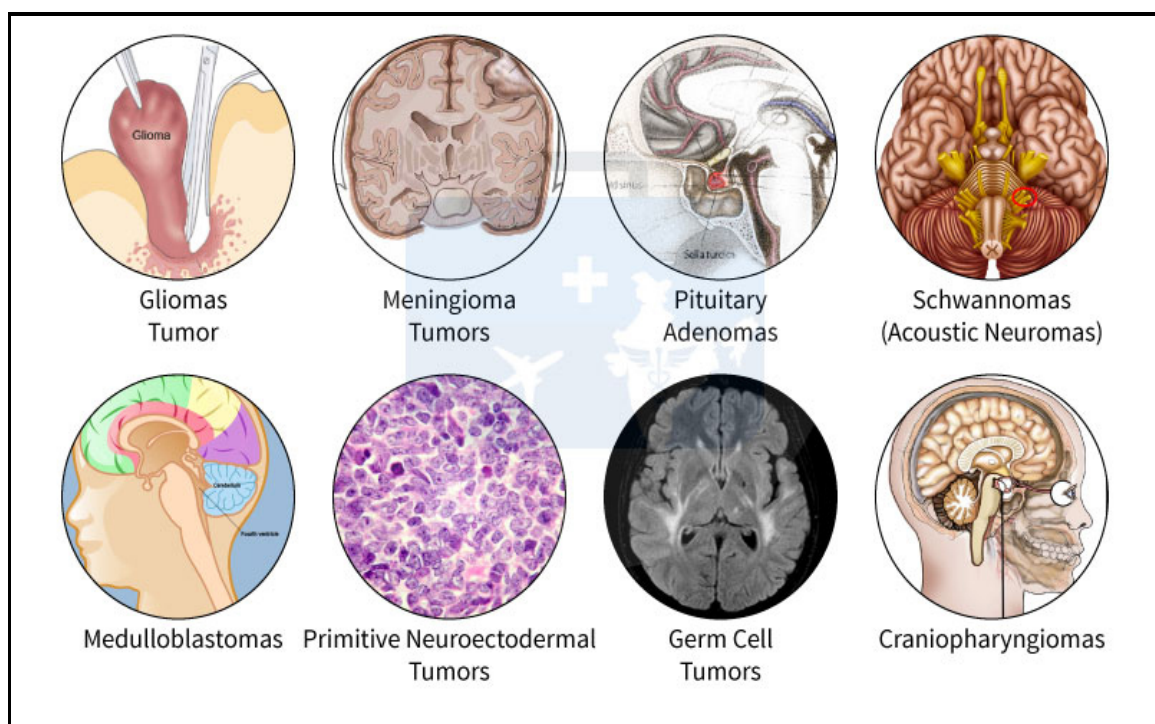


Figure I-2: The Most Common Brain Tumors [16]

I.3 Magnetic Resonance Imaging – MRI – an Overview

I.3.1 Introduction

Today, there are numerous imaging techniques, as shown in **Figure I-3**, often complementary. They have been developed from major physics discoveries of 20th century: X-rays and radio waves, natural and artificial radioactivity and finally the magnetic properties of the nuclei and atoms. They are based on the progress of medicine and advances in physics, chemistry, applied mathematics and computer science. Medical imaging continues to evolve and improve and it is increasingly used for diagnosis, in addition to a clinical examination and other investigations, such as biological examinations or neuropsychological tests. [17] [18]

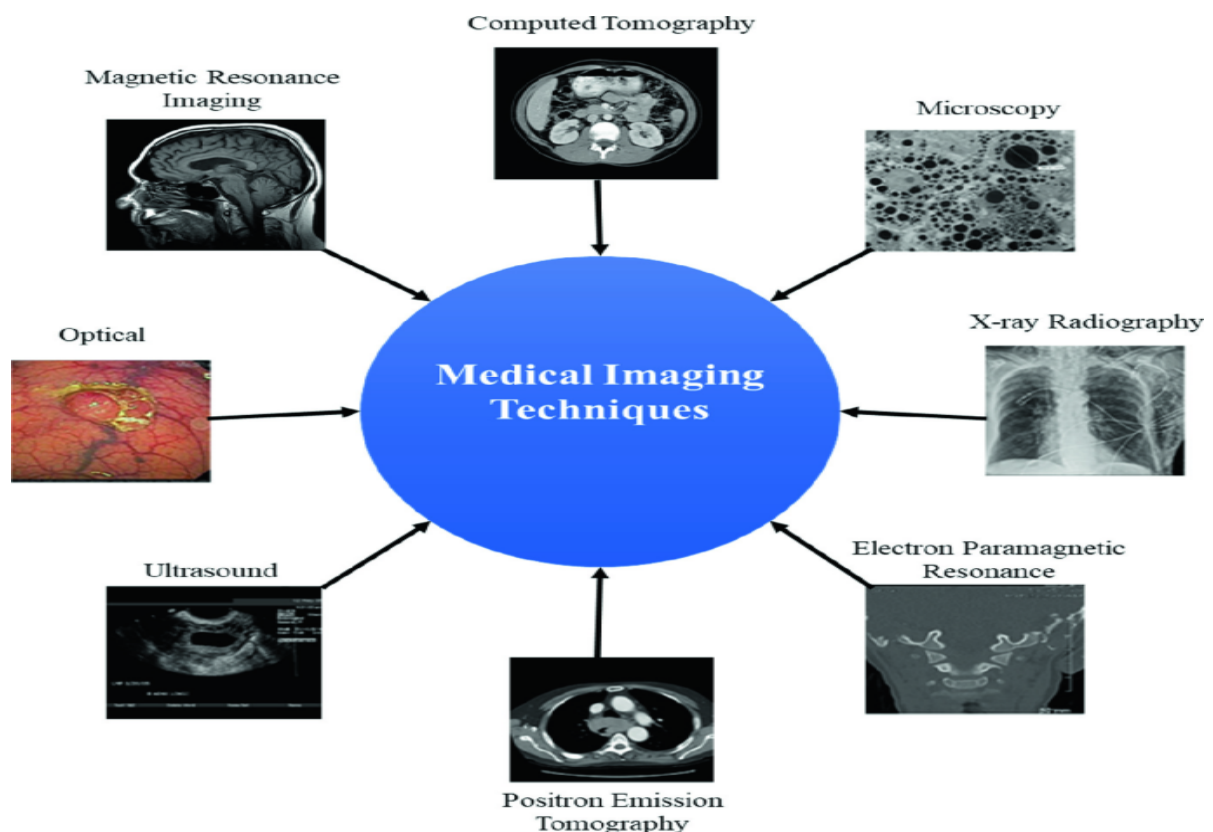


Figure I-3: Medical Imaging Techniques [19]

I.3.2 Overview of various imaging methods

Before delving into magnetic resonance imaging (MRI), the most widely used technique for visualizing brain tumors, this section presents an overview of the various imaging methods employed in brain studies. **Table I.2** offers a comparative analysis of these techniques. [17] [20] [21]

Table I.2 : Comparison of different imaging techniques [22]

Technique	Resolution (mm)	Source of Energy	Source of Image Contrast	Advantages	Limitations
CT	0.2 -1.0	X-Ray	Tissue density	Quick, high-resolution 3D reconstruction	Low soft tissue contrast, radiation exposure
MRI	0.3 -1.0	Radio-frequency	Multiple	Soft tissue contrast with various imaging techniques	Scan duration, sensitivity to metal, patient comfort
NUC MED	5-10	Gamma rays	Tissue biochemistry	Information on tissue function	Lower resolution, radioactive substances
PET	4-7	Positrons/ gamma rays	Tissue biochemistry	Functional information of tissues	Lower resolution, radioactive substances
SPECT	5-10	Gamma rays	Tissue biochemistry	Functional information of tissues	Lower resolution, radioactive substances
US	0.2-0.5	Acoustic (sound)	Tissue composition or flow	Quick, affordable, portable, real-time	Low image quality, restricted field of view
X-Ray	0.03-0.2	x-ray	Tissue density	Quick, affordable, and high-resolution	Limited to 2D, low soft tissue contrast

I.3.2.1 X-ray

X-ray imaging, or radiography, was the first and, for many years, the only method to visualize the inside of the body. It uses electromagnetic radiation that exposes tissues to ionizing radiation, accumulating over a patient's lifetime. Despite this, X-rays are quick, inexpensive, portable, and widely used in medicine. Specialized X-ray techniques include 2D mammography for breast imaging, 3D mammography (digital breast tomosynthesis) for breast cancer screening, and fluoroscopy, which produces real-time images. These methods show X-ray absorption differences in body tissues. However, X-rays only provide projection images, limiting internal organ views, prompting the development of other imaging techniques to address these limitations.[23]

I.3.2.2 Tomographic Imaging

MRI is one of several noninvasive techniques that generate cross-sectional (tomographic) images for radiologists and referring clinicians. Other commonly used tomographic modalities include computed tomography (CT), nuclear medicine, single

photon emission computed tomography (SPECT), positron emission tomography (PET), and ultrasound (US). [23]

I.3.2.2.1 Computed Tomography

Among the imaging methods, CT is most often compared to MRI because both produce detailed images of the body's anatomy with different shades of gray and can image any part of the body. However, the way images are created and how tissues appear in each method are very different.

Like MRI and other imaging techniques, CT creates an image by sending energy into the body and measuring how that energy is absorbed or changed by the body's tissues. In CT, x-ray beams are used. These beams pass through the body, and detectors on the opposite side measure how much energy gets through. This measurement shows how much energy was absorbed by the tissues. The x-ray beam is sent through the body at many different angles, and a computer processes these measurements to produce a cross-sectional image. [23]

I.3.2.2.2 Nuclear Medicine, SPECT, PET, and US

Nuclear medicine and SPECT use radioactive tracers introduced into the body to form images by measuring the decay of these tracers. The injected tracers emit gamma rays, which are similar to x-rays but have higher energy. A gamma camera detects these rays to create the final image. These methods are often used to measure blood flow and distribution in the heart and other organs. Compared to MRI, they produce lower resolution images but are specialized for assessing organ function.

PET also uses a radioactive tracer, but it detects tiny particles called positrons produced during decay. This allows PET to provide unique information about tissue metabolism. For example, a tracer can be attached to glucose to show how much glucose different tissues use, helping to distinguish normal from cancerous tissue. PET images have lower resolution than MRI but offer valuable insights into organ function. Hybrid systems like PET/CT and PET/MRI combine high-resolution anatomical images with metabolic images, allowing precise correlation between metabolic activity and anatomical structures, which is useful in tumor ablation.

Ultrasound is another tomographic imaging method and is the most widely available. It's relatively inexpensive, and the machines are small and portable. Ultrasound is commonly

used for fetal assessment during pregnancy and for scanning the heart, major arteries, liver, and kidneys. Unlike MRI and other methods, ultrasound doesn't use ionizing radiation but measures sound wave energy. However, because sound waves don't travel well through air or bone, ultrasound isn't optimal for imaging the lungs or skeleton. [23]

I.3.3 Magnetic Resonance Imaging (MRI)

MRI, as shown in **Figure I-4**, is undeniably fundamental in imaging brain tumors, significantly impacting every aspect of patient care, from diagnosis and treatment planning to monitoring treatment response and detecting recurrence. Presently, neuroimaging can detail both morphological and non-morphological (such as functional, hemodynamic, metabolic, cellular, microstructural, and occasionally genetic) features of brain tumors, substantially aiding in diagnosis and ongoing assessment [24]. MRI is a prominent medical imaging technique recognized for its ability to provide highly detailed visualizations of the human body. Its advanced technology is essential for the diagnosis and monitoring of a wide range of medical conditions. However, like any diagnostic method, MRI has both strengths and limitations. [23]



Figure I-4: Magnetic Resonance Imaging [25]

This section outlines the benefits of MRI, highlighting its safety, flexibility, and exceptional imaging quality, which make it a preferred tool in various clinical settings. It also addresses its drawbacks, including challenges related to cost, patient comfort, and accessibility, providing a balanced view of this critical imaging technology .

I.3.3.1 Advantages of MRI

MRI is a non-invasive imaging technique with numerous advantages, making it safe for repeated use and a valuable tool in medical diagnostics and neuroscience. Some of its key benefits include : [\[25\]](#)

- **Non-invasive and free of ionizing radiation:** MRI is a non-invasive imaging technique that, unlike X-rays and CT scans, does not require the use of ionizing radiation or invasive procedures like surgery, making it generally safe, reducing the risk of radiation exposure, and suitable for repeated examinations.
- **Excellent Soft Tissue Contrast:** MRI provides excellent contrast between different soft tissues, making it particularly useful for imaging the brain, muscles, joints, and organs like the liver and kidneys.
- **Multiplanar Imaging:** MRI allows imaging in multiple planes (axial, sagittal, and coronal), providing comprehensive views of the anatomy and facilitating the diagnosis of various conditions.
- **Functional Imaging:** Functional MRI (fMRI) can be used to assess brain activity by measuring changes in blood flow. This is valuable in neuroscience and can help identify areas of the brain associated with specific functions.

I.3.3.2 Disadvantages of MRI

Although MRI offers many advantages, it also has some drawbacks, including : [\[25\]](#)

- **Contrast Agents:** Some MRI scans may require the use of contrast agents (usually gadolinium-based) to enhance visibility of certain structures. While these agents are generally safe, there have been concerns about their long-term effects, especially in patients with kidney problems.
- **Noise and Claustrophobia:** The loud knocking and thumping noises produced during an MRI scan can be unsettling for some patients. Additionally, the enclosed space of the MRI machine can cause feelings of claustrophobia in some individuals.
- **Metallic Implant Interference:** Metal objects, such as pacemakers, artificial joints, and some dental implants, can interfere with the magnetic fields in an MRI machine, limiting its use in certain patients.

- **Cost:** MRI machines are expensive to purchase and maintain, making the cost of an MRI scan higher than some other imaging modalities.
- **Time-consuming:** MRI scans can be time-consuming, especially for certain types of studies. Patients may need to remain still for extended periods, which can be challenging for some individuals, such as young children or those with certain medical conditions.

I.3.3.3 Basic Principles of MRI

Magnetic Resonance Imaging is based on the principles of nuclear magnetic resonance (NMR) spectroscopy, which was initially developed for chemical analysis. In the context of medical imaging, MRI exploits the magnetic properties of certain atomic nuclei to produce detailed images of the human body. The basic principles of MRI involve the application of a strong magnetic field, radiofrequency (RF) pulses, and gradient magnetic fields to generate signals from the body that are used to construct images. Bellow a brief overview of these principles: [\[22\]](#) [\[26\]](#) [\[27\]](#)[\[28\]](#)

1. **Nuclear Magnetic Resonance (NMR):** The human body being made up on average of 70% water, we are in practice interested in the water molecule and in particular the hydrogen nucleus (proton). The hydrogen nucleus behaves like a charge rotating around its axis: this is the spin movement presented in Error! Reference source not found.. Protons can then be compared to magnetic dipoles. In the absence of any magnetic field, these will orient themselves in space in a random way. This movement gives the nucleus an angular momentum which depends on its mass and a magnetic moment which depends on its charge. In a magnetic field B_0 , the protons are then oriented relative to B_0 and describe around this field a precession movement, of constant angular speed.
2. **Magnetic Field:** MRI machines generate a strong, uniform magnetic field that aligns the magnetic moments of hydrogen nuclei (protons) in the body. The main magnetic field, denoted as B_0 , is typically several thousand times stronger than the Earth's magnetic field.
3. **RF Pulse and Resonance:** When a short burst of RF energy is applied at the resonant frequency of the protons (the Larmor frequency), it causes the protons to absorb energy and process (or wobble) out of alignment with the main magnetic field. This process is known as excitation or resonance.

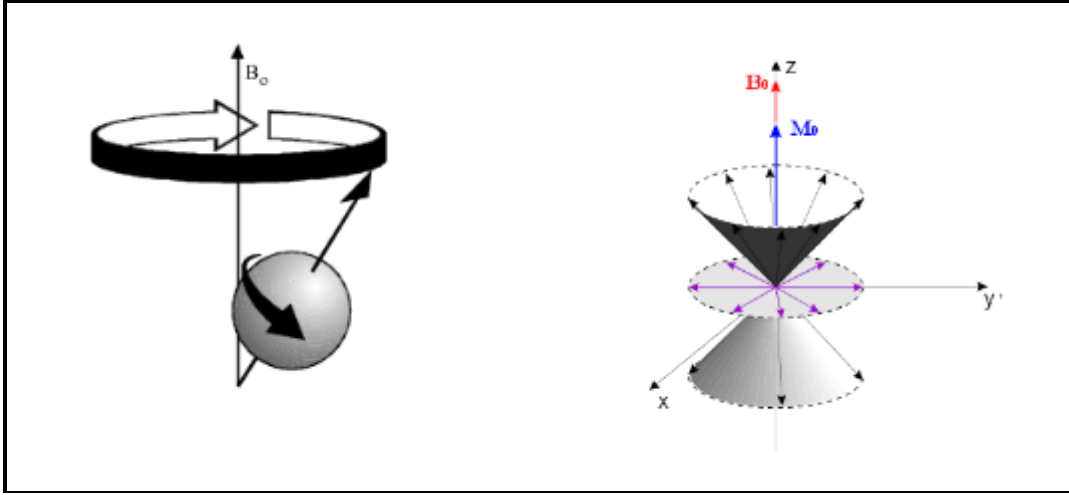


Figure I-5: The spin movement [22]

- 4. Relaxation Processes:** After the RF pulse is turned off, the protons gradually return to their equilibrium alignment with the main magnetic field. As presented in **Figure I-6**, There are two relaxation processes involved:
- Longitudinal Relaxation (T1):** Protons realign with the magnetic field, releasing energy in the form of RF signals. T1 relaxation affects the longitudinal magnetization (M_L), which is the component of the magnetization along the direction of the main magnetic field.
 - Transverse Relaxation (T2):** Protons lose phase coherence and dephase, leading to a loss of transverse magnetization (M_T). T2 relaxation is the process by which the transverse magnetization decays back to its equilibrium state.

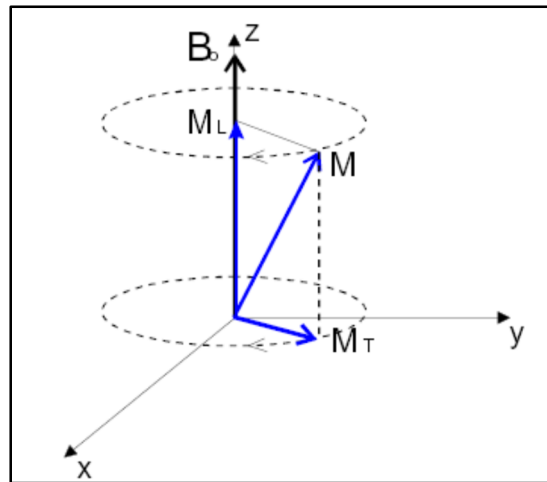


Figure I-6: Splitting of the magnetic moment M . [22]

- 5- Gradient Fields:** Gradient magnetic fields are applied in different directions, allowing spatial encoding of the signals. By varying the strength and timing of these gradients, different regions of the body can be selectively imaged.
- 6- Signal Detection:** To generate an MRI image, the patient is subjected to a magnetic field (B_0) and a radiofrequency wave (B_1) with a frequency matching the precession frequency of protons. This wave causes the protons to tilt at an angle (θ), typically 90 or 180 degrees relative to their initial state (M_0). When the radiofrequency pulse ends, the protons return to their equilibrium state, leading to a rapid decrease in the transverse moment (M_T) and a recovery of the longitudinal moment (M_L). During this return to equilibrium, the protons continue to precess, producing a Free Induction Decay (FID) magnetic field as shown in **Figure I-7**. This signal is captured by the receiving coils and converted into an electrical signal, which is then used to create the MRI image.

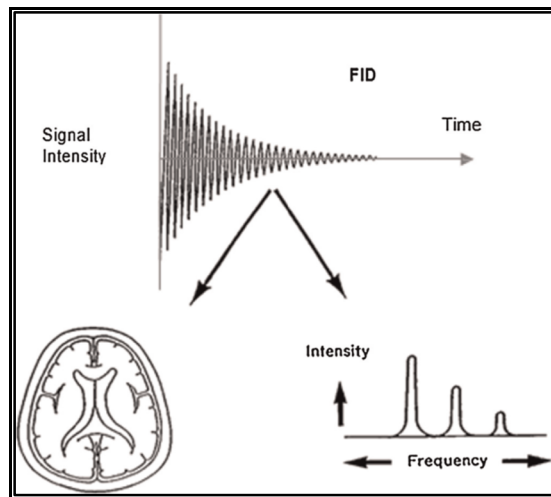


Figure I-7: The FID and signal detection to generate MR images. [27]

- 7- Image Reconstruction:** The signals detected by the receiving coils are processed by a computer to generate detailed images of the body. Various imaging sequences are presented in **Figure I-8**, such as T1-weighted, T2-weighted, and gradient-echo sequences, can be used to emphasize different tissue properties and provide different types of contrast in the images.

By manipulating these basic principles, MRI can produce detailed images of anatomical structures and physiological processes in the body with high spatial resolution and excellent soft tissue contrast, making it a versatile and powerful imaging modality in clinical practice.

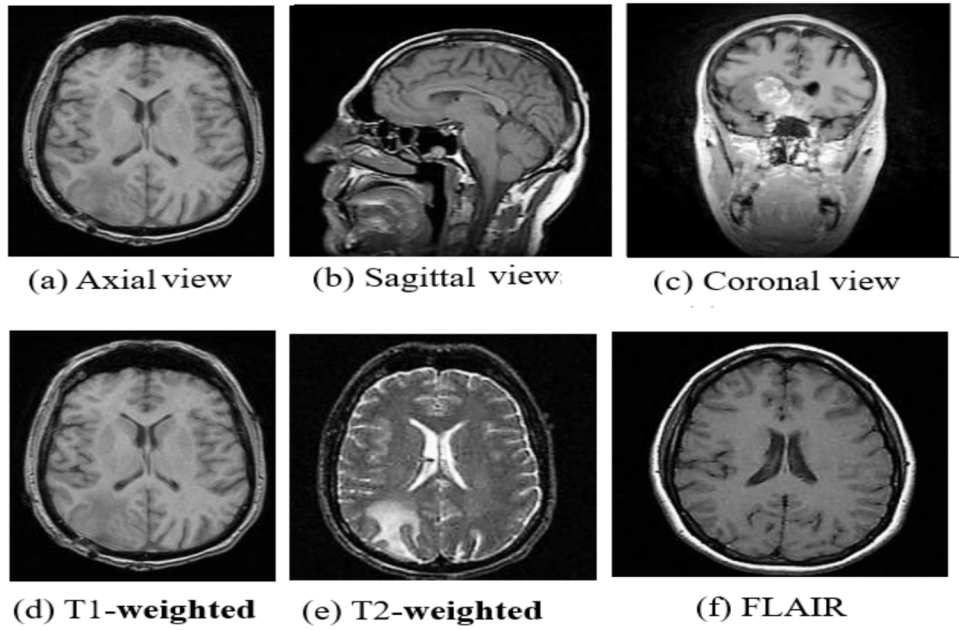


Figure I-8: Various MRI images sequences [29]

I.4 Conclusion

Brain tumors represent a complex and challenging medical condition, demanding accurate diagnosis and effective treatment strategies. MRI has emerged as an indispensable tool for brain tumor assessment, providing detailed insights into tumor characteristics and guiding clinical decision-making. Deep learning techniques have revolutionized the field of medical imaging, offering promising avenues for further enhancing brain tumor identification and classification using MRI data.

Chapter II

Materials and methods

II.1 INTRODUCTION	19
II.2 AI, ML AND DL PARADIGM	19
II.3 MACHINE LEARNING (ML):.....	20
II.3.1 DEFINITION	20
II.3.2 TYPES OF MACHINE LEARNING.....	20
II.3.3 CONCEPTS OF MACHINE LEARNING MODELS.....	21
II.4 DEEP LEARNING (DL).....	22
II.4.1 DEFINITION.....	22
II.4.2 HISTORY OF DEEP LEARNING.....	22
II.4.3 CONCEPTS OF DEEP LEARNING MODELS	24
II.4.4 TYPES OF ARTIFICIAL NEURAL NETWORK.....	30
II.5 DEEP LEARNING IN MEDICAL IMAGE ANALYSIS:	34
II.5.1 THE IMPACT OF DEEP LEARNING ON MEDICAL IMAGE ANALYSIS	34
II.5.2 APPLICATIONS IN MEDICAL IMAGING.....	34
II.5.3 DL TECHNIQUES FOR MEDICAL IMAGE ANALYSIS.....	35
II.5.4 ADVANTAGES OF DEEP LEARNING IN MEDICAL IMAGING	37
II.5.5 CHALLENGES AND LIMITATIONS	37
II.5.6 FUTURE DIRECTIONS	37
II.5.7 CNNs FOR MRI BRAIN TUMOR CLASSIFICATION	38
II.6 PERFORMANCE EVALUATION MEASUREMENTS.....	42
II.6.1 CONFUSION MATRIX	42
II.6.2 ACCURACY	42
II.6.3 SENSITIVITY.....	42
II.6.4 SPECIFICITY	43
II.6.5 F1-SCORE.....	43
II.6.6 ROC CURVE.....	43
II.7 CONCLUSION.....	44

Chapter II Materials and methods

II.1 Introduction

The integration of machine learning in MRI brain tumor detection promises to revolutionize clinical workflows by providing radiologists with powerful tools for early and accurate diagnosis. This chapter aims to provide a solid foundation and clear understanding of the tools and techniques employed in this research. We explore the domain of machine learning (ML), specifically focusing on deep learning (DL) techniques, and their transformative impact on medical image analysis. To ensure the robustness and reliability of the proposed models, the performance evaluation metrics used in this study are described.

II.2 Artificial intelligence, machine learning and deep learning paradigm

In the data sciences field, artificial intelligence (AI) aims to provide computers human-level intelligence. For this reason, Machine learning and deep learning, which are subfields of artificial intelligence, focus on developing algorithms and models that enable computers to learn from and make predictions or decisions based on data, without human intervention. They represent a powerful toolkit in achieving the ultimate goal of AI: intelligent machines [30]. **Figure II-1** visually represents this hierarchical relationship, with AI at the top level, followed by ML, and then DL as a specialized subset of ML.

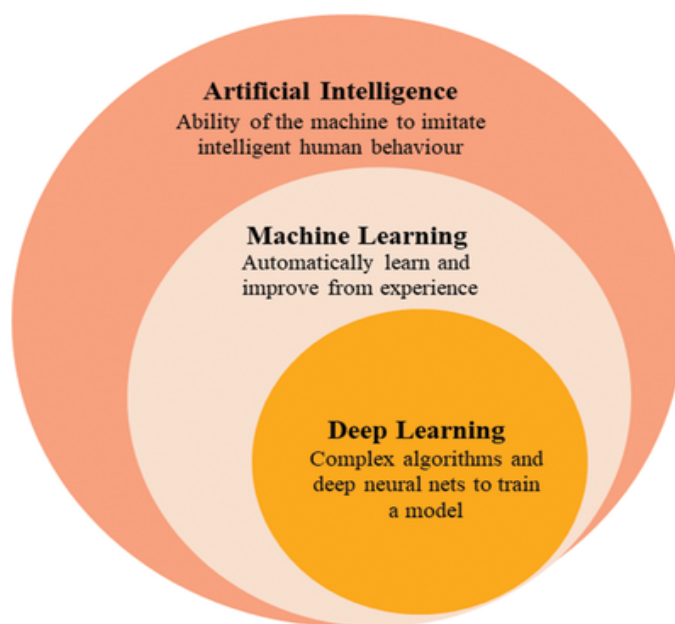


Figure II-1: AI, machine learning and deep learning paradigm [31]

II.3 Machine Learning (ML):

II.3.1 Definition

Machine learning is the study of computer algorithms that improve automatically through experience. It is a branch of artificial intelligence based on the idea that systems can learn from data, identify patterns, and make decisions with minimal human intervention. [32]

II.3.2 Types of Machine Learning

The effectiveness of machine learning models relies on the quality and quantity of data they are trained on. Depending on the nature of the data and the desired outcome, machine learning algorithms can be broadly classified into three main categories as illustrated in **Figure II-2**: supervised, unsupervised, and reinforcement learning. [30] [32]

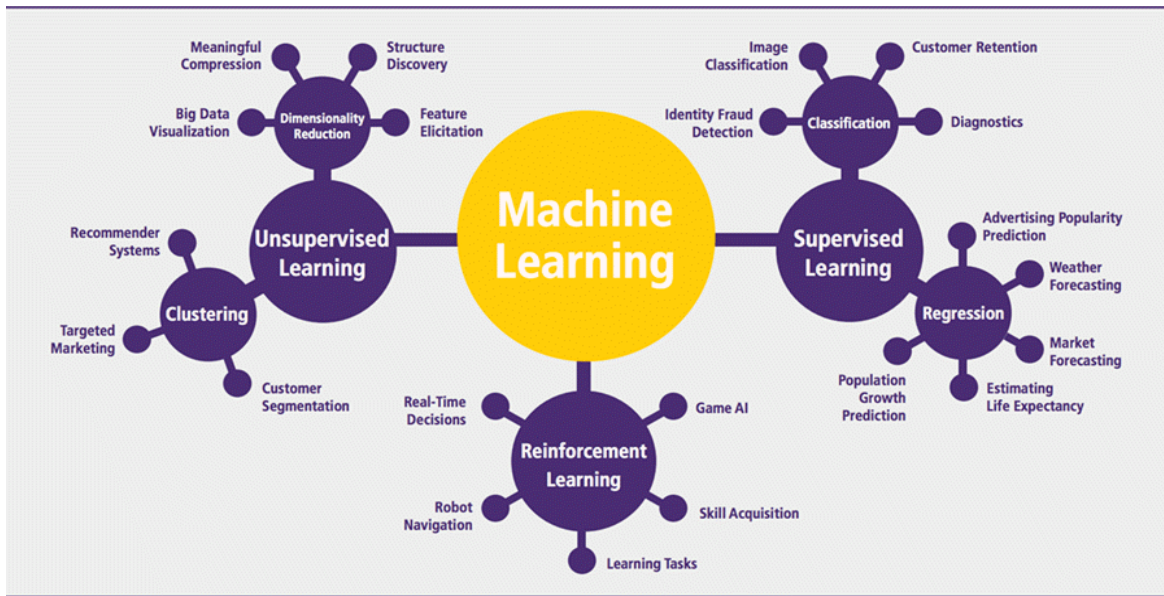


Figure II-2: Types of Machine Learning [33]

II.3.2.1 Supervised Learning:

The algorithm learns from labeled training data, making predictions or decisions based on input-output pairs. Common applications include classification and regression tasks.

II.3.2.2 Unsupervised Learning

The algorithm learns from unlabeled data, finding hidden patterns or intrinsic structures. Common applications include clustering and dimensionality reduction.

II.3.2.3 Reinforcement Learning

The algorithm learns through trial and error by interacting with an environment and receiving feedback in the form of rewards or penalties. It aims to maximize the cumulative reward over time.

II.3.3 Concepts of Machine Learning Models

The success of machine learning models hinges on a solid understanding of key concepts such as features, labels, model training, evaluation, and application areas. The typical process of ML is illustrated in **Figure II-3**. [34]

- **Features and Labels:** Features are input variables used to make predictions, while labels are the output variables to be predicted.
- **Model Training:** The process of fitting a model to training data by adjusting its parameters to minimize a loss function.
- **Model Evaluation:** Assessing the performance of a trained model on unseen data using evaluation metrics such as accuracy, precision, recall, F1-score, etc.
- **Applications:** Machine learning is widely used in various fields, including healthcare (diagnosis, prognosis), finance (fraud detection, risk assessment), and natural language processing (speech recognition, machine translation).

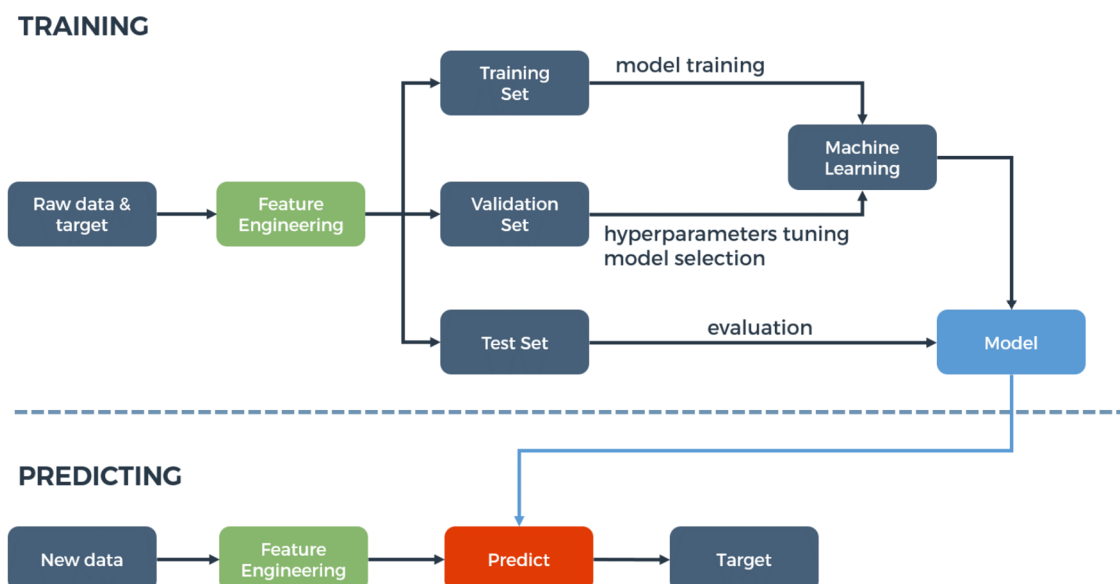


Figure II-3: The typical process of ML [30]

II.4 Deep Learning (DL)

II.4.1 Definition

Deep learning is a subset of machine learning that uses artificial neural networks to model and solve complex problems. It is characterized by the use of deep neural networks with multiple layers (deep architectures) as shown in **Figure II-4**. [35]

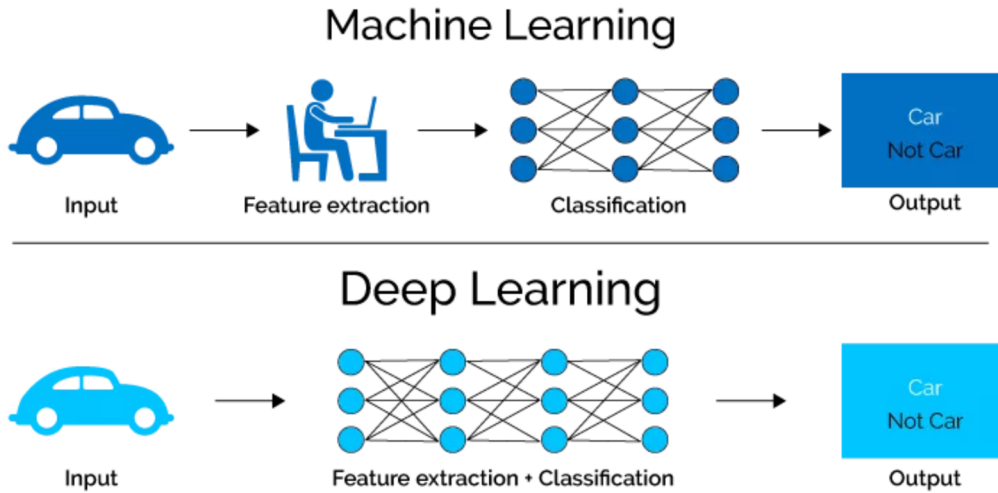


Figure II-4: Difference between ML and DL [30]

Machine learning encompasses a broader range of algorithms and techniques for learning from data, while deep learning focuses specifically on neural networks with multiple layers for solving complex problems. Deep learning has shown remarkable success in various applications, particularly in domains with large datasets.

II.4.2 History of Deep Learning

The history of Deep Learning goes back several decades, marked by the contributions of researchers and scientists in the field of neural networks and artificial intelligence. **Figure II-5** and **Table II.1** present a timeline of the main contributors and their contributions:

Table II.1: Timeline of the main contributions in the field of ANN [36]

Year	Contributer	Contribution
300 BC	• Aristotle	Introduced Associationism, marking the beginning of humanity's effort to understand the brain.
1873	• Alexander Bain	Introduced Neural Groupings as the first models of neural networks.
1943	• McCulloch & Pitts	The McCulloch-Pitts (MCP) model was introduced and is considered as the ancestor of artificial neural networks.
1949	• Donald Hebb	Regarded as the father of neural networks, he introduced the Hebbian Learning Rule, which forms the foundation of modern neural networks.
1958	• Frank Rosenblatt	Introduced the first perceptron.
1974	• Paul Werbos	Introduced Backpropagation
1980	• Teuvo Kohonen	Introduced Self Organizing Map
	• Kunihiko Fukushima	Introduced Neocogitron, which inspired Convolutional Neural Network
1982	• John Hopfield	Introduced Hopfield Network
1985	• Hilton & Sejnowski	Introduced Boltzmann Machine
1986	• Paul Smolensky	Introduced Harmonium, which is later known as Restricted Boltzmann Machine
	• Michael I. Jordan	Defined and introduced Recurrent Neural Network
1990	• Yann LeCun	Introduced LeNet, showed the possibility of deep neural networks in practice
1997	• Schuster & Paliwal	Introduced Bidirectional Recurrent Neural Network
	• Hochreiter & Schmidhuber	Introduced LSTM, solved the problem of vanishing gradient in recurrent neural networks
2006	• Geoffrey Hinton	Introduced Deep Belief Networks, also introduced layer-wise pretraining technique, opened current deep learning era.
2009	• Salakhutdinov & Hinton	Introduced Deep Boltzmann Machines
2012	• Geoffrey Hinton	Introduced Dropout, an efficient method for training neural networks

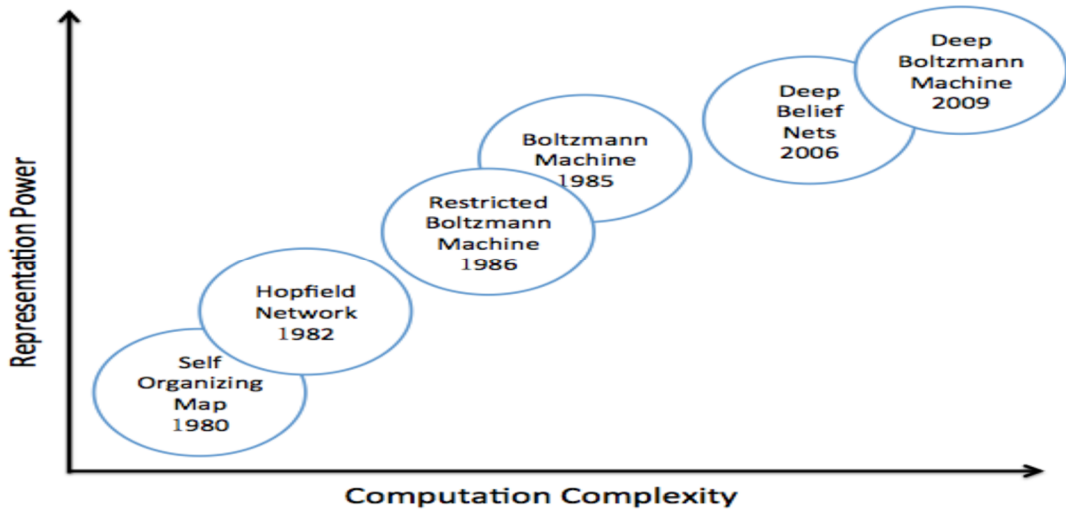


Figure II-5: Trade of representation power and computation complexity [36]

II.4.3 Concepts of Deep Learning Models

Artificial neural networks (ANNs) are inspired by the structure and function of the human brain. They consist of interconnected processing units called neurons, arranged in layers. This section presents the key components of an ANN architecture: [30]

II.4.3.1 Neurons

Neurons in a neural network act as information processors. They receive inputs from other neurons or the initial input layer. These inputs are then scaled by weights, which represent the strength of the connection between neurons. An optional bias term can be added to adjust the activation threshold of the neuron.

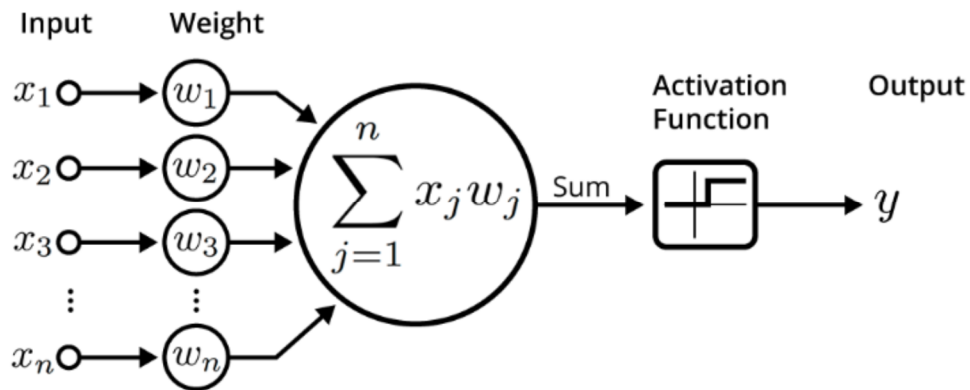


Figure II-6: Structure of a neuron [30]

Finally, the weighted sum is passed through an activation function. This function introduces non-linearity, allowing the network to learn complex patterns from data. The output of the activation function becomes the activation of the neuron, which is then sent onward to other neurons in the next layer, continuing the information processing chain.

As presented in **Figure II-6**, a neuron has three parameters: [37]

- **Weight:** When a signal (value) arrives, a neuron gets multiplied by a weight value. If a neuron has three inputs, it has three weight values which can be adjusted during training time.
- **Bias:** An additional input to neurons that is always set to 1, with its own connection weight. This ensures that even when all other inputs are absent (all 0s), there will still be activation in the neuron.
- **Activation Functions:** The primary role of any activation function in a neural network is to map the input to the output. This input is obtained by calculating the weighted sum of a neuron's inputs and adding a bias, if present. The activation function determines whether a neuron will fire for a given input by producing the corresponding output.

II.4.3.2 Activation Functions: The Decision Maker

An activation function in neural networks is a mathematical function that determines a neuron's output based on its input. It plays a key role in deciding how the network processes information, similar to how biological neurons function. Acting as a transfer function, it converts input values into corresponding outputs.

Neural network activation functions are categorized as binary step, linear, or non-linear. Linear functions produce outputs proportional to inputs. Binary step functions are threshold-based and simple. Non-linear functions, the most common and complex, enable diverse data processing. [38]

II.4.3.2.1 Binary Step Function

The binary step function, as shown in **Figure II-7**, determines neuron activation based on a threshold value. If the input exceeds the threshold, the neuron activates; otherwise, it remains inactive, preventing its output from being passed to the next hidden layer. [39]

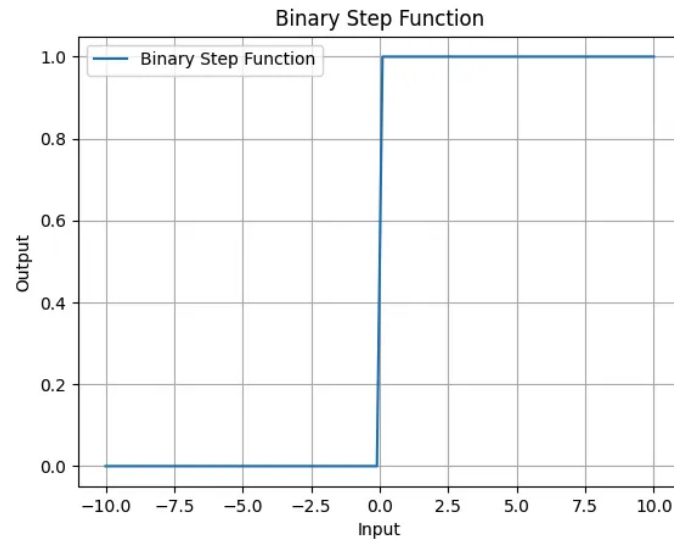


Figure II-7: Binary Step Function [39]

II.4.3.2.2 Linear Activation Function

A Linear Activation Function, as shown in **Figure II-8**, is represented by the equation $y = x$, forming a straight line. Regardless of the number of layers in a neural network, if all layers utilize linear activation functions, the final output remains a linear combination of the input. Linear activation functions are beneficial for certain tasks but need to be paired with non-linear functions to improve a neural network's learning ability and predictive performance.

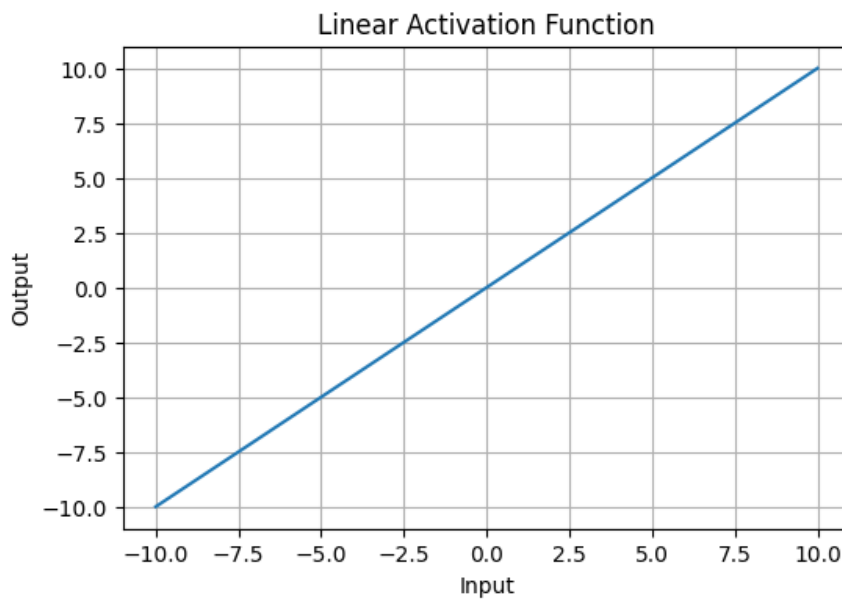


Figure II-8: Linear Activation Function [38]

II.4.3.2.3 Non-Linear Activation Functions

The success of artificial neural networks is largely attributed to their ability to model complex, non-linear functions in real-world data. Without non-linearity, even deep networks would be limited to solving only basic, linearly separable problems. Activation functions play a crucial role by introducing non-linearity, enabling neural networks to capture intricate data distributions and tackle advanced deep learning challenges. This flexibility allows the network to learn more abstract patterns and better fit input data, making activation functions essential for the effectiveness of neural networks. [38] [40]

- **Sigmoid Function :** The sigmoid activation function, also known as the logistic activation function, is a widely used non-linear function that maps input values to an output range between 0 and 1 as presented in **Figure II-9**. Unlike the binary step function, it produces continuous values within this range rather than just 0 or 1. [38] [40]

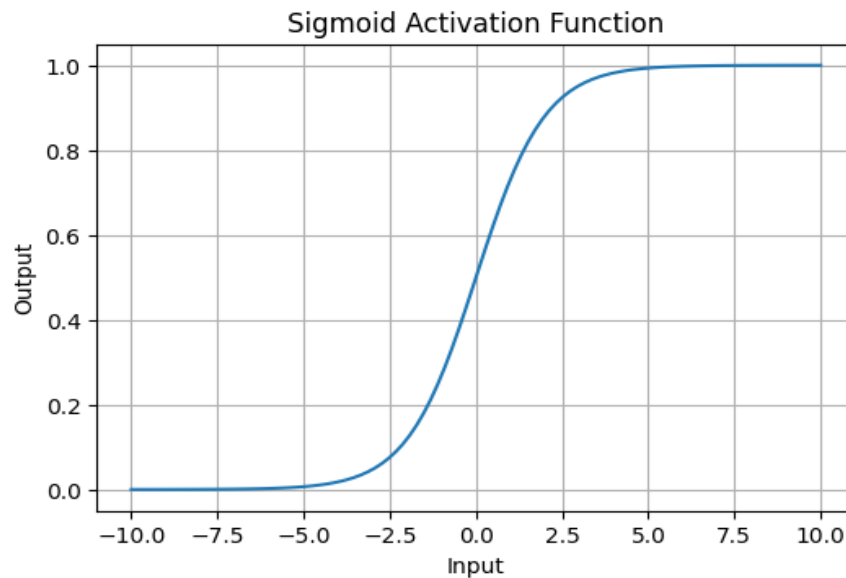


Figure II-9: Sigmoid Activation Function [38]

- **Tanh Activation Function :** The tanh activation function, as presented in **Figure II-10**, offers several advantages over sigmoid: it handles negative values better, is zero-centered for faster learning, and has stronger gradients that mitigate vanishing gradients somewhat. However, like sigmoid, it still suffers from the vanishing gradient problem, especially in deep networks. Tanh is commonly used in hidden layers, particularly when input data is zero-centered, for more efficient training. [38] [40]

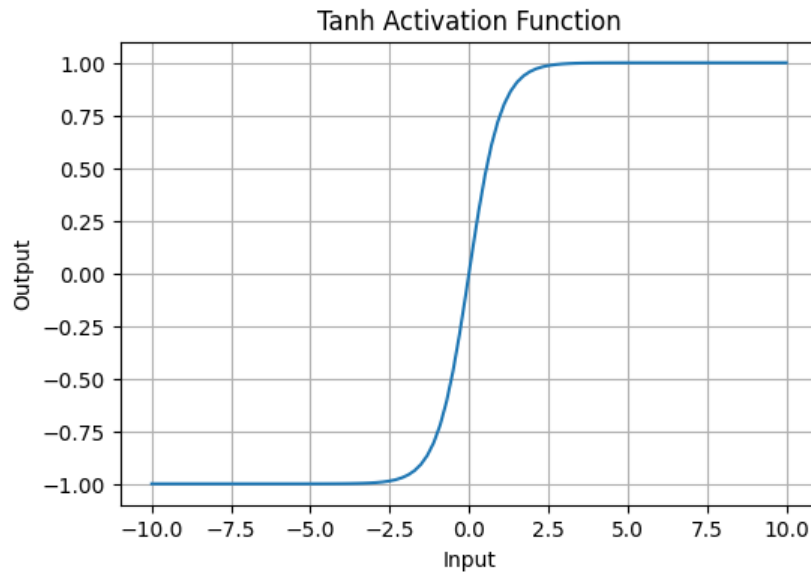


Figure II-10: Tanh Activation Function [38]

- **ReLU (Rectified Linear Unit) Function**

ReLU is a popular activation function that is known for its effectiveness and simplicity. It prevents gradient vanishing problems and speeds up computation by substituting 0 for negative values while keeping positive values unchanged, as shown in **Figure II-11**. Compared to neural networks that use sigmoid or tanh, those that use ReLU usually converge six times faster.[38] [40]

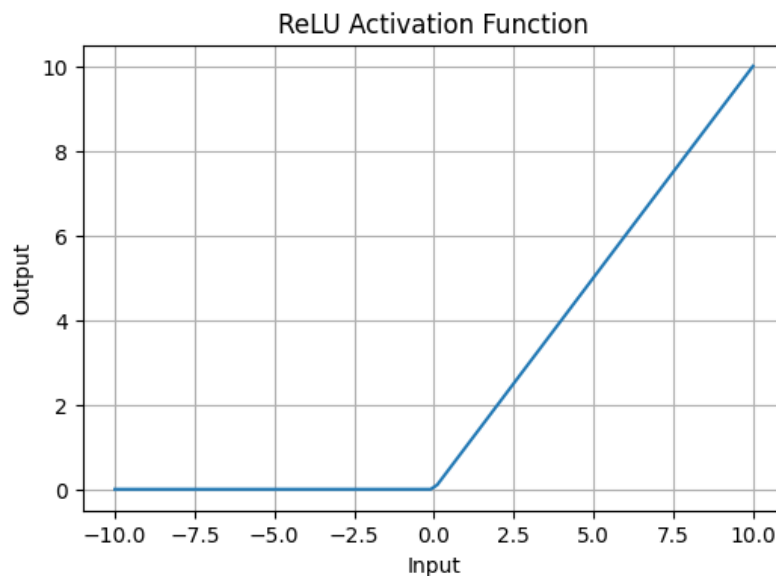


Figure II-11: ReLu Activation Function [38]

II.4.3.3 Artificial Neural Network

Artificial Neural networks (ANN) are a type of AI inspired by the structure and function of the brain. They are composed of interconnected nodes (or artificial neurons) that process information by passing signals to each other. These networks can learn and improve their performance over time by adjusting the weights of the connections between nodes.

There are typically three layers in an artificial neural network. Nodes that are connected to each other make up layers. The following provides a description of the three layers of ANN as illustrated in **Figure II-12**. [30]

- **Input layer:** This layer serves as the entry point, receiving raw data from the external world. This data can be anything from images and sounds to numerical values, depending on the network's purpose.
- **Hidden layers:** These layers, often consisting of multiple layers stacked upon each other, perform the core computations and information processing. They extract features and patterns from the raw data received from the input layer. The number of hidden layers and the number of neurons within each layer are crucial hyperparameters, influencing the network's complexity and its ability to learn and generalize from data.
- **Output layer:** The final layer of the network, the output layer, produces the network's final outcome. This output can take various forms, depending on the network's task. For example, it could be a classification decision (e.g., identifying a handwritten digit), a predicted value (e.g., stock price prediction), or even a generated image.

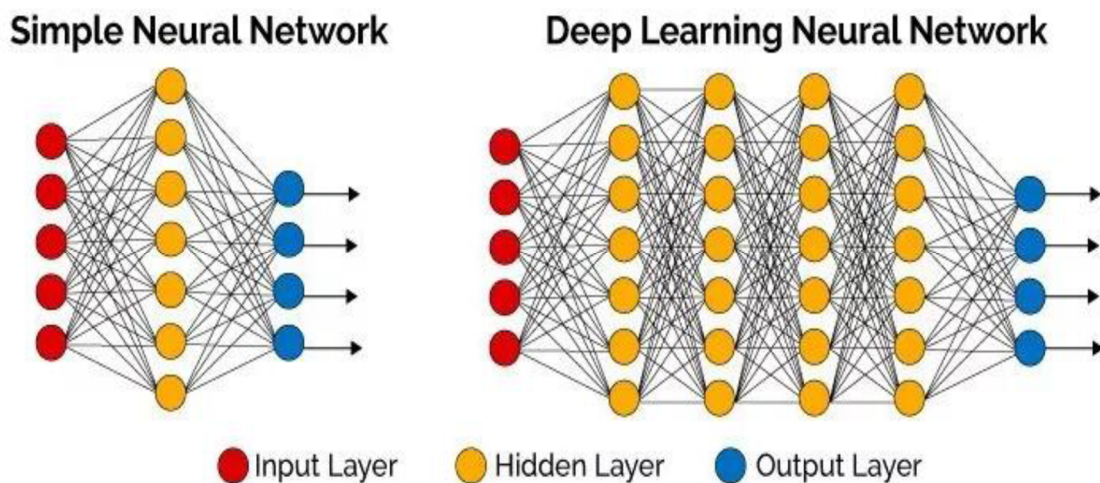


Figure II-12: Deep Neural Network [30]

II.4.4 Types of artificial neural network

There are many different types of neural networks, each with its own strengths and weaknesses. This section presents some of the most common types. [41][42]

II.4.4.1 Perceptron

The perceptron, as shown in **Figure II-13**, is the simplest type of neural network. It consists of a single layer of nodes and can only perform linear separations of data. Perceptrons are not very powerful on their own, but they are the building block of more complex neural networks. [43]

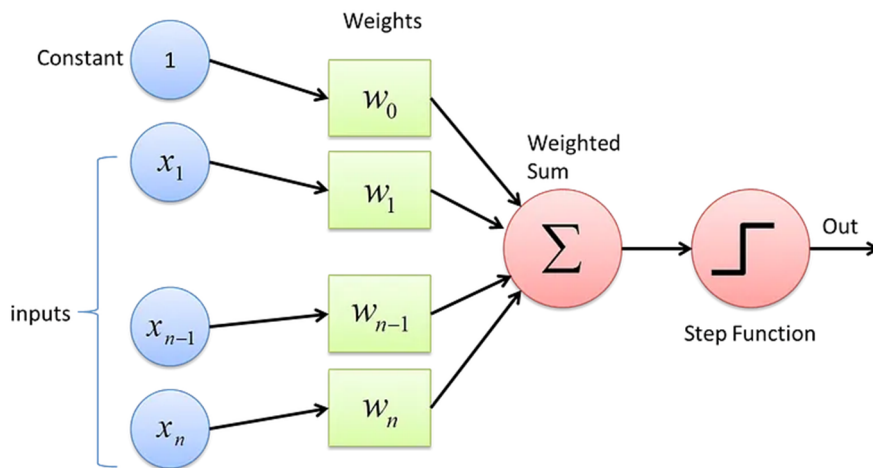


Figure II-13: Perceptron, Simple Neural Network [43]

II.4.4.2 Multilayer Perceptron (MLP)

MLPs are a type of feedforward neural network that consists of multiple layers of perceptron. The additional layers allow MLPs to learn more complex relationships between data. MLPs are a general-purpose type of neural network that can be used for a wide variety of tasks, such as image recognition and classification. [43]

II.4.4.3 Convolutional Neural Network (CNN)

CNNs are a type of neural network that is specifically designed for image recognition. CNNs, as shown in **Figure II-14**, use a special type of layer called a convolutional layer that is able to extract features from images. CNNs are very successful at image recognition tasks, such as face detection and object classification. [44] [45]

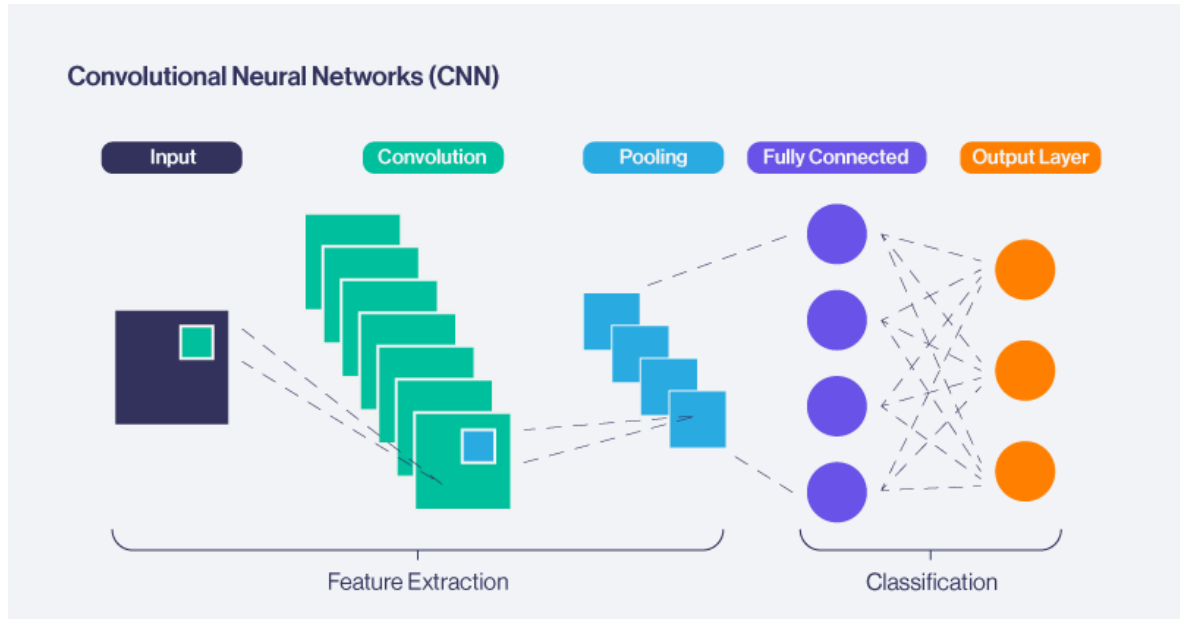


Figure II-14: Convolutional Neural Network Architecture [42]

II.4.4.4 Recurrent Neural Network (RNN)

RNNs are a specialized type of neural network designed for processing sequential data. Unlike traditional neural networks, they incorporate a feedback loop, as illustrated in **Figure II-15**, enabling them to retain information from previous inputs and use it to influence current processing. This memory-like capability makes RNNs particularly well-suited for tasks such as speech recognition, language translation, and time series prediction, including sales forecasting and stock market analysis. A key strength of RNNs is their ability to capture temporal dependencies, allowing them to learn from past data and make informed predictions about future events.[43] [44]

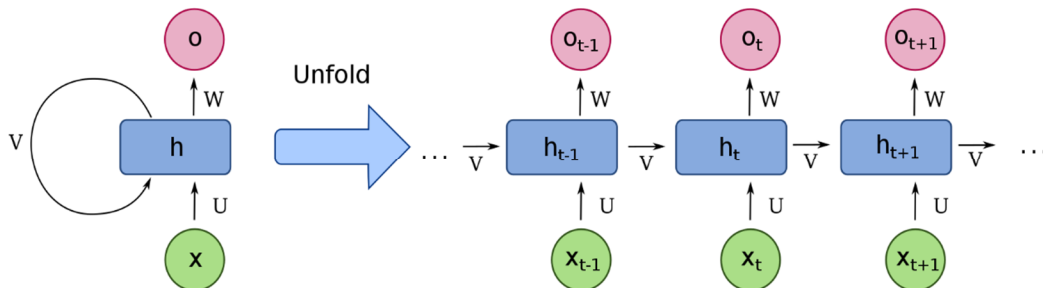


Figure II-15: RNN Architecture [43]

II.4.4.5 Long Short-Term Memory (LSTM)

LSTMs are a type of RNN that is specifically designed to address the problem of vanishing gradients. Vanishing gradients can occur in RNNs when processing long sequences of data. LSTMs have a special internal structure, as illustrated in **Figure II-16**, that allows them to store information for longer periods of time. LSTMs are very successful at tasks such as speech recognition and machine translation. [44] [46]

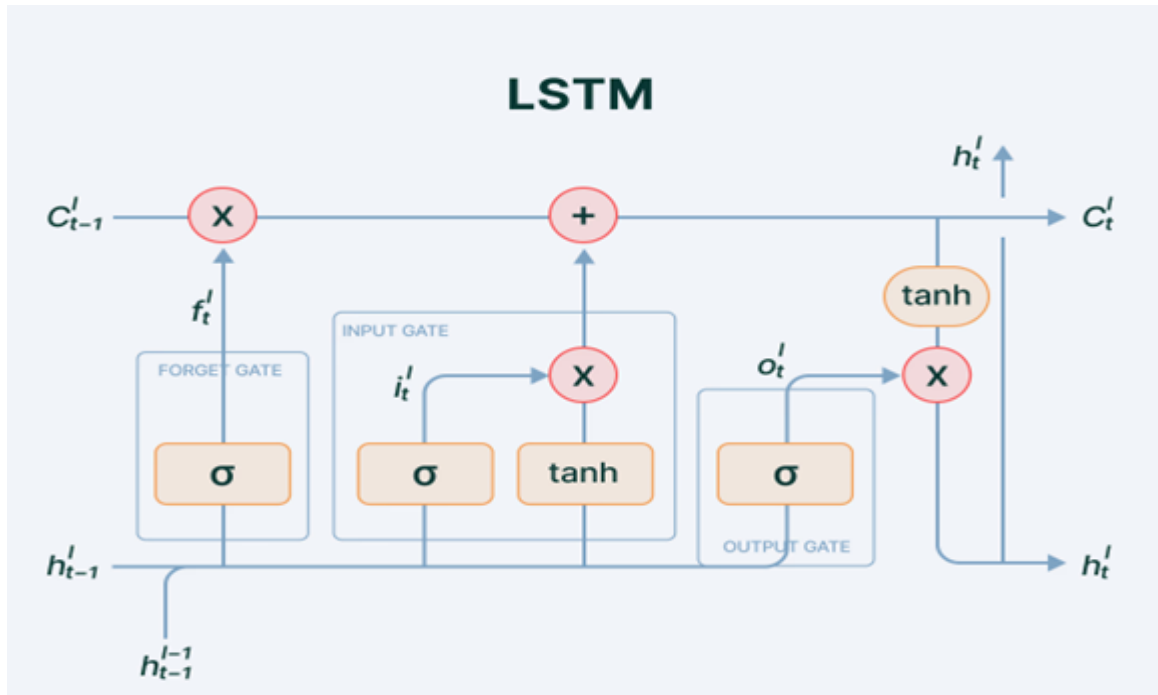


Figure II-16: LSTM Architecture [46]

II.4.4.6 Generative Adversarial Networks (GANs)

Generative adversarial networks are a type of artificial intelligence model developed by Ian Goodfellow and his colleagues in 2014. They are based on an adversarial training framework, where two neural networks, the generator and the discriminator, compete to generate highly realistic synthetic data. The generator is responsible for producing synthetic data, while the discriminator evaluates whether the data is real or artificially generated. Throughout training, the generator continuously improves its output to deceive the discriminator, while the discriminator enhances its ability to distinguish real from synthetic samples. This iterative process continues until the generator produces data that is nearly indistinguishable from real data, leading to a balanced state between the two networks. The architecture of GAN is illustrated in **Figure II-17**. [44][47]

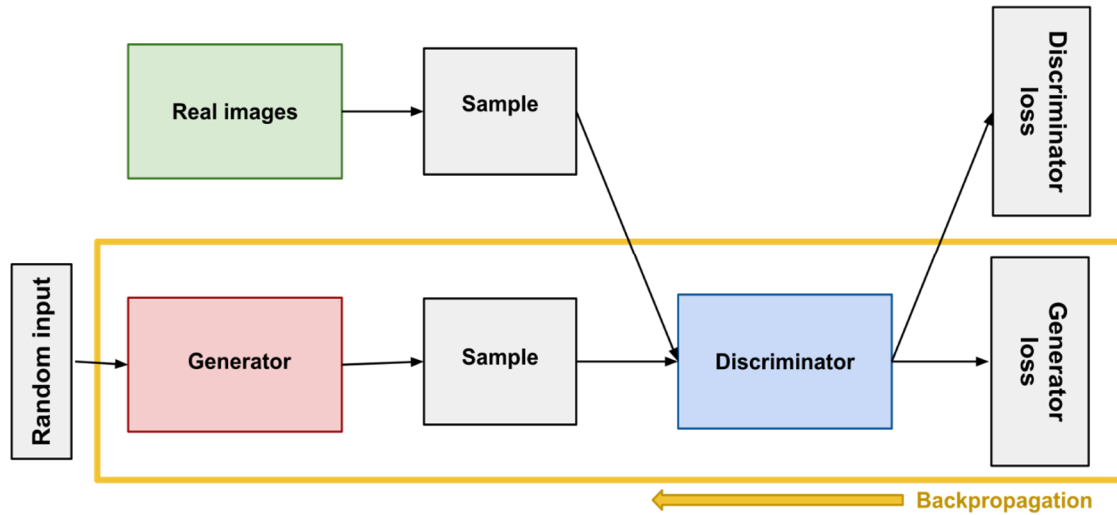


Figure II-17: GAN Architecture [47]

II.4.4.7 Sequence to Sequence Models (Seq2Seq)

Seq2Seq was first introduced by Google for machine translation, it revolutionized the word-by-word method that ignored sentence structure and syntax. Seq2Seq transformed translation by utilizing deep learning to take into account both the current input word and its context. There are two main parts, as shown in **Figure II-18**, to this model (Decoder and Encoder). Seq2Seq models are trained on input-output token sequences to predict the most likely output, making them effective for natural language processing (NLP) tasks like image captioning, text summarization, and machine translation. They often incorporate Attention mechanism to enhance performance by focusing on relevant input parts. Today, they are widely used in text generation, automated content creation, and conversational AI. [48]

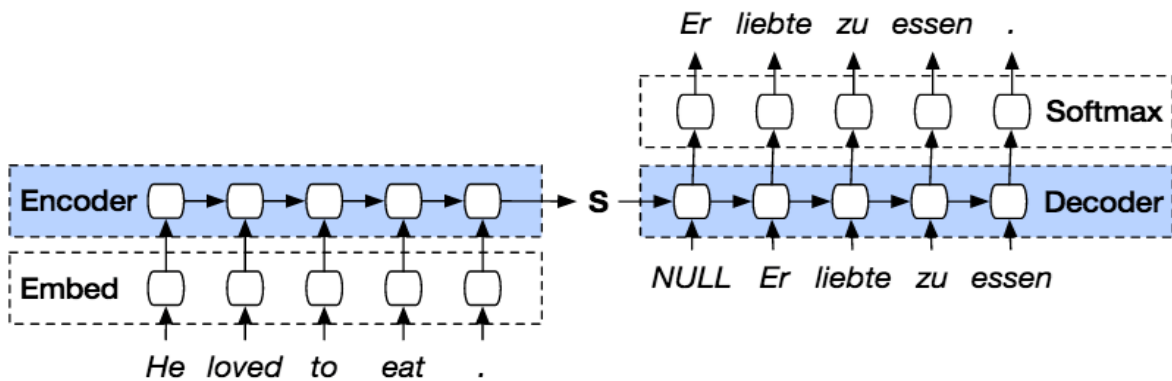


Figure II-18: Sequence to Sequence Model [48]

II.5 Deep Learning in medical image analysis:

Medical professionals have used imaging methods like CT, MRI, PET, mammography, ultrasound, and X-rays for decades in order to identify, diagnose, and treat diseases early [31]. Human specialists like radiologists and doctors have historically been in charge of interpreting these images. However, there is an increasing reliance on computer-aided techniques to support medical decision-making due to the complexity of anomalies and the possibility of human fatigue. Although image technology has advanced more quickly than computer-aided analysis, the use of machine learning has resulted in notable advancements. In particular, deep learning (DL) has revolutionized medical image analysis by enabling automated, accurate, and efficient interpretation of complex imaging data. Unlike traditional machine learning approaches that require handcrafted features and extensive domain expertise, deep learning models can autonomously learn hierarchical features from raw images. This capability has greatly enhanced diagnostic accuracy, disease classification, and treatment planning across various medical fields, including radiology, pathology, and oncology.[49]

II.5.1 The Impact of Deep learning on Medical Image Analysis

Deep learning, particularly Convolutional Neural Networks (CNNs), has fundamentally changed medical image analysis. By automating complex tasks like segmentation and disease classification with high accuracy, these algorithms are accelerating diagnoses, improving patient outcomes, and streamlining healthcare. Leveraging vast amounts of annotated data, deep learning enables earlier disease detection, enhances radiologist decision-making, and drives medical research, effectively revolutionizing patient care. [4] [44][43]

II.5.2 Applications in Medical Imaging

Deep learning has been widely applied to various medical imaging tasks [31][44] [45] [49] [50] [51] , including :

- **Tumor Detection and Classification:** Because of their strong feature extraction capabilities, CNNs are highly effective at accurately detecting and classifying cancers, such as brain tumors in MRIs, lung nodules in CT scans, and breast cancer in mammograms.

- **Medical Image Segmentation:** Organ and lesion segmentation is a crucial step for precise diagnosis and therapy planning, and U-Net and related architectures are frequently employed for this purpose.
- **Disease Prediction and Diagnosis:** By training on big datasets, deep learning models can detect and diagnose diseases such as diabetic retinopathy (based on visual imaging), Alzheimer's disease (based on brain MRI), and pneumonia (based on chest X-rays).
- **Image Enhancement and Reconstruction:** By reducing noise, enhancing resolution, and eliminating artifacts, methods such as GANs improve the quality of medical images, leading to better interpretation.
- **Image Registration:** To enhance analysis and treatment planning, image registration aligns medical images from several modalities, views, or times. VoxelMorph and other deep learning models improve speed and accuracy, which helps with radiation planning for accurate diagnosis and treatment, multi-modal fusion (MRI-PET), and disease tracking (MRI).
- **Image-Guided Interventions:** Deep learning is used in image-guided interventions to improve real-time imaging during operations and medical procedures. Robotic-assisted surgery benefits from reinforcement learning, while surgical tool tracking is aided by methods such as object detection. Applications that enhance accuracy and patient outcomes include real-time tissue segmentation, ultrasound-guided biopsies, and tumor localization in radiation therapy.

II.5.3 DL Techniques for Medical Image Analysis

Deep learning has transformed medical image analysis by improving feature extraction, classification, and segmentation. Key techniques include CNNs for object detection, RNNs and LSTMs for handling sequential medical data, and GANs for generating synthetic images to enhance datasets. Additionally, hybrid approaches combine deep learning with traditional methods to address challenges like data scarcity and interpretability, leading to more accurate and reliable diagnostic tools. These techniques collectively enhance medical decision-making and patient outcomes. [\[44\]](#)

- **Convolutional neural network for medical image analysis**

In the context of deep learning applications for medical image processing, CNNs are indispensable. Their capacity for automated feature extraction enables high performance in

object localization, segmentation, and classification. The hierarchical architecture of CNNs facilitates the identification of intricate patterns, resulting in improved diagnostic precision, increased procedural efficiency, and enhanced patient outcomes. [44] [52]

- **Recurrent neural network techniques for medical image analysis**

RNNs play a crucial role in medical image analysis with deep learning due to their ability to capture temporal dependencies and contextual information. They are particularly effective for tasks involving sequential or time-series data, such as analyzing medical image sequences or dynamic imaging modalities. By modeling long-term dependencies and leveraging information from previous time steps, RNNs facilitate pattern recognition, disease progression prediction, and tumor growth tracking. [44] [43]

- **Generative adversarial network techniques for medical image analysis**

GANs are crucial in medical image analysis because they enable the creation of realistic synthetic images, augment datasets, and eventually improve the precision of diagnoses and analyses. [44] [47]

- **Long short-term memory techniques for medical image analysis**

In medical image analysis, LSTM networks are essential for deep learning applications that require understanding sequential dependencies. Medical images often contain intricate spatial and temporal patterns that demand contextual awareness. As a type of RNN, LSTM excels at modeling these long-range dependencies and temporal dynamics, proving particularly useful for time series analysis, disease progression modeling, and image sequence analysis. By leveraging its memory and gating mechanisms, LSTM can effectively learn and retain pertinent information over time, resulting in more accurate and robust medical image analysis and contributing to better diagnostic outcomes and personalized treatment strategies. [44] [47]

- **Hybrid techniques for medical informatics**

Medical image analysis benefits greatly from hybrid approaches that blend deep learning with other methods. While deep learning excels at tasks like segmentation and classification, it can struggle with limited data or lack of transparency. Hybrid techniques address these issues by integrating traditional machine learning, statistical models, or expert knowledge. Combining diverse data sources, like images and patient reports, further

enhances understanding and improves medical decisions. This leads to more precise and dependable tools for healthcare professionals. [\[10\]](#) [\[44\]](#) [\[9\]](#)

II.5.4 Advantages of Deep Learning in Medical Imaging

Deep learning offers several key advantages for medical image analysis: [\[44\]](#) [\[53\]](#)

- **Automated Feature Extraction:** In contrast to traditional methods that require handcrafted features, deep learning algorithms learn pertinent features directly from data, minimizing human bias and effort.
- **High Accuracy and Robustness:** In many medical imaging tasks, deep learning has surpassed traditional techniques, sometimes attaining performance that is close to or even better than human.
- **Scalability and Generalization:** Deep learning models can effectively generalize across various imaging datasets and medical situations when given enough training data.

II.5.5 Challenges and Limitations

Despite its success, deep learning in medical image analysis faces several challenges: [\[53\]](#)

- **Data Availability and Annotation:** Deep learning models need large, well-annotated medical datasets for training, however collecting such data is frequently challenging because of privacy issues and a lack of expert annotations.
- **Interpretability and Explainability:** Since deep learning models operate as "black boxes," it is challenging to provide an explanation for their choices. Gaining the trust of clinicians in important medical applications requires interpretability.
- **Computing Requirements:** Significant computing resources, such as powerful GPUs and a lot of storage, are needed to train deep neural networks.

II.5.6 Future Directions

Deep learning research for medical image processing is moving forward to more efficient and interpretable models. To improve performance and explainability, methods like self-supervised learning, hybrid models that combine deep learning and rule-based systems (such as DRB classifiers) are being investigated. Federated learning, which enables the decentralized training of deep learning models without exchanging private patient data, is also showing promise as a remedy for privacy issues. Ongoing developments in model

architecture and training techniques are overcoming challenges like interpretability, computing demands, and data availability. Medical image analysis has been revolutionized by deep learning, which makes disease diagnosis quicker, more precise, more automated. Its incorporation with medical imaging has enormous potential to enhance clinical reasoning and, eventually, improve patient outcomes.

II.5.7 CNNs for MRI Brain Tumor Classification

The classification of MRI brain tumors is an intricate task requiring effective representation of spatial, structural, and textural features. CNNs have emerged as a powerful tool in medical image analysis, and several key advantages make them particularly well-suited for MRI brain tumor classification. These include their ability to automatically learn complex, hierarchical features; capture spatial and structural variations within MRI images; outperform traditional methods in classification accuracy; leverage transfer learning to improve performance with limited medical data; and integrate deep learning with handcrafted features. These strengths make CNNs a robust and dependable choice for this task, significantly advancing medical image analysis and enabling more accurate and reliable diagnoses.[\[44\]](#)

As shown in **Figure II-19** CNN is made up of several building blocks called layers. In this subsection, we will provide a detailed analysis of these layers and their roles in the CNN architecture.[\[42\]](#) [\[52\]](#)

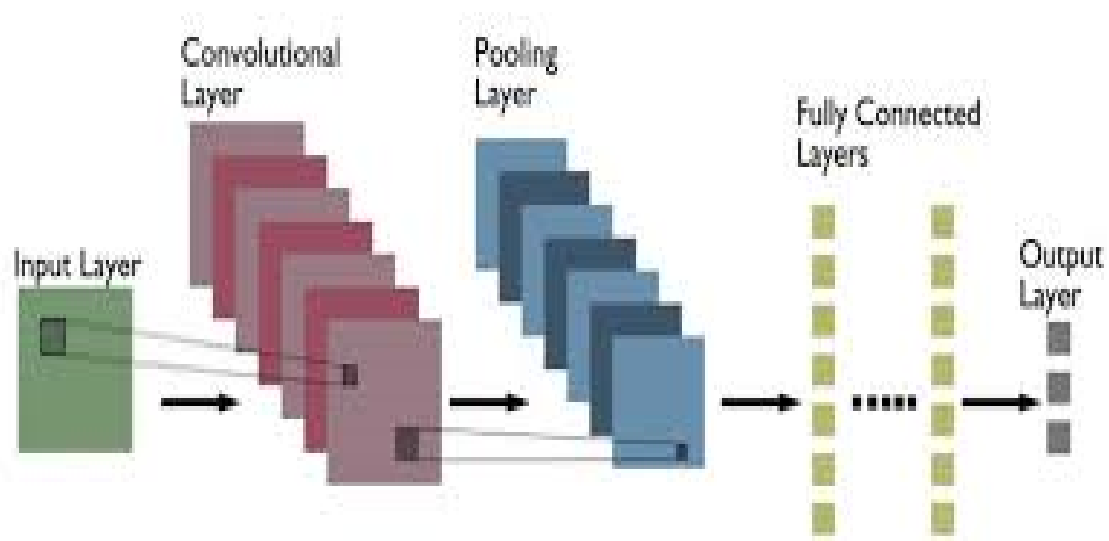


Figure II-19: Representation of Convolutional Networks [\[54\]](#)

II.5.7.1 Input layer

The input layer in CNN must contain data describing the image. Image data is represented by a three-dimensional matrix which generally needs to be reshaped into a single column (vector representation).

II.5.7.2 Convolutional Layer

The convolutional layer is sometimes called a feature extraction layer because image features are extracted in this layer as shown in **Figure II-20** and **Figure II-21**. First, a portion of the image is connected to the Convolutional layer to perform a convolution operation and calculate the dot product between the receptive field (a local region of the input image with the same size as the filter). The result of the operation is a single integer of the output volume. Then, we slide the filter over the next receptive field of the same input image by a stride and repeat the same operation. This operation is repeated by the same process over and over until the entire image is traversed.

- The Convolution layer also contains the ReLU activation so that all negative values are set to zero.

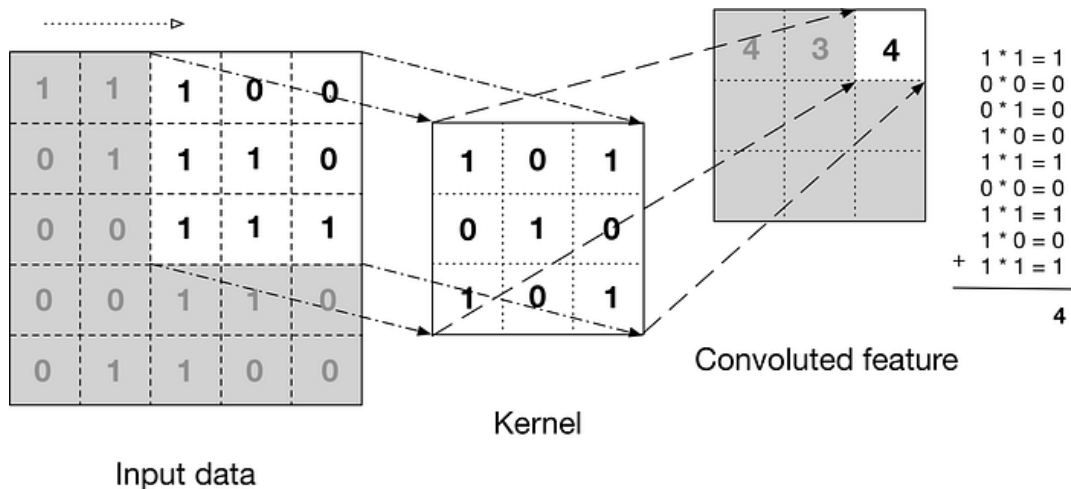


Figure II-20: Convolution Operation [37]

- The convolution layer plays a crucial role in CNNs by extracting relevant features from the input image, allowing the network to perform tasks like image recognition and object detection.

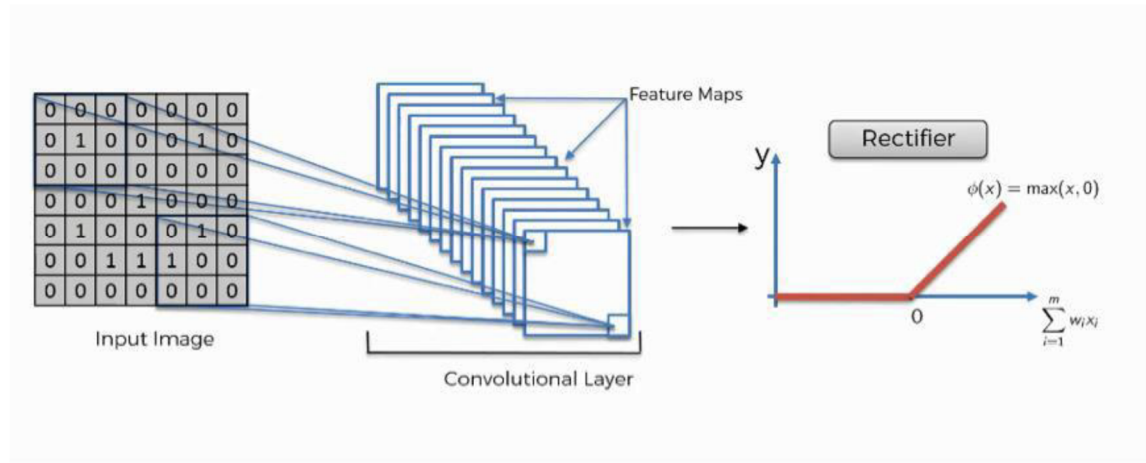


Figure II-21: Convolutional Layer [55]

II.5.7.3 Pooling Layer

Pooling layers are used to down sample the feature maps produced after convolution operations. They take large feature maps and shrink them to smaller sizes, preserving the most important features in each step. The pooling operation is defined by specifying the region size and stride, similar to the convolution operation. It is used between two convolutional layers. If we apply a Fully Connected (FC) layer after the Conv layer without applying pooling or maximum pooling, the computation will be costly. Thus, Different types of pooling techniques are used in various pooling layers, such as max pooling, min pooling, average pooling, gated pooling, and tree pooling. Max pooling is the most popular and commonly used technique as shown in **Figure II-22**.

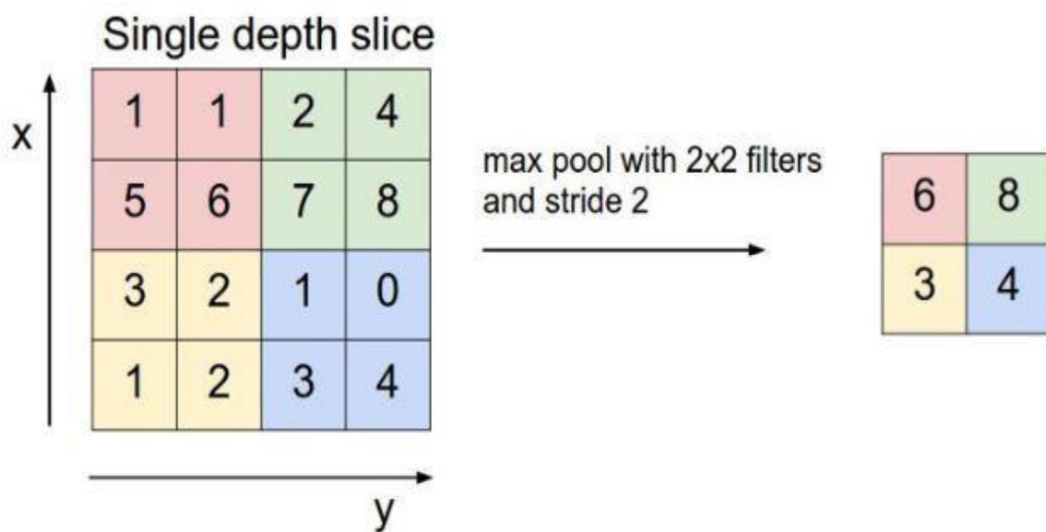


Figure II-22: Example of the Pooling Principle [56]

II.5.7.4 Fully Connected Layer

After several convolutional and max-pooling layers, high-level reasoning in the neural network is done through fully connected layers. They take the features extracted from the convolutional layers and connect them to a single output layer, performing classifications or predictions based on the learned features. Fully-connected layers are a type of feed-forward artificial neural network (ANN) that follow the principles of traditional multi-layer perceptron neural networks (MLP). These layers take input from the final convolutional or pooling layer, which is in the form of a set of matrices (feature maps). These matrices are flattened into a vector, which is then fed into the fully-connected layer to generate the final output of the CNN, as shown in **Figure II-23**.

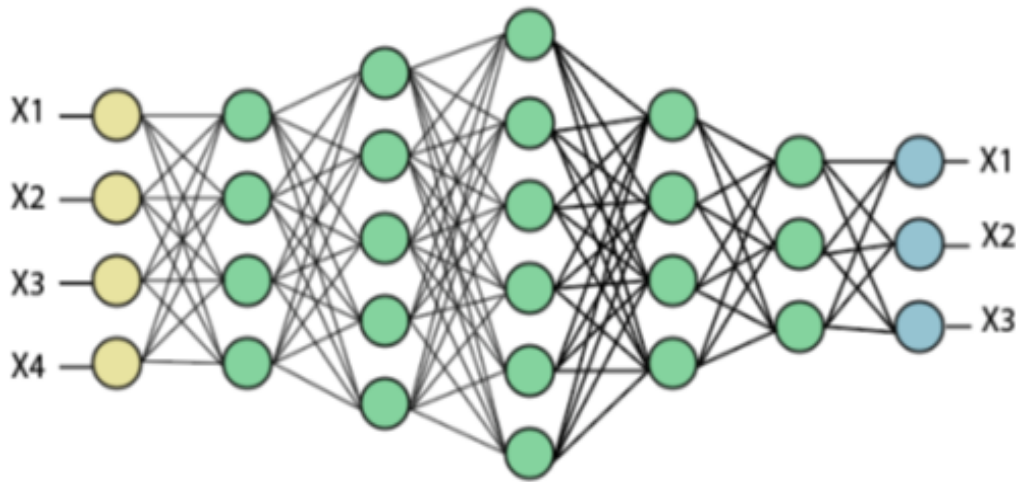


Figure II-23: Fully Connected Layers [30]

II.5.7.5 Logistic or Softmax Layer (LOSS)

The last layer of a CNN is the Softmax or Logistic layer, located at the end of the fully-connected layer. The Logistic layer is used for binary classification, while the Softmax layer is used for multi-class classification.

II.5.7.6 Output Layer: The Final Decision Maker

The output layer is the final layer in a Convolutional Neural Network. It receives the output from the preceding layers and generates the network's final prediction which is typically a classification or regression prediction.

II.6 Performance Evaluation Measurements

Evaluation metrics are crucial in assessing the performance of a deep learning algorithm. They provide a quantitative measure of a model's ability to generalize to new, unseen data. For classification tasks, these metrics can reveal the accuracy of predictions and the number of correct or incorrect predictions. Common metrics for such tasks include the confusion matrix (which visualizes classification performance and aids in calculating other metrics), accuracy, precision, recall (sensitivity), F1-score, specificity, and Receiver Operating Characteristic (ROC) curves .[57] [58]

II.6.1 Confusion Matrix

The confusion matrix, presented in **Table II.2** provides a summary of classification results, showing the number of correct and incorrect predictions for each class. The terms used in a confusion matrix and other evaluation metrics include true positives (TP), true negatives (TN), false positives (FP), and false negatives (FN). True positives are instances correctly identified as positive, while false positives are negatives incorrectly identified as positive. True negatives are correctly identified as negative, and false negatives are positives incorrectly identified as negative.[57] [59]

Table II.2: Confusion matrix

Expected outcome	Ground truth	
	Positive	Negative
Positive	TP	FP
Negative	FN	TN

II.6.2 Accuracy

Accuracy measures the proportion of instances correctly classified as either positive or negative out of the total number of instances. It is calculated by **Equation (II.1)**

$$\text{Accuracy} = \frac{\text{TP} + \text{TN}}{\text{TP} + \text{TN} + \text{FP} + \text{FN}} \quad (\text{II.1})$$

II.6.3 Sensitivity

Sensitivity, also known as recall or true positive rate, measures the proportion of actual positive instances that are correctly identified by the model. It is calculated by **Equation (II.2)**.

$$\text{Sensitivity} = \frac{TP}{TP+FN} \quad (\text{II.2})$$

II.6.4 Specificity

Specificity, also known as the true negative rate, measures the proportion of actual negative instances that are correctly identified by the model. It is calculated by **Equation (II.3)**.

$$\text{Specificity} = \frac{TN}{TN+FP} \quad (\text{II.3})$$

II.6.5 F1-score

F1-score is the harmonic mean of precision and recall and can be calculated by **Equation (II.4)**.

$$F1 - score = 2 \times \frac{\text{Precision} \times \text{Recall}}{\text{Precision} + \text{Recall}} \quad (\text{II.4})$$

II.6.6 ROC curve

The Receiver Operating Characteristic (ROC) curve is a graphical tool used to assess the performance of a classification model. It plots the True Positive Rate (sensitivity) against the False Positive Rate (1 - specificity) at various threshold settings. The ROC curve illustrates the balance between sensitivity and specificity for different thresholds.

The Area Under the ROC Curve (AUC) is a single value that summarizes the model's performance. An AUC of 1 indicates perfect classification, while an AUC of 0.5 suggests the model performs no better than random guessing. **Figure II-24** provides an illustration of a ROC curve.[\[58\]](#) [\[59\]](#)

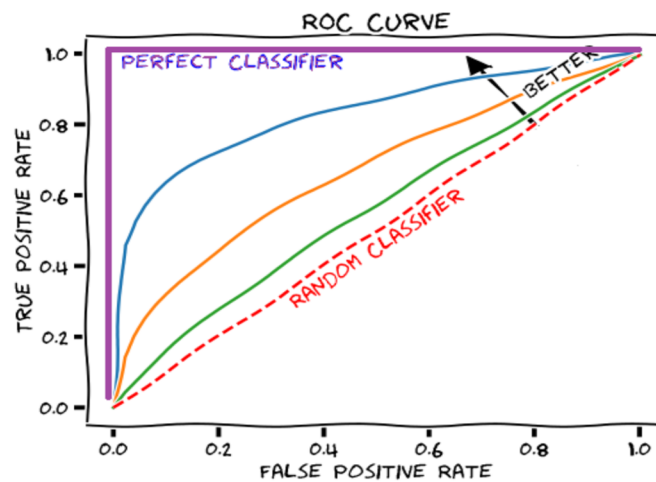


Figure II-24: Roc Curve [\[60\]](#)

II.7 Conclusion

This chapter provided a comprehensive overview of the theoretical foundations and methodologies employed in this study. It began by introducing the fundamental concepts of Artificial Intelligence, Machine Learning, and Deep Learning, emphasizing their relevance in medical image analysis. A detailed discussion of machine learning techniques, including supervised, unsupervised, and reinforcement learning, highlighted the different approaches to pattern recognition and decision-making.

The chapter then explored deep learning, covering its historical development, key architectures, and essential components, such as neurons, activation functions, and artificial neural networks. Various deep learning models, including CNNs, RNNs, LSTMs, and GANs, were examined, with a particular focus on CNNs due to their effectiveness in processing and analyzing medical images.

A dedicated section addressed the impact of deep learning in medical image analysis, showcasing its applications, advantages, and challenges. In particular, the role of CNNs in MRI brain tumor classification was detailed, explaining the functionality of each layer in the CNN pipeline.

Finally, the chapter concluded with an overview of performance evaluation metrics used to assess the effectiveness of classification models, including accuracy, sensitivity, specificity, F1-score, and the ROC curve. These metrics will be instrumental in analyzing and comparing the results obtained in subsequent experiments.

The insights and methodologies discussed in this chapter serve as a foundation for the experimental work that follows, ensuring a systematic approach to MRI brain tumor classification using deep learning techniques.

Chapter III

Brain Tumor Classification

III.1 INTRODUCTION.....	45
III.2 TAXONOMY OF MRI BRAIN IMAGE CLASSIFICATION ALGORITHMS.....	45
III.3 CLASSIFICATION PROCESS	48
III.3.1 PRE-PROCESSING STEP.....	49
III.3.2 FEATURE EXTRACTION STEP	49
III.3.3 CLASSIFICATION STEP:	53
III.4 OVERVIEW OF BRAIN TUMOR CLASSIFICATION	58
III.4.1 MACHINE LEARNING TECHNIQUES	58
III.4.2 DEEP LEARNING TECHNIQUES	59
III.5 DEEP RULE BASED CLASSIFIER FOR MRI BRAIN TUMOR CLASSIFICATION.....	60
III.5.1 GENERAL ARCHITECTURE OF THE DRB CLASSIFIER.....	60
III.5.2 MASSIVELY PARALLEL FRB	62
III.6 CONCLUSION	67

Chapter III : Brain Tumor Classification

III.1 Introduction

Magnetic Resonance Imaging is a powerful diagnostic tool widely used in the detection and characterization of brain tumors. The complex nature of brain tumor detection and classification necessitates the use of advanced computational techniques to assist radiologists in achieving accurate and timely diagnoses. Among these techniques, machine learning has emerged as a transformative approach, offering significant improvements over traditional methods in terms of accuracy, speed, and robustness.

Recent advancements in machine learning, particularly the rise of deep learning, have further enhanced the capabilities of brain tumor detection systems. Deep learning models, such as convolutional neural networks, have shown exceptional performance in image analysis tasks due to their ability to automatically learn hierarchical features from raw data. These models have been applied to MRI brain tumor detection with remarkable accuracy, outperforming traditional machine learning methods.

In this chapter, we delve into the various deep learning methodologies applied to MRI brain tumor detection. We explore the evolution of these techniques, their comparative performance, and the ongoing challenges that drive future research. We aim to provide a comprehensive overview of the state-of-the-art in deep learning applications, highlighting their transformative impact on brain tumor diagnostics.

III.2 Taxonomy of MRI Brain Image Classification Algorithms

The process of brain tumor detection and classification can be categorized into various methodological approaches. These include classical image processing techniques, machine learning algorithms, and more recently, deep learning methods. Each category encompasses a range of techniques and models designed to improve the accuracy and efficiency of tumor detection. The taxonomy presented in **Figure III-1** aims to provide a comprehensive overview of the various methods used in MRI brain tumor detection and classification. By categorizing and comparing classical image processing, machine learning, and deep learning techniques, we seek to highlight the evolution of this field and the strengths and limitations of each approach as shown in **Table III.1**. Understanding these methodologies will not only aid in selecting the appropriate techniques for specific clinical applications but also pave the way for future research and development in automated brain tumor detection systems.

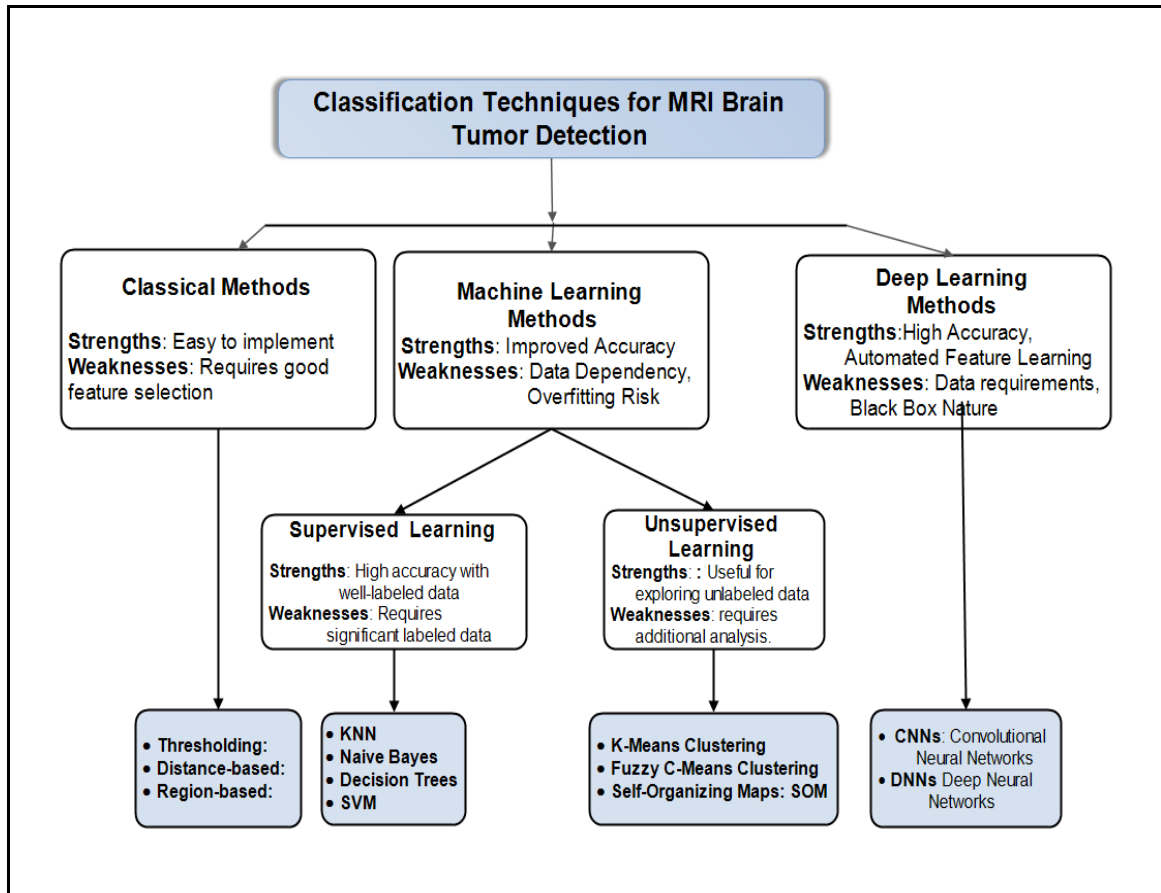


Figure III-1: Taxonomy of MRI Brain Tumor Classification Techniques

Classical Methods use simple techniques: thresholding isolates high-intensity regions, distance-based methods find similar patterns, and region-based methods segment structures but depend on good feature selection.

Supervised Machine Learning methods (e.g., KNN, Naive Bayes, Decision Trees, SVM) perform well with labeled data, balancing simplicity, interpretability, and scalability, but may face issues like overfitting or computational demands.

Unsupervised Machine Learning methods (K-means, Fuzzy C-Means, Self-Organizing Maps (SOM)) cluster data without labels, revealing natural patterns but requiring additional steps for interpretation.

Deep Learning methods, especially Convolutional Neural Networks (CNNs) and Deep Neural Networks (DNNs), demonstrate strong performance in MRI brain tumor classification by automatically learning spatial and hierarchical features. However, these models demand significant computational resources and are often seen as "black boxes" with limited interpretability, making them resource-intensive and challenging for clinicians to understand without further refinement.

Table III.1 serves as a guide to the different classification techniques, providing a basis for selecting the most appropriate method for MRI brain tumor analysis depending on resource constraints, interpretability needs, and dataset characteristics.

Table III.1: MRI Brain Tumor Classification Techniques

Category	Algorithm	Strengths	Weaknesses
Classical Methods	Thresholding	Isolates high-intensity regions	Lacks nuance
	Distance-based	Identifies similar patterns	Might miss subtle differences
	Region-based	Segments brain structures	Requires good feature selection
Machine Learning (Supervised)	KNN	Easy to implement, good for small datasets	Computationally expensive for large datasets
	Naive Bayes	Efficient for large datasets	Struggles with complex relationships
	Decision Trees	Handles mixed data, interpretable	Prone to overfitting
	SVM	Effective for high-dimensional data	Complex parameter tuning
Machine Learning (Unsupervised)	K-means Clustering	Identifies similar brain regions	Requires further investigation for class labels
	Fuzzy C-Means Clustering	More flexibility than K-means	Challenging interpretation
	SOM	Visualizes relationships, good for anomaly detection	Doesn't provide class labels directly
Deep Learning	CNN	Highly successful, learns spatial features	Computationally expensive, black box
	DNN	Powerful for complex tasks	Requires significant resources and expertise

III.3 Classification Process

Magnetic resonance imaging has become an essential tool for the diagnosis and monitoring of brain pathologies. With its ability to produce detailed images of brain anatomy, MRI allows for the visualization of a wide range of abnormalities, including tumors, strokes, infections, and neurodegenerative diseases. The analysis and classification of brain MRI images play a crucial role in interpreting data and establishing accurate diagnoses.

Brain MRI classification involves identifying and categorizing the different structures and abnormalities present in the images. This process typically involves several steps as shown in **Figure III-2**.

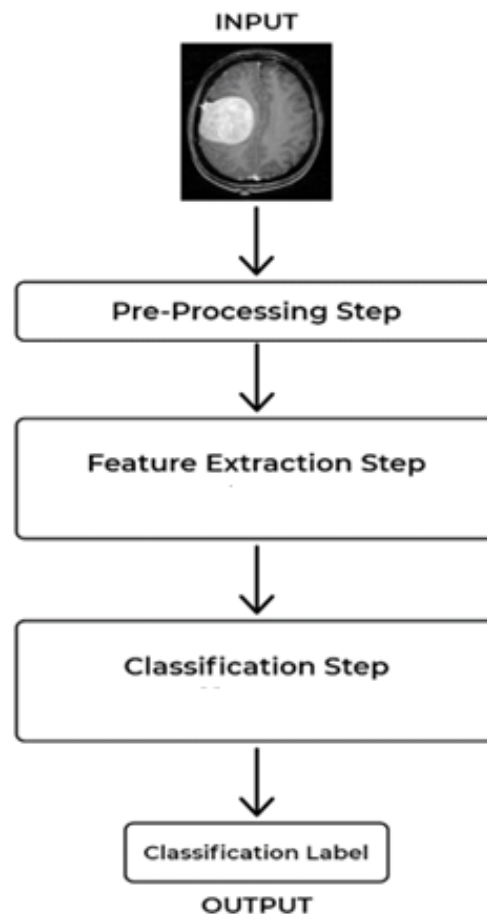


Figure III-2 Classification Process

III.3.1 Pre-processing step

The preprocessing step plays an important role in improving the quality of the image that leads to achieving better results in feature extraction and classification steps. It consists of fundamental pre-processing techniques such as binarization, normalization, rotation, resizing, and removal of undesired parts of MR images. Common preprocessing steps include :

- **Intensity Normalization:** MRI scans can exhibit variations in intensity due to scanner differences or acquisition protocols. Normalization techniques like scaling or histogram matching rectify these variations.
- **Skull Stripping:** This process removes the non-brain tissue (skull) from the MRI image, focusing analysis on the brain region of interest.
- **Noise Reduction:** MRI scans can be susceptible to noise caused by various factors. Techniques like filtering are employed to minimize noise and enhance image clarity.
- **Co-registration:** When using multiple MRI sequences, co-registration ensures their spatial alignment, allowing accurate feature extraction across modalities.

III.3.2 Feature extraction step

Feature extraction is also a vital step in the classification process. It consists of finding the most significant characteristics from the original data in order to improve the overall efficiency of the system.

Feature extractors can be categorized based on the information they capture. Intensity-based extractors provide basic statistics of pixel values. Textural extractors, like GLCM (Gray Level Co-occurrence Matrix), delve deeper to analyze the spatial arrangement of intensities, reflecting the tumor's texture. Morphological extractors focus on the tumor's shape and size. Finally, advanced techniques like Gabor filters or deep learning can capture intricate patterns within the image data. By strategically combining features from different categories, a comprehensive tumor representation can be achieved, potentially leading to superior classification accuracy [61]. **Figure III-3** provides a taxonomy for understanding the various types of feature extractors used in MRI brain tumor classification. Selecting the appropriate extractors and combining them effectively is crucial for building robust and accurate machine learning models for this critical medical application.

This section explores various feature extraction methods investigated in this research.

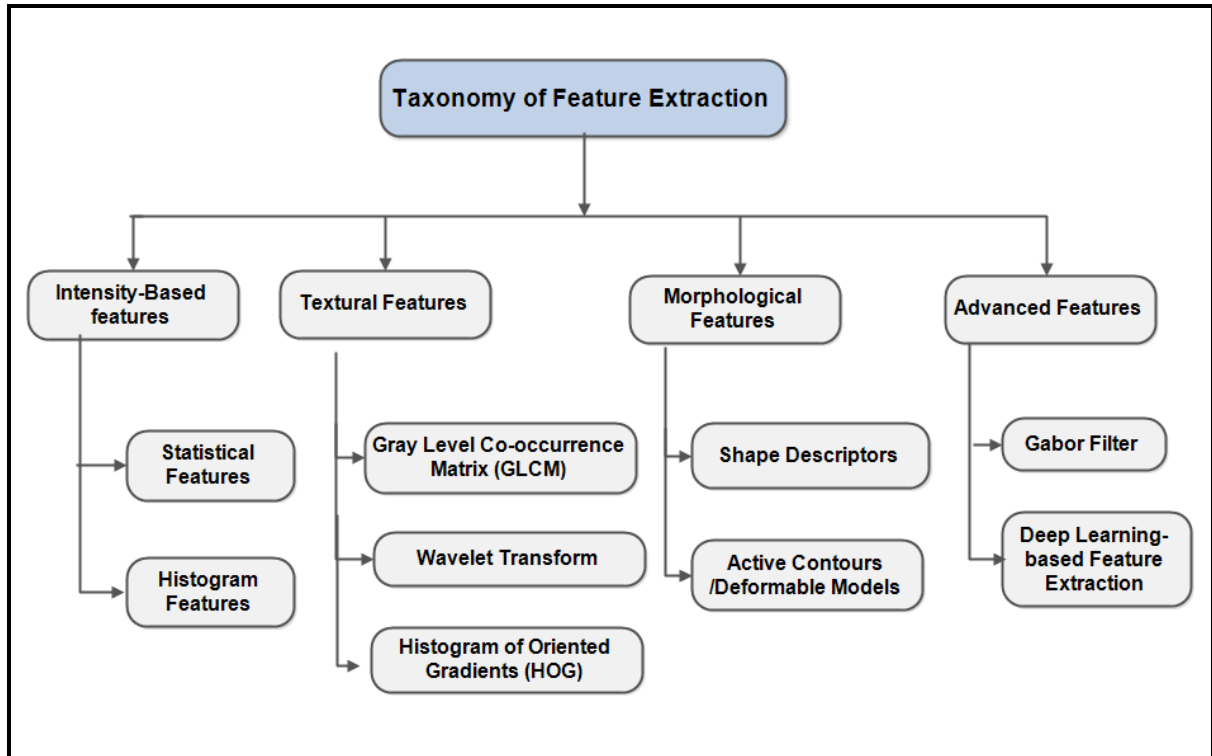


Figure III-3: Taxonomy of feature extraction used in MRI Brain Tumor Detection

III.3.2.1 Binarized Statistical Image Features (BSIF)

BSIF falls under the category of Statistical Feature Extractors but with a twist. Traditional statistical features directly analyze intensity values. BSIF, however, takes a more elaborate approach [62]:

- **Learns a statistical basis:** It utilizes techniques like Independent Component Analysis (ICA) to learn a set of basis vectors that capture the statistical properties of natural images.
- **Projects image patches:** small image regions (patches) around each pixel are projected onto this learned basis.
- **Binarizes the projections:** The resulting projection values are then thresholded, converting them into binary codes (0s and 1s).
- **Histogram representation:** Finally, a histogram is constructed to capture the frequency of these binary codes across the image.

Therefore, BSIF leverages statistical learning to create a novel feature representation based on intensity variations within local image patches [63].

III.3.2.2 Histogram of Oriented Gradients (HOG)

The HOG descriptor [64] is one of the most widely used methods for feature extraction in localized image regions, leveraging histograms of gradient orientations. The process for constructing the HOG feature vector involves several steps:

1. **Calculate the gradients of the image.** This can be done using a variety of filters, such as the Sobel filter or the Laplacian filter.
2. **Divide the image into cells.** The cells are typically 8x8 pixels in size.
3. **Calculate the histogram of oriented gradients for each cell.** For each cell, calculate the magnitude and orientation of the gradients at each pixel. Then, bin the gradients into a certain number of orientation categories. The histogram of oriented gradients for a cell is the count of gradients in each orientation category.
4. **Normalize the histograms.** This is done to ensure that the histograms are not affected by the overall brightness of the image.
5. **Concatenate the histograms together to form the final HOG descriptor.** The final HOG descriptor is a vector of numbers that represents the distribution of oriented gradients in the image.

HOG descriptors, as shown in **Figure III-4** are used in a variety of computer vision applications, such as object detection, image classification, and image matching.

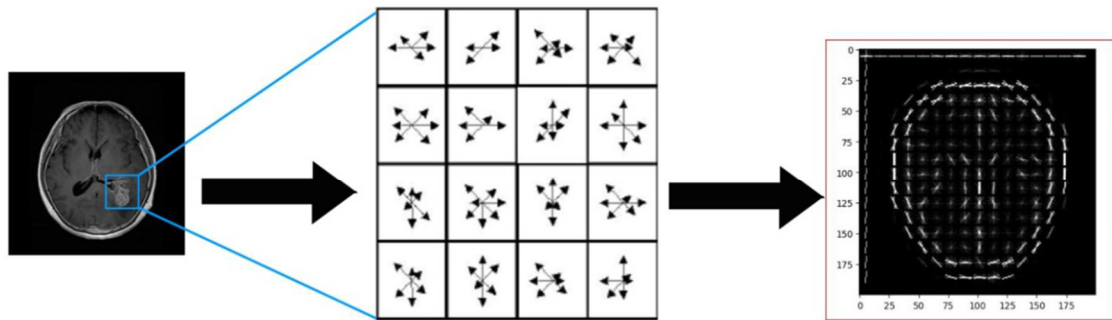


Figure III-4: HOG descriptor [64]

III.3.2.3 GIST Descriptor: A Low-Dimensional Image Representation

The GIST descriptor [65], is an image descriptor that relies on a low-dimensional representation known as the Spatial Envelope. It captures the dominant spatial structure of an image through a set of statistical attributes, including naturalness, openness, roughness, expansion, and robustness. GIST encapsulates gradient information, such as scales and orientations, for different regions of the image, providing a high-level approximation of its structure.

To extract the GIST features, the input grayscale image is first normalized by adjusting its intensity and local contrast. The image is then divided into a grid spanning multiple scales. For each cell in the grid, a set of Gabor filters is applied, and the resulting responses are combined to form the final feature vector. This process offers a compact and efficient summary of the image's spatial properties.

III.3.2.4 AlexNet

AlexNet, introduced by Krizhevsky et al., presented in **Figure III-5** [66], was the first CNN to win the ImageNet challenge in 2012, with a top 5 error of 16.4%. The use of rectified linear units (ReLUs) was also introduced in AlexNet. It includes five convolutional layers, three max pool layers, and three fully connected layers. This architecture uses a $[227 \times 227 \times 3]$ image as an input. In AlexNet, a 4096-dimensional feature vector represents the 227×227 image [67], [68].

III.3.2.5 VGG-16

The VGG (Visual Geometry Group) Net presented in **Figure III-6**, introduced by Simonyan and Zisserman [69], is a convolutional neural network (CNN) that gained prominence as one of the top-performing models in the ILSVRC-2014 (ImageNet Large Scale Visual Recognition Competition) for image classification. VGG Net was trained on the ImageNet dataset, which consists of over 14 million images across 1000 classes, with 1.3 million images for training, 50,000 for validation, and 100,000 for testing. The model achieved an impressive accuracy of 92.7% on the ImageNet dataset.

The input to the VGG Net must be an RGB image of size 224×224 . These images are passed through multiple convolutional layers, each with a fixed filter size of 3×3 and a stride of 1. The VGG-16 architecture, in particular, includes five max-pooling layers integrated within a series of convolutional layers, followed by three fully connected layers. The first two fully connected layers contain 4096 channels, while the third has 1000 channels, corresponding to the number of output classes. The final layer is a softmax layer, used for classification. [70]

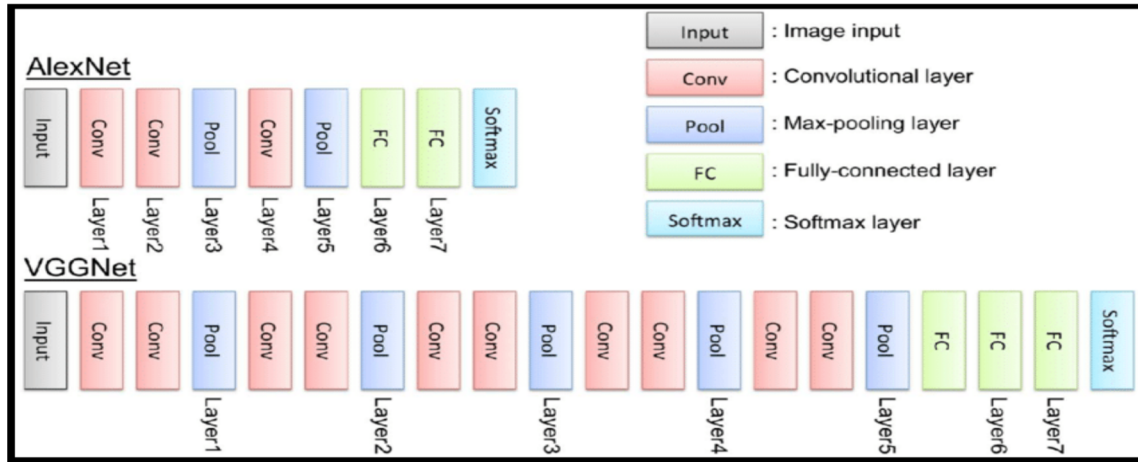


Figure III-5: VGG and Alexnet Architecture [71]

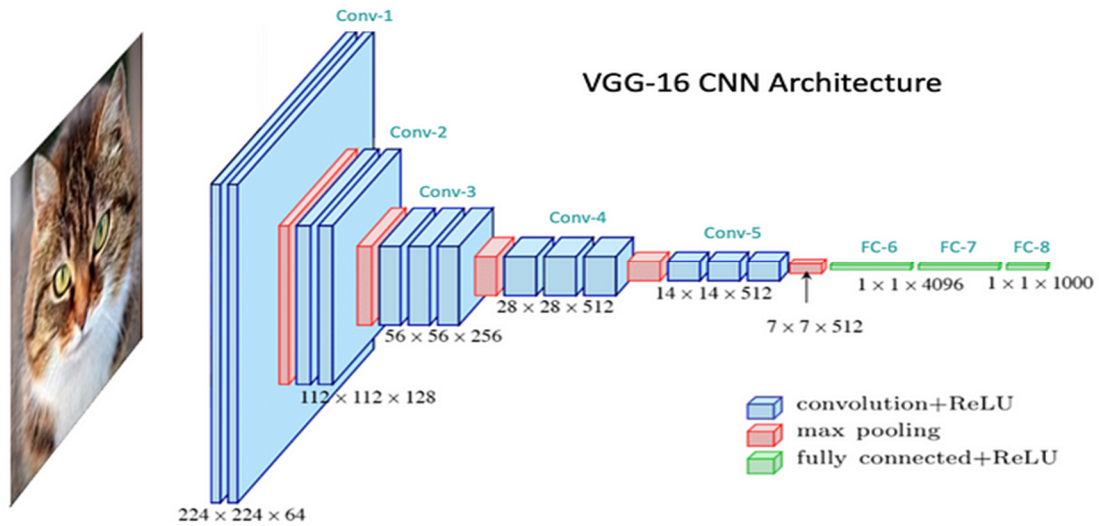


Figure III-6: VGG-16 CNN Architecture [69]

III.3.2.6 Residual Network (ResNet-50 and ResNet-18)

ResNet was proposed by He et al. [70], and it revolutionized CNN architecture by introducing the concept of residual learning in convolutional neural networks. This innovation provided an efficient methodology for training deep networks. ResNet introduced a deep CNN with 152 layers, which won the 2015 ILSVRC competition. The ResNet block architecture, 20 and 8 times deeper than AlexNet and VGG respectively, was one of the first to adopt batch normalization. Despite its depth, ResNet demonstrated lower computational complexity compared to previously proposed networks. [70] [72].

III.3.3 Classification step:

There exist several techniques for classification of data such as fuzzy clustering means (FCM), support vector machine (SVM), and artificial neural network (ANN).

Motivated by the high classification accuracy achieved by the DRB classifier in [73], we explore it for the classification of MRI brain tumors.

III.3.3.1 Naive Bayes

The Naive Bayes classifier is a probabilistic supervised algorithm that assumes the presence of a feature for a class, as showed in **Figure III-7**, is independent of the presence of other features, which is why it is described as "naive". For example, a person may be classified as a man based on their weight and height. Even though these characteristics are correlated in reality, a naive Bayes classifier treats them independently when making its classification.

Despite its extremely simplistic assumptions, this classifier delivers very good results in many complex real-world scenarios. In 2004, a study provided theoretical reasons behind this unexpected effectiveness [74]. However, a 2006 study showed that more recent methods (such as boosted trees and random forests) produce better results [75].

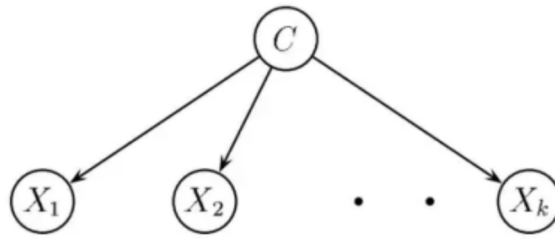


Figure III-7: The Naive Bayes classifier [75]

Naive Bayes algorithm offers good performance, but the predictions become inaccurate if the assumption of conditional independence is invalid.

III.3.3.2 K-Nearest Neighbor

The K-Nearest Neighbors (KNN) algorithm is a supervised classification algorithm. Each observation in the training set is represented by a point in an n -dimensional space, where n is the number of predictive variables. To predict the class of a new observation, the algorithm identifies the k closest points to this example. The class of the target variable is determined by the most represented class among the k nearest neighbors. Variants of the algorithm exist where the k observations are weighted based on their distance to the example being classified, with more distant observations considered less important. Example of classification with KNN is shown in **Figure III-8**. [76]

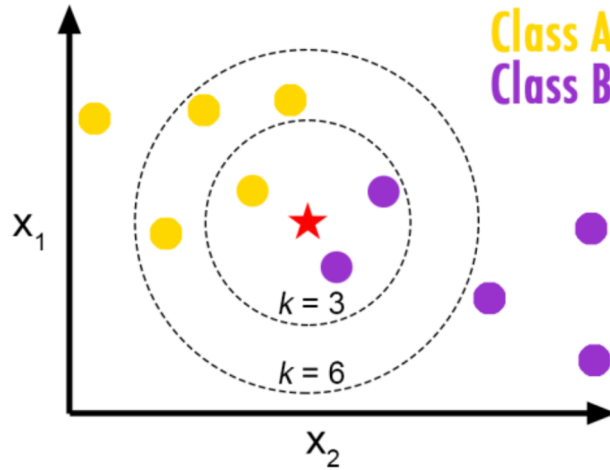


Figure III-8: Example of classification with KNN [77]

- **Advantages:** simple to design.
- **Disadvantages:** sensitive to noise, for a large number of predictive variables, the distance calculation becomes very costly.

III.3.3.3 Support Vector Machine (SVM)

Support Vector Machines [78] are very powerful non-linear binary classification algorithms. The principle of SVMs involves constructing a non-linear separating margin of maximum width that separates two sets of observations and using it to make predictions [79]. SVMs are classifiers based on two key ideas:

1. The first idea, in the case where the problem is linearly separable as shown in **Figure III-9** is to find a linear separator with maximum width, which is the concept of the maximum margin. The margin is the distance between the separating boundary and the closest samples, known as support vectors.

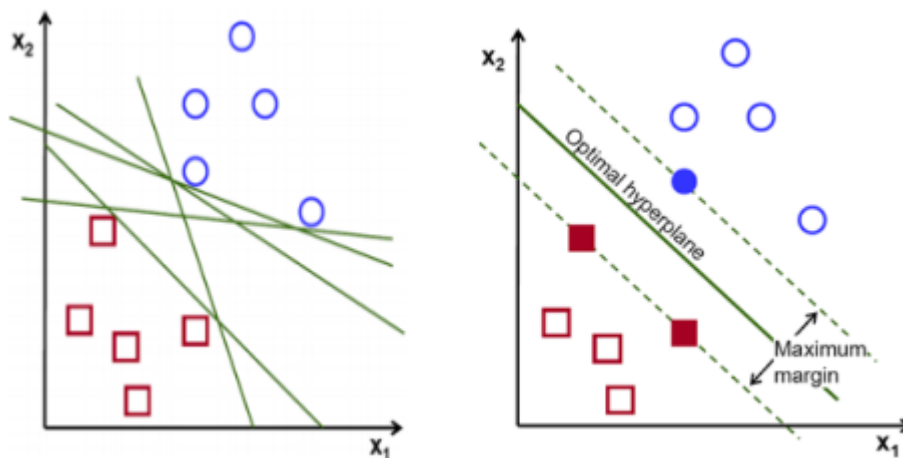


Figure III-9: Hyper plan of SVM classifier [80]

The problem is to find this optimal separating boundary. To solve this problem, there is a unique optimal hyperplane, defined as the hyperplane that maximizes the margin between the samples and the separating hyperplane.

2. To handle cases where data are not linearly separable, as shown in the example presented in **Figure III-10**, the second key idea of Support Vector Machines is to transform the input data representation space into a higher-dimensional space where a linear separation is more likely to exist. This is achieved using a kernel function, which must satisfy Mercer's theorem conditions and has the advantage of not requiring explicit knowledge of the transformation to be applied for the change of space. Kernel functions allow the transformation of a dot product in a high-dimensional space, which is computationally expensive, into a simple pointwise evaluation of a function. This technique is known as the kernel trick.

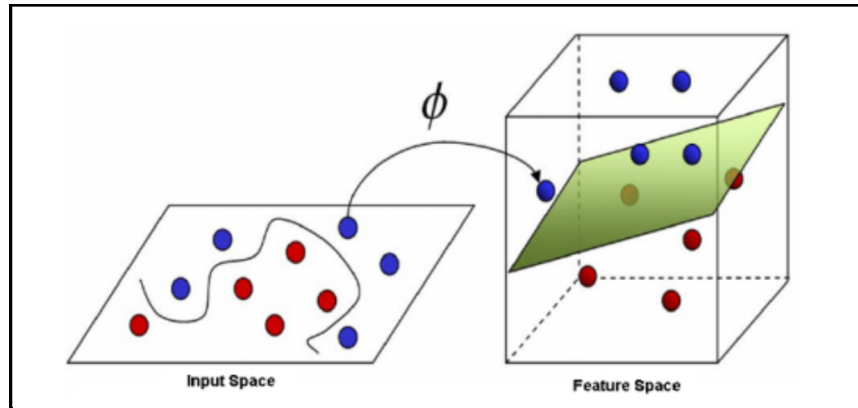


Figure III-10: Example of a non-linearly separable problem.[80]

Advantages of SVM:

- SVM can be used for both classification and regression tasks. They can also handle non-linear data by using kernel functions to transform the input space.
- SVMs are an alternative to neural networks because they are easier to train.

Disadvantages:

- Training an SVM can be computationally intensive, especially with large datasets. The algorithm's complexity and speed during the training process can be quite high.
- The performance of SVM is heavily dependent on the choice of kernel and the kernel parameters. Finding the best combination often requires extensive experimentation and cross-validation.
- SVMs can struggle with datasets where the classes overlap significantly. It's less effective when the classes are not well separated.

III.3.3.4 Decision Trees

Decision trees are supervised ML models that can be used for both classification and regression. A decision tree represents a function that takes an attribute vector as input and returns a decision, which is a single value. The inputs and outputs can be discrete or continuous. A decision tree makes decisions by executing a sequence of tests. Each internal node of the tree corresponds to a test of an attribute's value, and the branches coming out of the node represent the possible values of the attribute. The class of the target variable is determined by the leaf node reached by the observation after the sequence of tests. The learning phase consists of finding the right sequence of tests. For this, the right attributes must be chosen. A good attribute divides the examples into homogeneous sets, meaning they contain only observations belonging to the same class, while a useless attribute leaves the examples with almost the same proportion of values for the target variable. An example of a decision tree is illustrated in **Figure III-11**.

What is needed is a formal measure of "good" and "useless." For this, there are standard homogenized metrics to measure the homogeneity of a set. The most well-known are the Gini diversity index and entropy [81] [82].

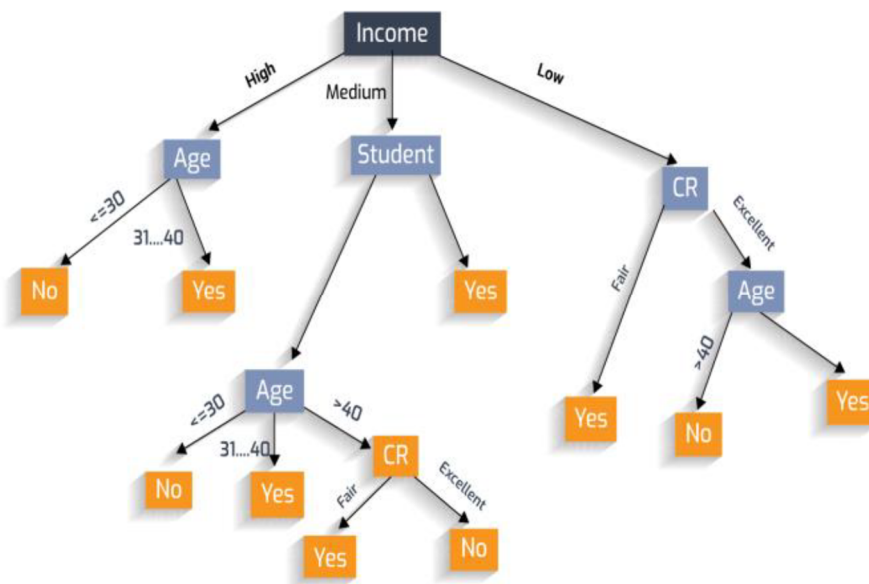


Figure III-11: Example of Decision Tree [82]

Advantages:

- It is a white-box model, simple to understand and interpret.
Requires little data preparation.
- The input predictive variables can be both qualitative and quantitative.
- Performs well on large datasets.

Disadvantages:

- There is a risk of overfitting if the tree becomes very complex. Pruning procedures are used to address this issue.
- Small changes in the data can result in a completely different tree being generated, leading to high variance in predictions.

III.4 Overview of Brain Tumor Classification

Numerous studies have investigated the classification of MRI brain images using machine learning and deep learning techniques. **Table III.2** provides a chronological summary of significant research works in this domain, highlighting each study's key features, classification methods, and achieved accuracy.

Table III.2: Summary of prior works on MRI brain tumor and classification system

Year	Authors	Features	Methods	Accuracy
2020	Badža <i>et al.</i> [2]	CNN	CNN	96.56%.
2018	Shree <i>et al.</i> [83]	Discrete wavelet Transformation (DWT)	PNN	100%
2015	Cheng <i>et al.</i> [5]	Intensity histogram, Gray Level Co-occurrence Matrix (GLCM), and Bag-of-Words (BoW) model	SVM	91.14%
2015	Zhang <i>et al.</i> [84]	Wavelet Packet Tsallis Entropy (WPTE),	FSVM	99.49%
2017	Bahadure <i>et al.</i> [85]	Berkeley Wavelet Transformation (BWT)	SVM	96.51%.
2012	Y. Zhang <i>et al.</i> [86]	Wavelet transform (WT) followed by Principal Component Analysis (PCA)	KSVM	99.38%
2017	Usman <i>et al.</i> [87]	Wavelet Texture Features	Random forest classifier	95.00%
2018	Ari <i>et al.</i> [88]	Convolutional Neural Network (CNN)	ELM-LRF	97.18%
2018	Byale <i>et al.</i> [89]	Grey Level Co-occurrence Matrix GLCM	ANN	93.33%.

III.4.1 Machine Learning Techniques

In the context of medical imaging, machine learning has demonstrated significant potential, particularly in the analysis of MRI brain images. Traditional machine learning

techniques such as Fuzzy Clustering Means (FCM), K-Nearest Neighbors (KNN), and Support Vector Machines (SVM) have been employed to detect and classify brain tumors, offering promising results. Here are some examples of methods utilizing machine learning:

- Zhang et al. [84] proposed a method using wavelet packet Tsallis entropy (WPTE) for feature extraction and fuzzy SVM for brain abnormality detection.
- Bahadure et al. [85] achieved 96.51% accuracy in classifying healthy and infected tissues using SVM with features extracted by Berkeley Wavelet Transformation (BWT).
- Y. Zhang et al. [86] developed an automatic classification method for MRI brain images using a kernel support vector machine (KSVM) and wavelet transform (WT) features, with Principal Component Analysis (PCA) to reduce feature size.
- Usman et al. [87] investigated the use of wavelet texture features with a random forest classifier to predict tumor labels in a multiclass classification scenario.
- Cheng et al. [5] focused on classifying three specific tumor types using a combination of feature extraction methods and bag-of-words for improved accuracy.

III.4.2 Deep Learning Techniques

The application of deep learning in MRI brain tumor detection encompasses a variety of architectures and techniques. Convolutional Neural Networks (CNNs), for instance, have been extensively used for their ability to capture spatial hierarchies in images. Here are some examples of methods utilizing deep learning:

- Ari et al. [88] designed a method using extreme learning machines for classifying tumors as benign or malignant, achieving 97.18% accuracy.
- Shree et al. [83] achieved near-perfect accuracy using discrete wavelet transformation for feature extraction and a probabilistic neural network for classification.
- Byale et al. [89] proposed a binary classification system using neural networks with features extracted from Gray Level Co-occurrence Matrix (GLCM), achieving 93.33% accuracy.
- Badža et al. [2] presented a new convolutional neural network (CNN) architecture specifically designed for brain tumor classification from imbalanced datasets, achieving 96.56% accuracy.

Recent advancements in deep learning have facilitated significant improvements in the accuracy and robustness of tumor detection models. These models not only assist in

distinguishing between tumor and non-tumor regions but also contribute to the classification of tumor types, aiding in the development of personalized treatment plans. Moreover, the ability of deep learning models to generalize across different datasets and imaging conditions underscores their potential for widespread clinical adoption.

III.5 Deep Rule Based Classifier for MRI Brain Tumor Classification

Deep learning, particularly deep convolutional neural networks (DCNNs), has gained significant popularity due to advances in computational resources.[90][76] DCNNs have shown high accuracy in various image processing tasks such as handwritten digit recognition [91], object recognition [92], human action recognition, and more [93]. Despite their success, DCNNs have limitations: they require large amounts of training data, lack transparency, involve complex decisions on structure, have limited parallelization, and struggle with uncertainty and unseen classes.

In contrast, traditional fuzzy rule-based (FRB) systems are efficient at handling uncertainties and offer transparent, interpretable structures. Recent data-driven FRB classifiers can autonomously learn from data but still lag behind deep learning classifiers in performance.

The Deep Rule-Based (DRB) system is a new approach, combining FRB systems with the multi-layer structure of deep learning. The DRB system employs a massively parallel set of 0-order fuzzy rules and self-organizes a transparent IF-THEN structure. Its training process is fully autonomous, online, non-iterative, and non-parametric, starting classification from the first image and self-evolving with new data, making it suitable for real-time applications.

The DRB approach is simpler and entirely data-driven compared to DCNNs, performing highly accurate classification without the need for accelerated hardware. It is faster, non-parametric, and highly parallelizable. The DRB system can be easily adapted for various classification and prediction problems, offering a human-interpretable, self-evolving structure.

III.5.1 General Architecture of the DRB Classifier

The general architecture of the DRB classifier is illustrated in **Figure III-12**. As depicted, the DRB approach consists of the following layers:

1. Pre-processing block;
2. Feature extraction layer;
3. Massively parallel ensemble of highly interpretable IF...THEN... rules;
4. Decision-maker.

The preprocessing step is crucial for enhancing image quality, leading to improved results in feature extraction and classification. It involves fundamental techniques such as binarization, normalization, rotation, resizing, and removing unwanted parts of MRI images.

For the feature extraction layer, the DRB classifier can utilize various types of feature descriptors commonly used in computer vision.

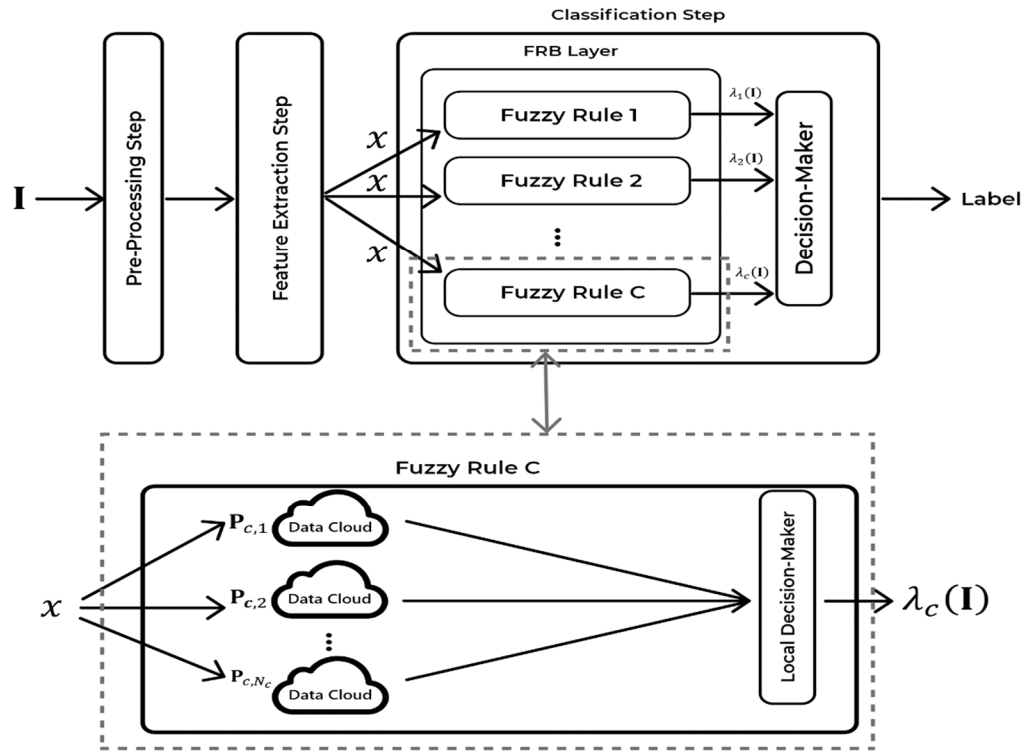


Figure III-12: General Architecture of the DRB Classifier

The DRB block is composed of two main sections. The first section forms the foundation of the DRB classifier during the training phase. It consists of a set of parallel IF...THEN rules based on self-developed FRB models, specifically the AnYa type. These non-parametric rules do not require the definition of a membership function [94][95]. Instead, they are derived from data patterns using the concept of Empirical Data Analytics [96]. Each fuzzy rule, as shown in Table III.3, takes the form of a disjunction (logical OR) between multiple fuzzy sets, which are determined by several prototypes representing the most characteristic data clusters.

The second section serves as the decision-maker during the validation phase. This process employs a "winner-takes-all" strategy to assign the label of the winning class. The final decision is made by a local decision-maker, based on the outcomes [97], [98]. For greater clarity, key notations and their definitions are provided in **Table III.3**.

Table III.3: Key Notation Descriptions of the DRB Classifier

Notations	Description
C	The number of classes in the dataset
d	Dimensionality of the feature vector
k	The number of current time instance
I	A single instance image
x	The associated feature vector of I
\bar{x}	Vector normalization
N_c	Identified prototypes number of the C^{th} class
μ_c	The global mean of feature vectors of the training images of the C^{th} class
D	Data density
$I_{c,k}$	The k^{th} training image of the C^{th} class
$x_{c,k}$	The corresponding feature vector of $I_{c,k}$
$P_{c,i}$	The i^{th} prototype of the C^{th} class
$p_{c,i}$	The mean of feature vectors of the training images associated with $P_{c,i}$
$S_{c,i}$	The number of training images associated with $P_{c,i}$
$r_{c,i}$	The radius of the area of influence of the <i>dataclouds</i> d associated with $P_{c,i}$
λ_c	The score of confidence given by the local decision-maker of the C^{th} fuzzy rule
Sg_i	The i^{th} segment of the image I or local information

III.5.2 Massively parallel FRB

The fuzzy rule-based (FRB) layer consists of a set of highly parallel IF...THEN rules, presented by **Equation (III.1)**, based on the AnYa type 0-order fuzzy rules. These non-parametric rules do not require a predefined membership function. Instead, following the Empirical Data Analytics concept, the fuzzy rules naturally emerge from patterns in the data. [95] [96] .

$$\text{IF}(I \sim P_{c,1}) \text{OR} \dots \text{OR}(I \sim P_{c,N_c}) \text{ THEN (class } C) \quad (\text{III.1})$$

Where "~" signifies a resemblance that can be interpreted as a fuzzy degree of satisfaction, membership, or typicality; I represents a specific image; $c=1,2,...,C$; N_c refers to the number of prototypes in the C^{th} class. The identified prototypes are represented by P .

III.5.2.1 Training process of the DRB system

This section provides an overview of the primary procedure involved in training a specific FRB subsystem as depicted in **Figure III-13**. Due to the highly parallel structure of the DRB system, we focus on the C^{th} fuzzy rule, where $c=1, 2, \dots, C$.

We begin by initializing the $k^{th} (k \leftarrow 1)$ training image to verify condition 1 and distinguish stage 0 from the other stages.

Condition1:

$$IF(k = 1) THEN (start with stage 0) \quad (III.2)$$

If condition 1 is satisfied, it indicates that this is the first image received, and the system is initialized by following stage 0. If condition 1 is not met, the system has already been initialized, and we proceed directly to stage 1.

Stage 0: System Initialization.

We initialize the C^{th} fuzzy rule using the first image of the corresponding class, denoted as $I_{c,1}$ with the global feature vector represented by $x_{c,1} (x_{c,1} = [x_{c,1,1}, x_{c,1,2}, x_{c,1,d}])$, where d is the dimensionality. The system's meta-parameters are then initialized following **Equation (III.3)**.

$$k \leftarrow 1; \mu_c \leftarrow \bar{x}_{c,1}; N_c \leftarrow 1; P_{c,N_c} \leftarrow I_{c,1}; p_{c,N_c} \leftarrow \bar{x}_{c,1}; S_{c,N_c} \leftarrow 1; r_{c,N_c} \leftarrow r_c; \quad (III.3)$$

Where k represents the current time instance, μ_c is the global mean of all the observed data samples for the C^{th} class. p_{c,N_c} is the mean of feature vectors of the images associated with the first data cloud with the visual prototype P_{c,N_c} , S_{c,N_c} denotes the number of images associated with the data cloud. r_{c,N_c} is the radius of the area of the data cloud, r_0 is a small value introduced to stabilize the initial status of the newly formed data clouds.

Stage 1: System preparation.

At this stage, we calculate the densities to verify the condition 2. First, we read the newly arrived $k^{th} (k \leftarrow k + 1)$ training image ($I_{c,k}$) belonging to the C^{th} class. Next, we

update the global mean μ_c and compute the data densities of all existing prototypes $\mathbf{P}_{c,i}$ using the following Equations (III.4, III.5, III.6):

$$\mu_c \leftarrow \frac{k-1}{k} \mu_c + \frac{1}{k} \bar{x}_{c,k} \quad (\text{III.4})$$

$$D(\mathbf{P}_{c,i}) = \frac{1}{1 + \|\mathbf{p}_{c,i} - \mu_c\|^2 / \sigma_c^2} \quad (\text{III.5})$$

$$D(\mathbf{I}_{c,k}) = \frac{1}{1 + \|\bar{x}_{c,k} - \mu_c\|^2 / \sigma_c^2} \quad (\text{III.6})$$

where $\sigma_c^2 = 1 - \|\mu_c\|^2$

Stage 2: System update.

In this stage, we check the condition 2, if the $\mathbf{I}_{c,k}$ becomes a new prototype or we find the nearest prototype to $\mathbf{I}_{c,k}$ using the $D(\mathbf{P}_{c,i})$ and $D(\mathbf{I}_{c,k})$ calculated in the previous stage. Then, we update the system and meta-parameters.

Condition 2:

$$\begin{aligned} \text{IF } \left(D(\mathbf{I}_{c,k}) > \max_{i=1,2,3,\dots,N_c} (D(\mathbf{P}_{c,i})) \right) \text{ OR } \left(D(\mathbf{I}_{c,k}) < \min_{i=1,2,\dots,N_c} (D(\mathbf{P}_{c,i})) \right) \\ \text{THEN } (\mathbf{I}_{c,k} \text{ is new prototype}) \end{aligned} \quad (\text{III.7})$$

If condition 2 is met, then $\mathbf{I}_{c,k}$ is new prototype with new data cloud.

$$N_c \leftarrow N_c + 1; \mathbf{P}_{c,N_c} \leftarrow \mathbf{I}_{c,1}; P_{c,N_c} \leftarrow \bar{x}_{c,1}; S_{c,N_c} \leftarrow 1; r_{c,N_c} \leftarrow r_c; \quad (\text{III.8})$$

If condition 2 is not satisfied, we find the nearest prototype $\mathbf{P}_{c,n}$ to $\mathbf{I}_{c,k}$ following the Equation (III.9).

$$\mathbf{P}_{c,n} = \arg \min_{j=1,2,\dots,N_c} (\|\bar{x}_{c,k} - \mathbf{P}_{c,j}\|) \quad (\text{III.9})$$

Before associating the $\mathbf{I}_{c,k}$ with the data cloud of $\mathbf{P}_{c,n}$, we must check the last condition 3 to determine whether $\mathbf{I}_{c,k}$ is located in the area of influence of $\mathbf{P}_{c,n}$:

Condition 3:

$$\text{IF } (\|\bar{x}_{c,k} - \mathbf{p}_{c,n}\| \leq r_{c,N_c}) \text{ THEN } (\mathbf{I}_{c,k} \text{ is assigned to } \mathbf{P}_{c,n}) \quad (\text{III.10})$$

If the condition 3 is satisfied, the meta-parameters are updated and $\mathbf{I}_{c,k}$ assigned to the data cloud of the prototype $\mathbf{P}_{c,n}$ using (III.11).

$$S_{c,n} \leftarrow S_{c,n} + 1; \mathbf{p}_{c,n} \leftarrow \frac{S_{c,n}-1}{S_{c,n}} \mathbf{p}_{c,n} + \frac{1}{S_{c,n}} \bar{x}_{c,k}; \quad (\text{III.11})$$

If the *condition 3* not met, then $\mathbf{I}_{c,k}$ is considered outside the influence area of the nearest data cloud, and it is treated as a new prototype according to **Equation (III.8)**.

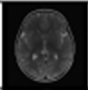
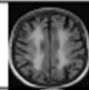
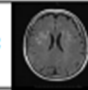
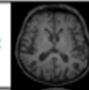
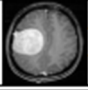
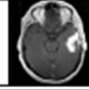
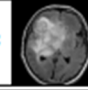
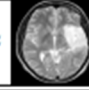
After completing Stage 2, the DRB system updates the fuzzy rule accordingly following the equation (III.12). The value of K is then incremented by 1 ($k \leftarrow k + 1$), and the system returns to Stage 1 to process the next image, initiating a new cycle.

Stage 3: Generate Fuzzy rule based (FRB).

Once all the training data has been processed, the system generates a fuzzy rule (Rule_c) based on the identified prototypes. Samples of AnYa type fuzzy rules derived from the brain tumor dataset are shown in **Table III.4**.

$$\text{Rule}_c : \text{IF } (\mathbf{I} \sim \mathbf{P}_{c,1}) \text{ OR } \dots \text{OR } (\mathbf{I} \sim \mathbf{P}_{c,N_c}) \text{ THEN } (\text{Class } C) \quad (\text{III.12})$$

Table III.4: Samples of AnYa-type fuzzy rules derived from the brain tumor dataset

fuzzy rule								
IF(I \approx	)OR(I \approx	)OR(I \approx	)OR...OR(I \approx		THEN no tumor
IF(I \approx	)OR(I \approx	)OR(I \approx	)OR...OR(I \approx		THEN tumor

III.5.2.2 Validation process of the DRB system

At the end of the training process, the DRB system generates C fuzzy rules corresponding to the C classes. For each testing image, the system produces c confidence score $\lambda_c(\mathbf{I})$ by its local (per rule) decision-maker based on the feature vector of \mathbf{I} , denoted by \mathbf{x} :

$$\lambda_c(\mathbf{I}) = \arg \max_{j=1,2,\dots,N_c} \left(\exp(-\|\mathbf{x} - \mathbf{p}_{c,j}\|^2) \right) \quad (\text{III.13})$$

III.5.2.3 Decision Maker

Thus, for each image, we obtain C confidence scores $\lambda_c(\mathbf{I}) = [\lambda_1(\mathbf{I}), \lambda_2(\mathbf{I}), \lambda_3(\mathbf{I}), \dots, \lambda_c(\mathbf{I})]$. These scores serve as inputs of the overall decision-maker of the DRB classifier (the final layer in **Figure III-12**), which assigns a label to the testing image using the “winner-takes-all” principle as follows:

$$\text{label}(\mathbf{I}) = \arg \max_{c=1,2,\dots,C} (\lambda_c(\mathbf{I})) \quad (\text{III.14})$$

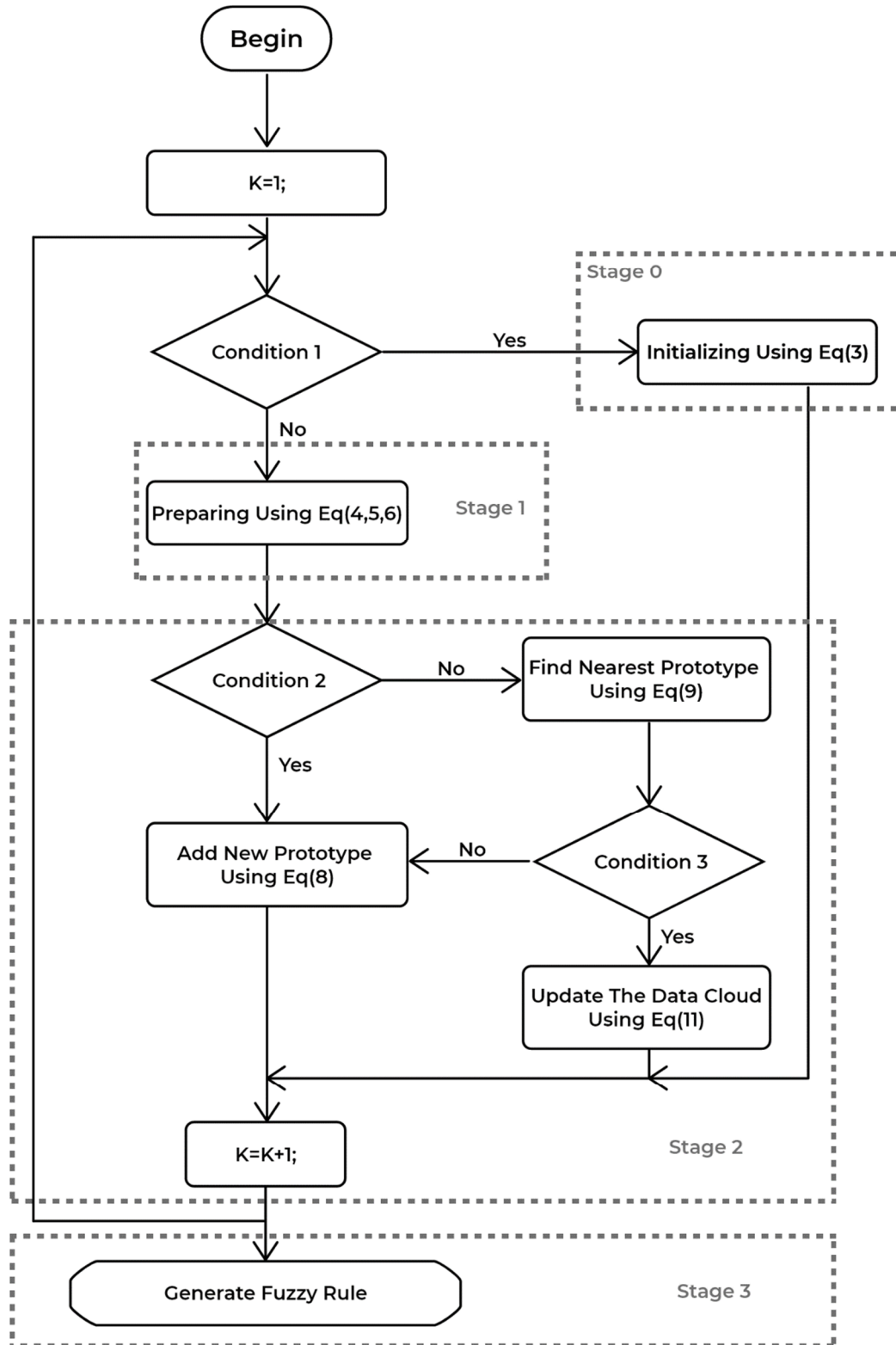


Figure III-13: Flowchart of the training process of the FRB subsystem

The pseudo code of the training process is as follows.

Algorithm 1 training process of the deep rule-based classifier

```

K=1;
While the new feature vector  $x_{c,k}$  of the  $k^{th}$  image  $I_{c,k}$  of the  $C^{th}$  class is
available Do
IF (K=1) THEN
    1. Initialization using Eq. (III.3);
    2. Generate the Anya type fuzzy rule Eq. (III.12);
ELSE
    1. Update  $\mu_c$  using Eq. (III.4);
    2. Calculate  $D(P_{c,i})$  and  $D(I_{c,k})$  using Eq. (III.5, III.6);
    If (condition 2 is met) then
        • Initialize a new data cloud using Eq. (III.8);
    Else
        • Find  $P_{c,n}$  using Eq. (III.9);
    If (condition 3 is met) then
        ▪ Update the existing data cloud using Eq. (III.11);
    Else
        ▪ Initialize a new data cloud using Eq. (III.8);
    End if
End if
    Update the Anya type fuzzy rule using Eq. (III.12);
End if
K=k+1;
End while

```

III.6 Conclusion

This chapter has provided a comprehensive overview of MRI brain image classification. We explored the evolution of classification techniques, ranging from classical image processing methods to advanced machine learning and deep learning algorithms. A taxonomy of these approaches was introduced to clearly outline their respective strengths and limitations in the context of brain tumor detection. Additionally, we detailed the classification process, emphasizing key steps such as preprocessing, feature extraction, and classification. A significant highlight of this chapter is the introduction of the Deep Rule-Based classifier, a hybrid approach that combines the transparency and interpretability of traditional fuzzy rule-based systems with the powerful hierarchical learning capabilities of deep learning. By understanding the challenges and comparative strengths of various classification techniques, this chapter paves the way for the development of more accurate, robust, and reliable tumor detection systems. These insights will contribute to future advancements in automated brain tumor diagnosis, improving clinical decision-making and patient outcomes.

Chapter IV: DRB-BBSIF for Brain Tumor Classification

IV.1 INTRODUCTION.....	68
IV.2 THE ARCHITECTURE OF PROPOSED DRB-BBSIF CLASSIFIER	68
IV.2.1 EXTRACTION OF THE REGION OF INTEREST (ROI)	69
IV.2.2 EXPLORING BINARIZED STATISTICAL IMAGE FEATURES (BSIF)	69
IV.2.3 DEEP RULE-BASED CLASSIFIER FOR MRI BRAIN TUMOR CLASSIFICATION..	71
IV.3 EXPERIMENTS AND RESULTS.....	72
IV.3.1 DATABASE	72
IV.3.2 EXPERIMENT 1: CONSTRUCTION OF BANK OF BSIF FILTERS	73
IV.3.3 EXPERIMENT 2: IMPACT OF FEATURE EXTRACTOR METHODS.....	78
IV.3.4 EXPERIMENT 3: EVALUATION OF THE DRB-BBSIF MODEL	80
IV.4 CONCLUSION.....	83

Chapter IV: DRB-BBSIF for Brain Tumor Classification

IV.1 Introduction

Brain tumor identification and classification using MRI play a crucial role in medical diagnosis but remain a challenging task due to the inherent complexity of tumor analysis. Traditional approaches heavily depend on the expertise of radiologists, which can introduce subjectivity and variability in interpretation. Additionally, the process is often time-consuming and costly, limiting its efficiency in clinical practice. This chapter presents our first contribution, which aims to automate and improve brain tumor classification using MRI data. To this end, we propose a novel model called DRB-BBSIF (Deep Rule-Based Classifier using Bank of Binarized Statistical Image Features), designed to address the shortcomings of conventional methods by focusing on two key aspects:

- **Enhanced Feature Extraction:** BSIF effectively extracts texture information from images, offering a good balance of simplicity and performance. However, its dependence on hand-crafted features can limit its ability to capture complex patterns. To address this, we introduced Bank-BSIF, an improved version of BSIF that utilizes optimized parameter settings for enhanced performance.
- **Automated Classification with Deep Rules:** The model employs a Deep Rule-Based Classifier for automated classification. DRB leverages a self-organizing set of fuzzy rules guided by prototypes, providing a robust and efficient approach for tumor classification.

IV.2 The Architecture of Proposed DRB-BBSIF Classifier

The flowchart of DRB-BBSIF classifier is presented in **Figure IV-1**. The framework contains four steps:

- **Step 1:** It consists of the extraction of the ROI in the medical image, which is very important to improve the classification performance.
- **Step 2:** The features are extracted from the ROI using BSIF descriptor.
- **Step 3:** The DRB classifier is applied to classify the given ROI of MRI brain tumor into different pathological types.
- **Step 4:** The final step consists of the decision maker, which decides the class label that tested image belongs to.

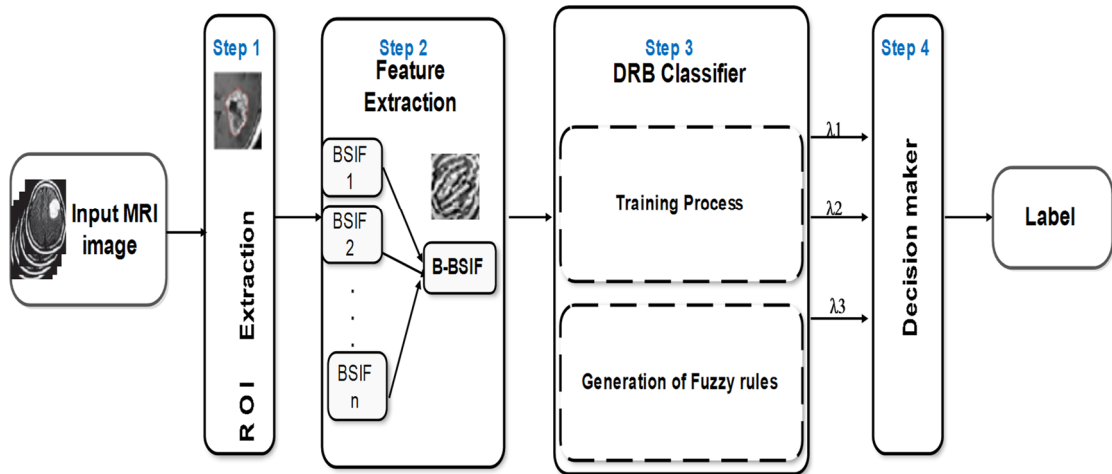


Figure IV-1: DRB-BBSIF Classifier Architecture

IV.2.1 Extraction of the Region of Interest (ROI)

For medical images, the region of interest is the lesion area for doctors, which contains the main disease information. In this work, the procedure employed for the extraction of the ROI is same as used in [5]. The ROI extraction technique is as follows: first, the tumor region is augmented by image dilation and used as the ROI rather than the initial tumor region, because tumor-neighboring tissues can provide significant indications for the identification of tumor types. Second, the augmented tumor region is fragmented to progressively fine ring-form sub regions. Finally, we can apply a local feature descriptor to extract the features from the extracted ROI.

IV.2.2 Exploring Binarized Statistical Image Features (BSIF)

Good feature descriptor is important to produce satisfactory classification results [99]. Several local image descriptors are proposed in the literature, e.g., WLD (Weber Local Descriptor) [100] [101], PHOG (Pyramid of Histogram of Oriented Gradients) [102], LBP (Local Binary Pattern) [103], LPQ (Local Phase Quantization) [104] and BSIF (Binarized Statistical Image Features) [63]. Motivated by the success of BSIF technique in natural images classification and iris recognition [63] [105] [106], we have explored this technique in this work of MRI brain tumor classification.

BSIF is a local image descriptor based on the LBP and LPQ techniques. Unlike these methods, BSIF does not rely on predefined set of filters but instead learns the filters from natural images. These learned filters are then applied to describe each pixel of the ROI as a

binary string, representing the binarized responses of learned convolutional filters. Further, the histogram of the binary string values for each pixel generates BSIF features, which efficiently describe the texture proprieties of the image sub regions. A set of filters with patch size $l \times l$ are learned from input images using independent component analysis (ICA) [63][62]. Patch size l is given as:

$$l = (2 * n + 1) \quad (IV-1)$$

Where $n \in \{1, 2...8\}$. The pre-learned filters from natural images are used to extract texture features from the images. Suppose an image be represented as $I(x, y)$ and the filter be denoted by $h_i(u, v)$, where i indicates the basis of filter, the linear response of filter s_i can be expressed as:

$$s_i = \sum_{x,y} I(u, v) h_i(u, v) \quad (IV-2)$$

Where x and y stand for the dimension of image and filter, respectively. Hence, the response is binarized based on the obtained response value. Specifically, if the linear filter response exceeds the threshold, a value of 1 is assigned; otherwise, a value of 0 is given. This process is defined as follows:

$$b_i = \begin{cases} 1 & \text{if } s_i > 0 \\ 0 & \text{otherwise} \end{cases} \quad (IV-3)$$

The responses obtained from different bases are used to create a new gray code for the pixel values. Since the descriptors are built using filters learned from a set of natural images, the responses of these filters are maximally independent in terms of statistical significance. Because the descriptor is derived from the statistical properties of the image, the resulting feature set is known as Binarized Statistical Image Features [62] [63]. The BSIF features are represented as a histogram of pixel binary codes, which effectively captures the texture components of the MRI image. The BSIF descriptor relies on two key factors: the filter size and the length of the filter. Single filters with a fixed length may not effectively generalize brain tumor patterns with varying intensities, scales, and orientations. Therefore, we propose using a bank of high-performing filters with different scales, referred to as B-BSIF, to capture significant features, as detailed in the experimental section. **Figure IV-2** illustrates an example of an MRI image processed with BSIF filters. **(a)** shows the input ROI MRI image. **(b)** displays a learned BSIF filter with a size of 17×17 and a length of 11 bits. **(c)** shows the results of convolving the ROI MRI image with the respective BSIF filters. **(d)**

presents the final BSIF-encoded feature/image.

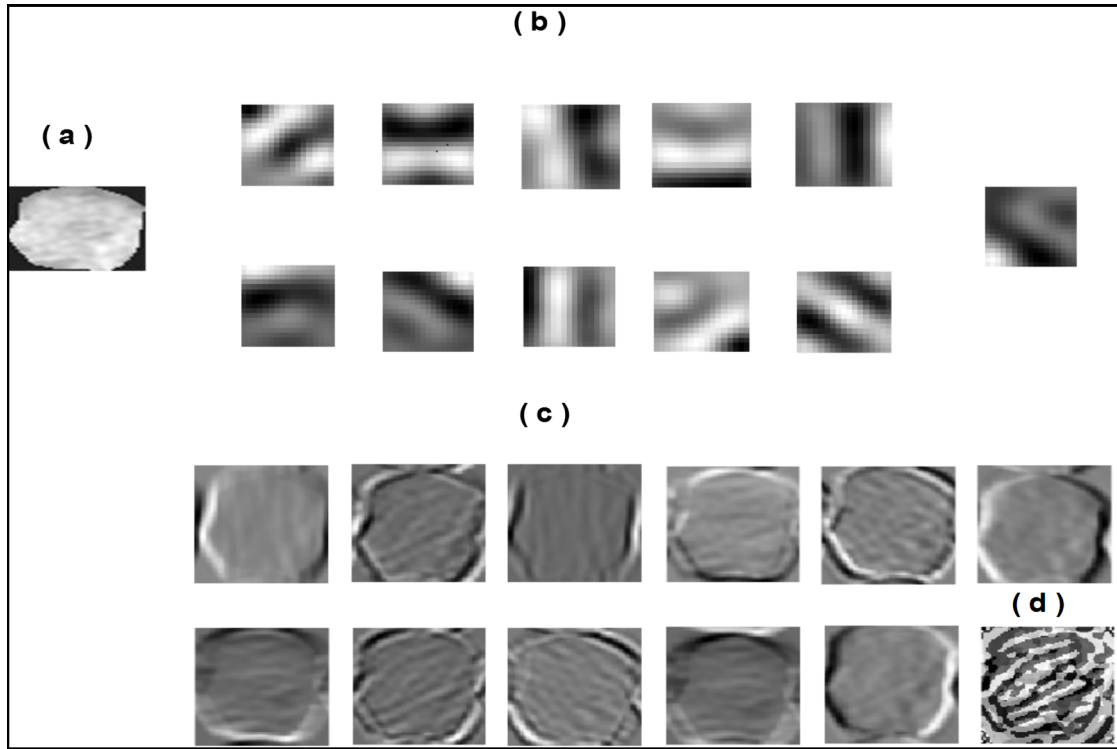


Figure IV-2: An example of an MRI image processed with BSIF filters

IV.2.3 Deep Rule-Based Classifier for MRI Brain Tumor Classification

Various techniques have been proposed for data classification. Inspired by the high classification accuracy achieved by the DRB classifier in [73], we investigate its application for classifying MRI brain tumors. To the best of our knowledge, this is the first study to employ this technique for MRI brain tumor classification. The advantage of the DRB classifier approach lies in its combination of two powerful and proven techniques that have demonstrated efficiency and high accuracy in various image processing tasks [94][96]. However, both techniques have certain limitations, which the DRB system addresses. The first technique is Deep Convolutional Neural Networks (DCNNs), known for their ability to achieve very high classification accuracy. The major drawback of DCNNs is that they require a large amount of training data and need to be fully retrained when new classes of images are introduced. They also perform well only when the test images share similarities with the training data and struggle with handling uncertainties. Additionally, their parameters are often opaque and not easily interpretable [98]. In contrast, the second technique, the traditional Fuzzy Rule-Based (FRB) system, is effective at managing uncertainties by providing a clear and

interpretable structure. However, it doesn't perform at the same high level as DCNNs due to its relatively small internal structure [98][96][95]. The DRB classifier addresses these limitations by merging the strengths of the FRB system with deep learning, incorporating a multi-layer fuzzy structure for image classification.

In this study, we explored the FRB layer, which functions as the "engine" of the DRB classifier and is built on the autonomously self-developing fuzzy rule-based models of the AnYa type [96]. The AnYa model employs a set of IF...THEN... fuzzy rules that are non-parametric, meaning they do not require predefined membership functions. Instead, these rules are derived automatically from data patterns, following the concept of Empirical Data Analytics. This layer involves two key processes: training and the generation of fuzzy rules. The process involves three stages: system initialization, preparation, and updating. A large dataset is utilized to train the DRB system, and after training is complete, each subsystem generates a fuzzy rule for its respective class based on the identified prototypes. The fuzzy rules produced by our proposed BRB-BSIF system are shown in **Table IV.7**.

IV.3 Experiments and results

This section presents the experimental evaluation of the proposed DRB-BBSIF classifier, which is based on the Bank of BSIF (BBSIF) filters. The experiments are designed to assess the classifier's performance and explore the effectiveness of different feature descriptors. Three distinct experiments are conducted: Experiment 1 involves the creation of a BSIF filter bank and a comparison between standard BSIF and B-BSIF; Experiment 2 examines the impact of various feature descriptors when used with the DRB classifier; and Experiment 3 focuses on evaluating the DRB-BBSIF model specifically for MRI brain tumor classification.

IV.3.1 Database

The proposed model is evaluated on the publicly available brain T1-weighted CE-MRI dataset. This database was collected by Cheng et al [5] from Nanfang Hospital, Guangzhou, China, and General Hospital, Tianjing Medical University, China, from 2005 to 2010. Where, 3064 slices were collected from 233 patients, having 708 slices infected by Meningiomas, 1426 slices infected by Gliomas, and 930 slices infected by Pituitary tumors. The images contained an original size of 512 x 512 in pixels. Three examples are illustrated in **Figure IV-3**.

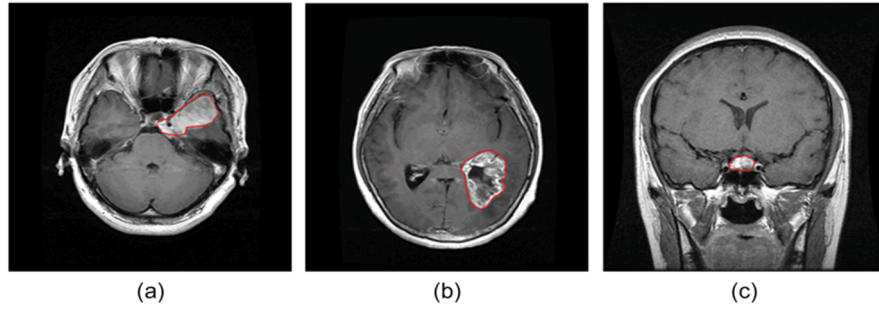


Figure IV-3: Illustrations of three typical brain tumors [5]

(a) meningioma; (b) glioma; and (c) pituitary tumor. Red lines indicate the tumor border.

IV.3.2 Experiment 1 – Construction of Bank of BSIF Filters

IV.3.2.1 Objectives and Methodology

The objective of this experiment is to enhance the system's accuracy by constructing a bank of BSIF filters. To identify the optimal BSIF parameters and corresponding filters, several sub-experiments were conducted, with the results summarized in **Table IV.1**. We tested various filters with different parameters, such as filter size (k) and filter length (n). The parameters achieving the highest performance were selected and used to build the BSIF filter bank (BBSIF).

These selected parameters, listed in **Table IV.2**, are fixed and will be used as the estimated parameters for subsequent experiments. **Figure IV-4** illustrates the B-BSIF descriptor model, showing an example using B-BSIF. As seen, the bank comprises different BSIF descriptor sizes, namely 17×17 , 15×15 , 13×13 , and 11×11 , with a length of 11 bits. This filter bank serves as an input to the DRB classifier.

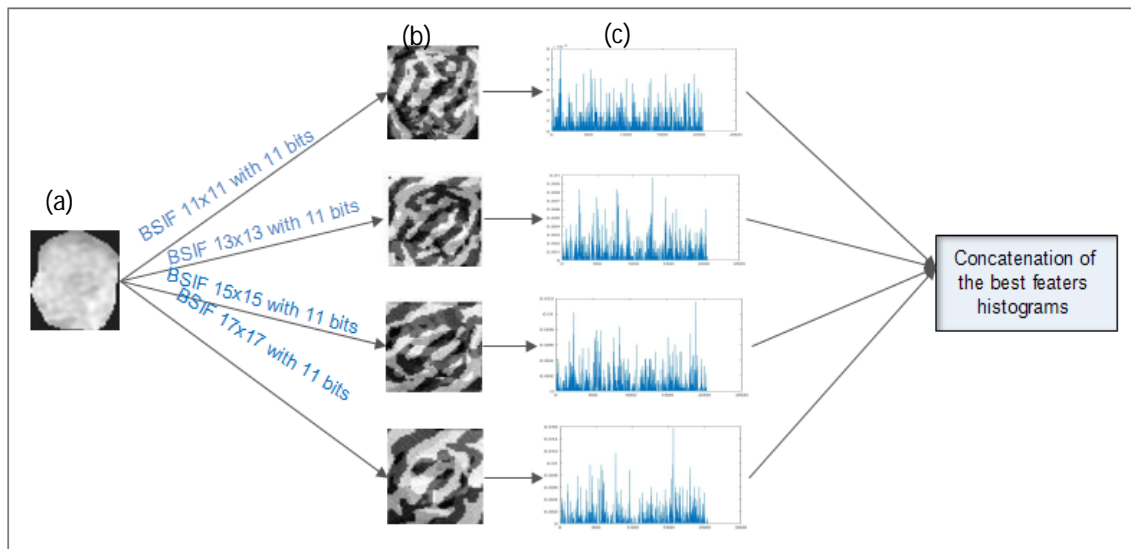


Figure IV-4: The model of the B-BSIF descriptor:

(a) input ROI of MRI, (b) results of applying the different BSIF descriptor (BSIF code images), and (c) the histograms of the BSIF code images.

Table IV.1: All parameters of BSIF applied on the MRI brain tumor

Parameters		Accuracy (%)	Sensitivity (%)	Specificity (%)
K	N			
17×17	12	81.79	85.88	80.56
17×17	11	84.30	86.44	83.66
17×17	10	83.39	85.88	82.64
15×15	12	82.08	84.89	81.24
15×15	11	83.71	85.59	83.15
15×15	10	83.26	88.42	81.71
13×13	12	81.89	84.04	81.24
13×13	11	82.70	86.86	81.45
13×13	10	82.25	86.86	80.86
11×11	12	80.97	83.05	80.35
11×11	11	82.60	85.03	81.88
11×11	10	83.62	85.03	83.19

IV.3.2.2 Analysis of Results

The results of applying various BSIF filters reveal several key trends in terms of accuracy, sensitivity, and specificity:

1. Filter Size and Performance :

- Larger filter sizes (17×17) tend to deliver higher accuracy compared to smaller sizes (11×11). For example, the 17×17 filter with a length of 11 bits achieves the highest accuracy (84.30%), whereas the smallest filter (11×11) with the same bit length reaches an accuracy of 82.60%.
- However, the performance gap between different filter sizes is not drastic. For instance, the 15×15 filter with 11 bits still performs comparably, with 83.71% accuracy.

2. Sensitivity and Specificity:

- Sensitivity remains relatively high across all filters, with the best sensitivity (88.42%) being observed with the 15×15 filter at 10 bits, indicating that this configuration is particularly effective in detecting true positives.
- Specificity also stays within a narrow range, generally between 80% and 83%, indicating a consistent ability to correctly identify true negatives. The highest specificity (83.66%) occurs with the 17×17 filter at 11 bits.

3. Bit Length Influence :

- Shorter bit lengths (10 or 11 bits) tend to provide slightly better overall performance than longer bit lengths (12 bits). For example, the 17×17 filter at 11 bits outperforms the same filter at 12 bits in accuracy, sensitivity, and specificity.

4. Best Configuration :

- The optimal performance in terms of accuracy (84.30%) is achieved with the 17×17 filter at 11 bits, offering a balanced performance across all metrics.
- The 15×15 filter at 10 bits stands out for sensitivity, making it a strong candidate if detecting positive cases is prioritized.

In summary, the BSIF filters perform consistently across different configurations, with the 17×17 filter at 11 bits being the most optimal in terms of accuracy and specificity. Sensitivity, on the other hand, peaks with a 15×15 filter at 10 bits, highlighting that different configurations may be preferable depending on the specific performance metric emphasized in the analysis.

Table IV.2: Best BSIF filters

Parameters	
k	n
17×17	11
15×15	11
13×13	11
11×11	11

The experiment comparing the BSIF and B-BSIF descriptors demonstrates a clear improvement in performance when using the B-BSIF (Bank BSIF) approach. The results in **Table IV.3** indicate that the B-BSIF consistently outperforms the standard BSIF in terms of accuracy, sensitivity, and specificity.

Table IV.3: Comparison between BSIF descriptor and Bank BSIF

Feature descriptor	Accuracy (%)	Sensitivity (%)	Specificity (%)
BSIF	84.30	86.44	83.66
BBSIF	84.73	87.57	83.87

1. **Accuracy:** The accuracy of the B-BSIF (84.73%) slightly surpasses that of the BSIF (84.30%). Although the difference is small, it highlights the enhanced capacity of the B-BSIF filter bank to capture more discriminative features.
2. **Sensitivity:** A more notable improvement is seen in sensitivity, where the B-BSIF reaches 87.57%, compared to 86.44% for the BSIF. This suggests that the B-BSIF is more effective at detecting true positive cases, which is particularly important in medical image analysis for identifying brain tumors.
3. **Specificity:** The specificity of the B-BSIF (83.87%) is also marginally higher than that of the BSIF (83.66%), indicating a slight improvement in identifying true negative cases.

These results demonstrate that the construction of a filter bank (B-BSIF) improves classification performance over the individual BSIF descriptor. The enhancements in sensitivity are especially valuable, as they indicate the model's improved ability to detect positive cases more reliably. Therefore, the B-BSIF descriptor can be considered a more robust and effective feature extraction method for MRI brain tumor classification.

IV.3.2.3 Interpretation of Results

The superior performance of the B-BSIF (Bank BSIF) descriptor compared to the standard BSIF can be justified based on several factors related to feature extraction and the flexibility of the filter bank approach:

1. Increased Diversity in Feature Representation

The B-BSIF approach involves using a bank of BSIF filters with varying sizes and parameters. This diversity allows the model to capture a broader range of texture and spatial features in the MRI images. Different filter sizes respond to different scales of detail, enabling the model to extract both detailed and general features. The standard BSIF, with a single set of filters, is limited in its ability to capture such multi-level information.

2. Adaptability to Image Variability

MRI brain images exhibit significant variation in tumor size, shape, texture, and intensity patterns. The B-BSIF bank, with its varied filters, adapts more effectively to this variability compared to a single BSIF descriptor. The flexibility of the filter bank ensures that features are captured across different resolutions and orientations, contributing to improved sensitivity and accuracy.

3. Improved Generalization

By combining multiple filters, the B-BSIF bank can generalize better across different datasets or image conditions. In medical imaging, such robustness is crucial, as the same type of tumor can manifest differently in different patients. The B-BSIF's ability to integrate information from multiple descriptors improves the model's ability to generalize and detect true positives (tumors) more reliably, which is reflected in the higher sensitivity.

4. Enhanced Discriminative Power

The combination of different filters in B-BSIF increases the discriminative power of the features used by the classifier. The subtle differences in texture and intensity patterns, which might not be captured by a single filter set, are more likely to be detected by the varied filters in the bank. This is likely why B-BSIF achieves better specificity, as it reduces false positives by distinguishing between normal and abnormal tissue more accurately.

5. Reduction in Overfitting

A single BSIF filter set may be prone to overfitting, particularly if the parameters are not well-suited to the full variability present in the images. The B-BSIF, by incorporating multiple filter sets, reduces the likelihood of overfitting to specific patterns, thus offering a more balanced performance across accuracy, sensitivity, and specificity.

IV.3.2.4 Key findings

In summary, the B-BSIF's ability to capture a wider range of image features, its adaptability to MRI image variability, and its improved generalization contribute to its better performance in accuracy, sensitivity, and specificity compared to the standard BSIF.

IV.3.3 Experiment 2: Impact of Feature Extractor Methods

IV.3.3.1 Objective of Experiment 2

The goal of this experiment is to evaluate the impact of various feature descriptor methods (LBP, LPQ, WLD, PHOG, BSIF, and B-BSIF) on the performance of the DRB classifier for MRI brain tumor classification. The experiment compares the accuracy, sensitivity, and specificity of the DRB classifier when paired with each feature descriptor, to determine which combination yields the best results. **Table IV.4** presents the findings.

Table IV.4: Performance of feature descriptor methods with the DRB classifier

DRB with	LBP	LPQ	WLD	PHOG	BSIF	B-BSIF
Accuracy (%)	73.99	77.15	75.78	79.31	84.30	84.73
Sensitivity (%)	57.77	74.72	64.97	74.29	86.44	87.57
Specificity (%)	78.86	77.89	79.03	80.81	83.66	83.87

IV.3.3.2 Analysis of results

The results of **Experiment 2**, illustrate the performance of different feature descriptor methods used with the DRB classifier, highlighting the effectiveness of the B-BSIF descriptor. From this experiment, we can make several key observations:

1. Accuracy:

Among the feature extractors tested, the **B-BSIF** achieves the highest accuracy (84.73%), followed closely by the **BSIF** (84.30%). These outperform other methods such as **PHOG** (79.31%), **LPQ** (77.15%), and **LBP** (73.99%). This indicates that the BSIF-based methods, particularly B-BSIF, provide superior feature extraction capabilities for use with the DRB classifier.

2. Sensitivity:

B-BSIF also leads in sensitivity (87.57%), indicating that it is more effective at correctly identifying positive cases (e.g., true tumor cases). This is significantly higher than **LBP** (57.77%) and even better than **PHOG** (74.29%). The high sensitivity makes B-BSIF particularly useful for medical image analysis where detecting true positives is crucial.

3. Specificity:

In terms of specificity, the B-BSIF (83.87%) and BSIF (83.66%) show the highest values, indicating better performance in correctly identifying negative cases (e.g., healthy tissue). This suggests that the B-BSIF descriptor reduces the number of false positives more effectively compared to other methods like **LPQ** (77.89%) and **WLD** (79.03%).

IV.3.3.3 Interpretation of results

The following interpretation of results provides insights into the performance of various feature descriptor methods utilized with the DRB classifier, focusing on their strengths and limitations in capturing local features essential for effective MRI brain tumor classification.

- **Nature of Local Features:** While all the methods tested represent images as histograms of local features, the differences in performance stem from the types of local features each descriptor captures. The **B-BSIF** method is more robust because it uses a diverse bank of filters that capture multi-scale and multi-orientation texture features, resulting in more comprehensive feature representation.
- **BSIF and B-BSIF Advantages:** BSIF-based methods (particularly B-BSIF) excel in medical image classification because they are particularly good at capturing fine-grained textural information in MRI images, which is essential for distinguishing between healthy and abnormal tissues. B-BSIF's improved performance over BSIF is likely due to the added flexibility of using a bank of filters, which enhances its ability to capture subtle variations in tumor texture and structure.
- **LBP and LPQ Limitations:** Descriptors like **LBP** and **LPQ** perform worse in sensitivity and accuracy, as they may not capture the complex texture patterns present in medical images as effectively as the BSIF-based methods. **LBP**, for example, is a simple descriptor that may miss finer details, leading to its relatively low sensitivity.

IV.3.3.4 Key findings

In summary, The B-BSIF descriptor clearly outperforms other feature extraction methods when paired with the DRB classifier, achieving the best balance of accuracy, sensitivity, and specificity. This makes B-BSIF the most suitable choice for MRI brain tumor classification in this context. The results demonstrate that using a more sophisticated filter bank, like B-BSIF, significantly enhances the classification performance compared to more traditional descriptors like LBP or PHOG.

IV.3.4 Experiment 3: Evaluation of the DRB-BBSIF Model

IV.3.4.1 Objective of Experiment 3

The objective of experiment 3 is to evaluate the performance of the proposed DRB-BBSIF model for MRI brain tumor classification, specifically focusing on its effectiveness in accurately distinguishing between three tumor types: meningioma, glioma, and pituitary tumors. This experiment aims to conduct a comparative analysis between the DRB-BBSIF model and the KNN classifier, while also generating fuzzy rules, as presented in **Table IV.7**, to enhance interpretability and improve decision-making within the classification process.

IV.3.4.2 Analysis of Results

In this section, we delve into the performance of the DRB-BBSIF model for MRI brain tumor classification based on the results obtained in Experiment 3. The analysis covers three key areas: Per-class performance, a comparison with the K-Nearest Neighbors (KNN) classifier, and the contribution of fuzzy rules to the classification process.

1. Performance by Class:

- **Table IV.5** shows the system's accuracy for each class. The highest accuracy is observed for **gliomas** (88.71%), followed closely by **meningiomas** (87.57%). However, the system shows lower performance in classifying **pituitary tumors**, with an accuracy of **76.45%**. This suggests that the DRB-BBSIF model is highly effective for glioma and meningioma classification, but further improvements may be needed for pituitary tumor detection.
- Misclassification is evident, particularly between glioma and pituitary tumors. For instance, 115 out of 930 pituitary tumors were misclassified as meningiomas, indicating a possible overlap in feature representation or limitations in distinguishing these specific classes.

Table IV.5: Performance of the DRB-BBSIF for each class

	Meningioma	Glioma	Pituitary
Meningioma	620/708	33/708	55/708
Glioma	95/1426	1265/1426	66/1426
Pituitary	115/930	104/930	711/930
Accuracy	87.57	88.71	76.45

2. Comparison with K-Nearest Neighbors (KNN):

- **Table IV.6** presents a comparison between the proposed DRB-BBSIF system and various configurations of the KNN classifier (with different k values). The DRB-BBSIF consistently outperforms KNN, achieving an accuracy of 84.73%, while the KNN variants range from 80.01% (1NN) to 83.37% (15NN).
- The superiority of DRB-BBSIF over KNN suggests that the feature extraction process using the BSIF descriptor, coupled with the DRB classifier, provides a more robust approach for capturing tumor-specific features in MRI images compared to the KNN classifier, which relies on proximity-based decision-making and may not capture the complex textures of tumors as effectively.

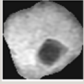
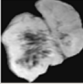
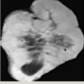
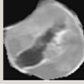
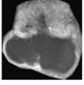
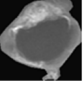
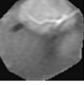
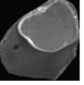



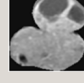
Table IV.6: Comparison of the DRB-BSIF with KNN

Method	DRB-BBSIF	1NN	3NN	7NN	15NN	45NN
Accuracy (%)	84.73	80.01	81.69	83.14	83.37	83.09

3. Fuzzy Rules:

Table IV.7 outlines the fuzzy rules generated during the training process, which are used to classify the MRI images into different tumor categories. These rules, constructed from the feature descriptors, help the system make more nuanced decisions by considering various combinations of MRI features that are indicative of each tumor type. This further supports the flexibility and adaptability of the DRB-BBSIF model compared to more rigid classifiers like KNN.

Table IV.7: Fuzzy rules generated through the training process

Fuzzy rules				
(IF MRI ~ )	OR (MRI ~ )	OR (MRI ~ )	OR (MRI ~ )	THEN (Meningioma)
(IF MRI ~ )	OR (MRI ~ )	OR (MRI ~ )	OR (MRI ~ )	THEN (Glioma)
(IF MRI ~ )	OR (MRI ~ )	OR (MRI ~ )	OR (MRI ~ )	THEN (Pituitary)

IV.3.4.3 Interpretation of Results

To justify the choice of the BSIF (Binarized Statistical Image Features) filter among other feature extractors, we can highlight several key aspects:

1. Theoretical Strengths of BSIF:

- **Texture Representation:** BSIF excels at capturing rich texture information, which is crucial for distinguishing fine details in MRI brain tumor images. Tumors often exhibit subtle texture differences, making BSIF particularly effective in capturing these variations.
- **Data-Driven Filter Design:** Unlike other feature extractors like LBP or LPQ, BSIF uses filters learned from natural image statistics, leading to more discriminative features tailored to the data. This makes it well-suited for complex medical images where the statistical structure is crucial for classification.

2. Robustness to Noise :

- **Performance in Noisy Environments:** MRI images often suffer from noise due to acquisition methods. BSIF's ability to binarize features and leverage learned filters provides robustness against such noise, potentially offering more stable performance compared to other methods like LPQ, which may be more sensitive to variations in lighting or noise.

3. Comparison with Other Feature Extractors:

- **BSIF vs. LBP/LPQ/WLD:** While methods like LBP and LPQ capture local texture and phase information, BSIF can extract more complex, high-level patterns, leading to better feature abstraction. LBP and LPQ are based on predefined filters, while BSIF adapts its filters from data, making it more flexible and potentially more powerful for classification tasks where fine details matter, such as in brain tumor classification.
- **BSIF vs. Deep Features:** While deep learning architectures like AlexNet or ResNet extract hierarchical features, BSIF is computationally less demanding and can work well when the dataset is smaller, which is common in medical imaging. It offers a good balance between simplicity and performance without requiring large-scale training data.

IV.3.4.4 Key Finding

The experiment demonstrates that the DRB-BBSIF model outperforms KNN for MRI brain tumor classification, particularly for meningiomas and gliomas. However, the lower accuracy for pituitary tumors highlights an area for further optimization. The use of fuzzy rules in the DRB-BBSIF model also adds to its strength by allowing for more precise classification through complex feature combinations. In summary, the results confirm the effectiveness of the proposed system in tumor classification, while highlighting areas where further improvements are needed in certain cases.

IV.4 Conclusion

The first contribution of this thesis presents the DRB-BSIF (Deep Rule-Based Classifier using Binarized Statistical Image Features) model, a significant advancement in the automated classification of MRI brain tumors. This model effectively addresses the limitations of traditional classification methods through two core innovations: enhanced feature extraction and automated classification utilizing deep rules.

The results from the three experiments conducted under this contribution demonstrate the efficacy of the DRB-BSIF model. Experiment 1 established the optimal parameters for the BSIF filter bank, Experiment 2 highlighted the comparative performance of various feature extraction methods with the DRB classifier, and Experiment 3 validated the superior classification performance of the DRB-BBSIF model compared to traditional classifiers like KNN. The findings indicate that the DRB-BBSIF model excels in accurately distinguishing

between meningioma, glioma, and pituitary tumors, showcasing its potential as a reliable tool for automated MRI brain tumor diagnosis.

In conclusion, the DRB-BBSIF model represents a significant contribution to the field of medical image analysis, offering a robust and interpretable framework for brain tumor classification. This work not only advances existing methodologies but also sets the stage for future research focused on refining automated classification techniques in medical imaging.

Chapter V: DRB with Deep Feature Extraction

V.1 INTRODUCTION	85
V.2 PROPOSED METHODOLOGY	85
V.2.1 PRE-PROCESSING STEP	86
V.2.2 FEATURE EXTRACTION STEP.....	86
V.2.3 CLASSIFICATION STEP.....	86
V.3 DATABASE.....	86
V.4 EXPERIMENTS AND RESULTS.....	87
V.4.1 EXPERIMENT 1: ALEXNET WITH 4 DIFFERENT CLASSIFIERS.	88
V.4.2 EXPERIMENT 2: VGG-16 WITH 4 DIFFERENT CLASSIFIERS.	92
V.4.3 EXPERIMENT 3: RESNET-50 WITH 4 DIFFERENT CLASSIFIERS.....	96
V.4.4 EXPERIMENT 4: RESNET-18 WITH 4 DIFFERENT CLASSIFIERS.....	100
V.4.5 COMPREHENSIVE ANALYSIS OF RESULTS	103
V.5 COMPARISON BETWEEN THE TWO CONTRIBUTIONS.....	108
V.6 HIGH PERFORMANCE OF THE DRB CLASSIFIER	109
V.6.1 CHARACTERISTICS OF DRB CLASSIFIER.....	109
V.6.2 PERFORMANCE METRICS OF THE DRB CLASSIFIER:.....	110
V.6.3 COMPARISON WITH OTHER CLASSIFIERS:.....	110
V.7 CONCLUSION.....	111

Chapter V: DRB with Deep Feature Extraction

V.1 Introduction

The second contribution focuses on the synergistic integration of deep learning and rule-based classification. We propose a novel, simple, and automatic DRB-based scheme for MRI brain tumor classification. This model leverages the power of deep learning for feature extraction and combines it with the effectiveness of DRB for classification.

- **Deep Feature Extraction:** The model utilizes pre-trained deep learning architectures like AlexNet, VGG-16, ResNet-50, and ResNet-18 to extract deep features from MRI images. These deep features capture complex patterns and relationships within the data, leading to improved classification performance.
- **DRB for Classification:** Similar to the first contribution, the model employs DRB for classification. DRB utilizes the extracted deep features to automatically generate a set of fuzzy rules, enabling accurate tumor identification.

V.2 Proposed methodology

The primary objective of this study is to develop a method for MRI brain tumor classification utilizing deep learning techniques. The proposed approach, outlined in **Figure V-1**, consists of three stages: preprocessing, feature extraction, and classification. Both the feature extraction and classification stages rely on deep learning methods.

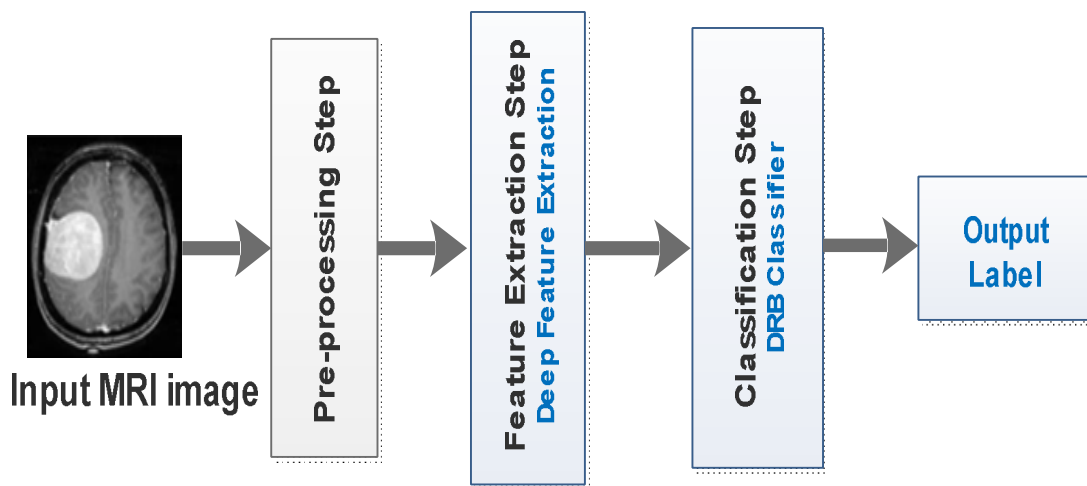


Figure V-1: Block diagram of the proposed method.

V.2.1 Pre-processing step

The preprocessing step is crucial for enhancing the image quality, which leads to achieve better performance in the feature extraction and classification stages. This process involves essential techniques such as binarization, normalization, rotation, resizing, and the removal of irrelevant parts from the MR images.

V.2.2 Feature extraction step

Feature extraction is a crucial part of the classification process, as it focuses on identifying the most important characteristics from the original data to enhance the system's efficiency. In this study, we employ deep learning-based feature descriptors to achieve this goal. Specifically, we used four pre-trained convolutional neural networks (CNNs): AlexNet, VGG-16, ResNet-18, and ResNet-50. These pre-trained models were applied to extract relevant features from MRI images. A summary of the CNN models used is provided in **Table V.1**.

Table V.1: Summary of CNN's models

Network	depth	Parameters (millions)	Image input size
AlexNet	8	60	$[227 \times 227]$
VGG-16	16	138	$[224 \times 224]$
ResNet-18	18	11.7	$[224 \times 224]$
ResNet-50	50	25.6	$[224 \times 224]$

V.2.3 Classification step

Various techniques exist for data classification, including fuzzy clustering means (FCM), support vector machines (SVM) [5] [85], and artificial neural networks (ANN) [89]. Inspired by the high classification accuracy demonstrated by the DRB classifier in [73], we investigate its use for MRI brain tumor classification.

V.3 Database

In this study, we utilized two publicly available datasets from the Kaggle website. As outlined in **Table V.2**, the first dataset consists of 253 images categorized into 2 classes (no tumor, pathological), while the second dataset includes 3264 images classified into 4 classes (Glioma tumor, Meningioma tumor, Pituitary tumor, No tumor). The "no tumor" data were obtained from the Novoneel Chakraborty Kaggle data set. (available at:

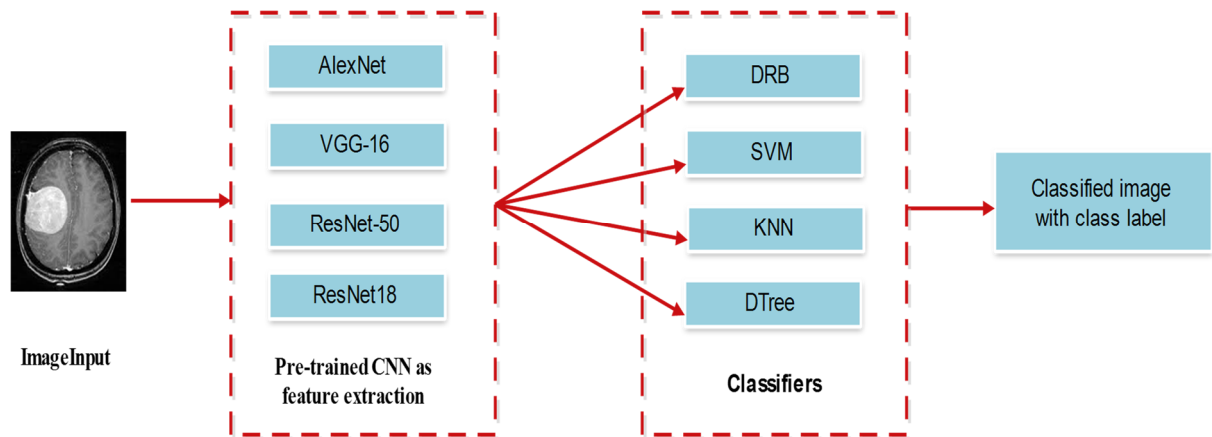
<https://www.kaggle.com/datasets/navoneel/brain-mri-images-for-brain-tumor-detection>).

Table V.2: Datasets descriptions

Dataset	Classes	Number of images	Images type
Dataset1	Tumor	155	JPG
	No tumor	98	
Dataset2	Glioma tumor	926	JPG
	Meningioma tumor	937	
	No tumor	500	
	Pituitary tumor	901	

V.4 Experiments and results

The objective of this section is to provide a comprehensive evaluation of the proposed deep features-based MRI brain tumor classification system using a series of experiments. Each experiment assesses the performance of different classifiers (DRB, SVM, KNN, and Decision Tree) in combination with features extracted from pre-trained CNN models (AlexNet, VGG-16, ResNet-50, and ResNet-18).

**Figure V-2:** Experimental evaluation of the proposed system.

The primary aim is to determine which combination of feature extractor and classifier yields the best classification results across two MRI brain tumor datasets. The evaluation is based on several key performance metrics, including accuracy, sensitivity, specificity, precision, and F-measure, allowing for a detailed comparison of the system's effectiveness in both binary and multi-class classification tasks.

V.4.1 Experiment 1: AlexNet with 4 different classifiers

In this experiment, we investigated the performance of different classifiers on pre-extracted features from a pre-trained convolutional neural network (CNN) called AlexNet (as illustrated in **Figure V-3**).

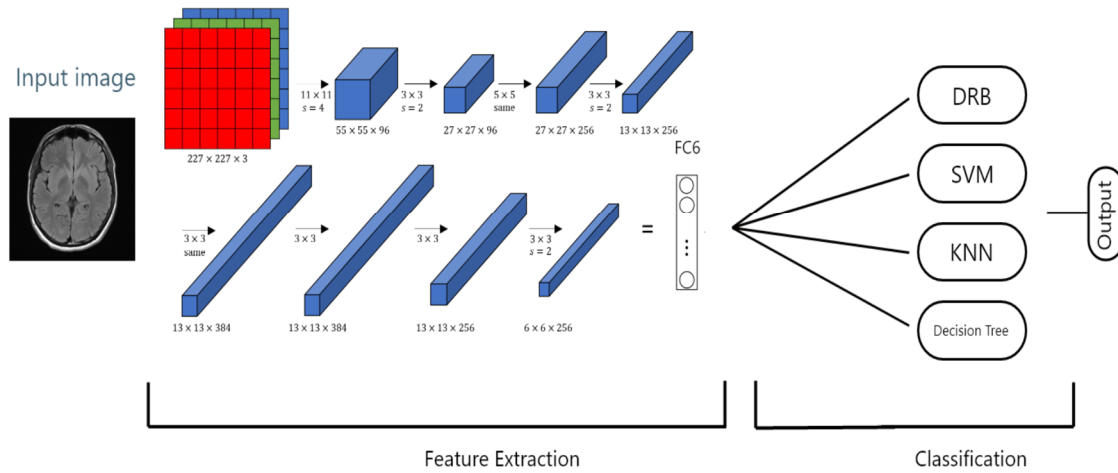


Figure V-3: Architecture of experiment1

Table V.3 outlines the architecture of **AlexNet**, showing key layers such as convolutional layers, max pooling, and fully connected layers.

Table V.3: Details of AlexNet layers

Layer	Number of kernels	Kernel size	Stride	padding	Output size
Input					$[227 \times 227 \times 3]$
Conv1	96	$11 \times 11 \times 3$	4	-	$[55 \times 55 \times 96]$
Maxpool1		3×3	2	-	$[27 \times 27 \times 96]$
Norm1				-	$[27 \times 27 \times 96]$
Conv2	256	$5 \times 5 \times 48$	1	2	$[27 \times 27 \times 256]$
Maxpool2		3×3	2	-	$[13 \times 13 \times 256]$
Norm2					$[13 \times 13 \times 256]$
Conv3	384	$3 \times 3 \times 256$	1	1	$[13 \times 13 \times 384]$
Conv4	384	$3 \times 3 \times 192$	1	1	$[13 \times 13 \times 384]$
Conv5	256	$3 \times 3 \times 192$	1	1	$[13 \times 13 \times 256]$
Max pool3		3×3	2	-	$[6 \times 6 \times 256]$
FC6 ReLu Dropout (0.5)	1				4096
FC7 ReLu Dropout (0.5)	1				4096
FC8 Softmax	1				1000

By extracting features from AlexNet and using them with different classifiers, we can evaluate how well each classifier performs with deep features. This process allows us to compare traditional machine learning classifiers (SVM, KNN, Decision Tree) with the DRB classifier and assess which approach yields the best performance in MRI brain tumor classification.

V.4.1.1 Analysis of Results

Table V.4 below highlights the comparative performance of each classifier on both datasets. The analysis explores how the classifiers performed in distinguishing between tumor and non-tumor cases, offering insights into which models are most effective for this classification task.

Following this table, a detailed breakdown of the results will be provided for each dataset, followed by key observations regarding classifier performance and dataset complexity.

Table V.4: Comparative performance of AlexNet with 4 different classifiers

AlexNet with 4 different classifiers						
Data set	Architecture	Accuracy	Sensitivity	Specificity	Precision	F-measure
Data set1	DRB	85.23%	0.9375	0.8036	0.7317	0.8219
	SVM	79.55%	0.8438	0.7679	0.6750	0.7500
	KNN	89.77%	0.8750	0.9107	0.8485	0.8615
	Decision Tree	69.32%	0.6563	0.7143	0.5676	0.6087
Data set2	DRB	79.19%	0.3500	0.9422	0.6131	0.4605
	SVM	75.63%	0.2000	0.9456	0.5556	0.2941
	KNN	60.66%	0.3700	0.6871	0.2868	0.3231
	Decision Tree	71.32%	0.4000	0.8197	0.4301	0.4145

1. Performance on Dataset 1 :

- The **K-Nearest Neighbors (KNN)** classifier performs best in terms of accuracy, achieving **89.77%**, which is significantly higher than the other classifiers.
- **DRB** and **SVM** also demonstrate solid results with **85.23%** and **79.55%** accuracy, respectively.
- **Decision Tree** performs the worst, with an accuracy of **69.32%**.
- In terms of **sensitivity** (true positive rate), **DRB** achieves the highest value (**93.75%**), which suggests that it is most effective in identifying positive cases (tumors).

- **Specificity** (true negative rate) is highest for **KNN** at **91.07%**, indicating that KNN is better at correctly identifying negative cases (non-tumors).
- **Precision** (the ratio of true positives to all predicted positives) is also strongest for **KNN** at **84.85%**, meaning it is more reliable in predicting the positive class.

2. Performance on Dataset 2 :

- The performance of all classifiers drops on Dataset 2, which may suggest that this dataset is more complex or challenging.
- **DRB** achieves the best accuracy on this dataset with **79.19%**, followed by **SVM** at **75.63%**. Both **KNN** and **Decision Tree** show significantly lower accuracies, with **60.66%** and **71.32%**, respectively.
- **DRB** again shows strong **specificity** (**94.22%**), indicating that it effectively identifies negative cases, while **Decision Tree** shows a slightly lower value (**81.97%**).
- In terms of **sensitivity**, **DRB** shows a notable drop, achieving only **35%**, indicating that it struggles with detecting positive cases in Dataset 2.
- **Precision** and **F-measure** are also higher for **DRB** and **SVM**, reinforcing that these classifiers are more consistent in performance across both datasets.

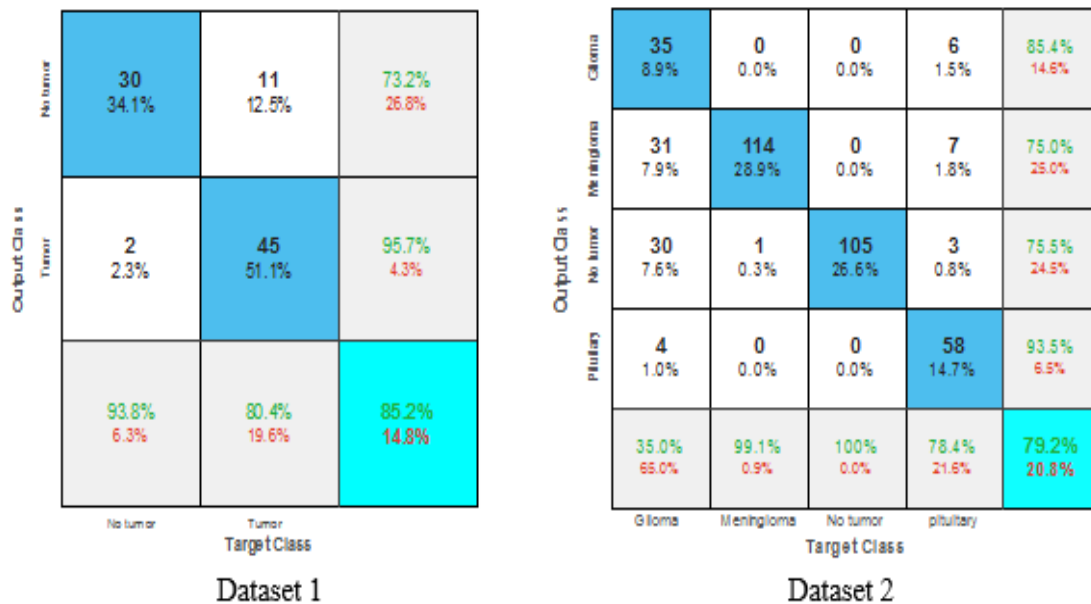


Figure V-4: Confusion matrix of DRB with data 1 and Data 2.

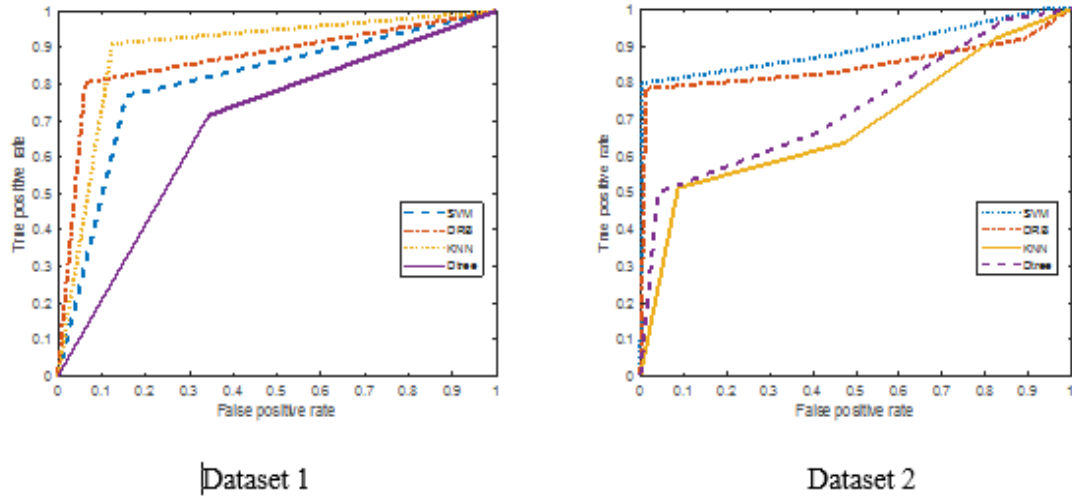


Figure V-5: ROC curves of dataset 1 and dataset 2.

V.4.1.2 Key Finding

The key findings of Experiment 1 reveal important insights into the performance of various classifiers when used with features extracted by the AlexNet deep learning model on two different MRI brain tumor datasets:

- **KNN** achieves the highest performance on Dataset 1, while **DRB** outperforms other classifiers on Dataset 2, but with a trade-off in sensitivity.
- **SVM** provides relatively balanced performance across both datasets but doesn't outperform DRB or KNN in accuracy or sensitivity.
- **Decision Tree** generally performs the worst, especially in terms of sensitivity and F-measure, indicating it is less suited for this classification task.
- The difference in performance between datasets suggests that the second dataset might be more difficult to classify, potentially due to increased complexity or variations in the images.

The ROC curves for both datasets in **Figure V-5** illustrate these variations in classifier performance, showing how the models balance sensitivity and specificity across different thresholds.

The results show that the choice of classifier can significantly impact the performance depending on the dataset, with DRB being the most balanced classifier.

V.4.2 Experiment 2: VGG-16 with 4 different classifiers

VGG-16 is a popular convolutional neural network model, as presented in **Figure V-6**, known for its deep structure and efficient use of small convolutional filters. These 3x3 filters help capture spatial patterns effectively across different scales. The architecture of VGG-16, as shown in **Table V.5**, is designed to progressively reduce the spatial resolution while increasing the depth, ultimately producing a high-dimensional feature representation that can be fed into fully connected layers for classification.

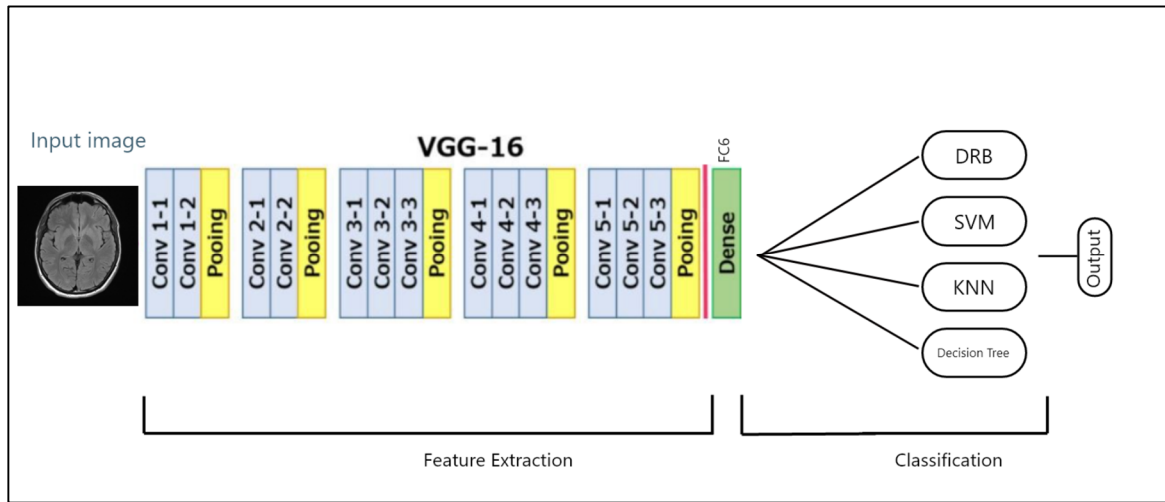


Figure V-6: VGG-16 with the classifiers

Table V.5: Architecture of VGG-16 layers

Layer	Feature map	Size	Kernel size	Stride
Input	1	$[224 \times 224 \times 3]$	-	-
Conv	64	$[224 \times 224 \times 64]$	3×3	1
Max-pooling	64	$[112 \times 112 \times 64]$	3×3	2
Conv2	128	$[112 \times 112 \times 128]$	3×3	1
Max-pooling	128	$[56 \times 56 \times 128]$	3×3	2
Conv3	256	$[56 \times 56 \times 256]$	3×3	1
Max-pooling	256	$[28 \times 28 \times 256]$	3×3	2
Conv4	512	$[28 \times 28 \times 512]$	3×3	1
Max-pooling	512	$[14 \times 14 \times 512]$	3×3	2
Conv5	512	$[14 \times 14 \times 512]$	3×3	1
Max-pooling	512	$[7 \times 7 \times 512]$	3×3	2
Fully connected		25088		
Fully connected		4096		
Fully connected		4096		
Fully connected		1000		

V.4.2.1 Analysis of results

Table V.6 compares the performance of the four classifiers using the VGG16 feature extractor on two datasets (Dataset1 and Dataset2). With this approach, an accuracy of **86.36%** was achieved with **KNN** on Dataset1, while an accuracy of **81.73%** was obtained with **DRB** on Dataset2.

Table V.6: Comparative performance of VGG-16 with 4 different classifiers

VGG-16 with 4 different classifiers						
Data set	Architecture	Accuracy	Sensitivity	Specificity	Precision	F-measure
Data set1	DRB	79.55%	0.8125	0.7857	0.6842	0.7429
	SVM	84.09%	0.7500	1	0.6957	0.8205
	KNN	86.36%	0.9063	0.8393	0.7632	0.8286
	Decision Tree	75.00%	0.7500	0.7500	0.6316	0.6857
Data set2	DRB	81.73%	0.4800	0.9422	0.7059	0.5714
	SVM	77.16%	0.2900	0.9456	0.6042	0.3919
	KNN	61.93%	0.4400	0.6871	0.3188	0.3697
	Decision Tree	72.84%	0.3800	0.8197	0.4578	0.4153

From Table V.6 , we can draw the following observations:

1- Performance on Dataset 1 :

- **DRB:** Achieved an accuracy of **79.55%**, showing relatively balanced performance across the metrics. Sensitivity and precision were moderate, with a solid F-measure of **0.7429**, indicating it handles both positive and negative predictions effectively.
- **SVM:** Outperformed other classifiers with the highest sensitivity (**0.8125**) and perfect specificity (**1**), leading to a high accuracy of **84.09%** and an F-measure of **0.8205**. This indicates SVM's strong capability to detect positive cases, though its precision and sensitivity could be better balanced.
- **KNN:** Showed the highest accuracy (**86.36%**) and strong sensitivity (**0.9063**), indicating high effectiveness in identifying true positives. Its F-measure of **0.8286** suggests that KNN was the best overall classifier on Dataset 1.
- **Decision Tree:** Had the lowest accuracy (**75.00%**) and the weakest performance across all metrics. Its F-measure of **0.6857** reflects a struggle to maintain a balance between precision and sensitivity, suggesting that it was less effective on this dataset.

2- Performance on Dataset 2 :

- **DRB:** Provided the best results on this dataset with an accuracy of **81.73%**. Its F-measure of **0.5714** reflects good performance despite having a lower sensitivity (**0.4800**), meaning it was effective at distinguishing different classes but less sensitive in detecting positives.
- **SVM:** Performed worse than on Dataset 1, achieving **77.16%** accuracy. With a lower sensitivity (**0.2900**), SVM struggled with false negatives on Dataset 2, but it maintained high specificity (**0.9456**), indicating it was good at identifying negatives.
- **KNN:** Showed a drop in performance compared to Dataset 1, with **61.93%** accuracy and a low F-measure (**0.3697**), indicating that KNN was less effective in this multi-class scenario.
- **Decision Tree:** Slightly outperformed KNN but still underperformed with **72.84%** accuracy and an F-measure of **0.4153**, showing it was not very effective on this dataset either.

V.4.2.2 Key Findings

The key findings of Experiment 2 reveal important insights into the performance of various classifiers when used with features extracted by the VGG-16 deep learning model on two different MRI brain tumor datasets:

- KNN and SVM performed better on Dataset 1 (binary classification), with KNN achieving the highest accuracy.
- DRB outperformed all classifiers on Dataset 2 (multi-class classification) with the best accuracy.
- Decision Tree consistently underperformed across both datasets, particularly in terms of precision and F-measure.
- Overall, DRB and KNN were the most effective classifiers depending on the dataset, while Decision Tree lagged behind.

These findings highlight the idea that the performance of classifiers is highly dependent on the nature of the dataset and the complexity of the classification task. KNN and SVM excel in simpler, binary classification tasks like Dataset 1, while DRB is more robust in multi-class scenarios like Dataset 2. Decision Tree underperforms due to its overfitting tendencies and difficulty handling complex, high-dimensional features. The

combination of high-dimensional features extracted by VGG-16 and the intricacies of MRI brain tumor classification means that DRB's rule-based approach is more effective for handling complex tasks, while traditional classifiers like KNN and SVM excel in simpler cases.

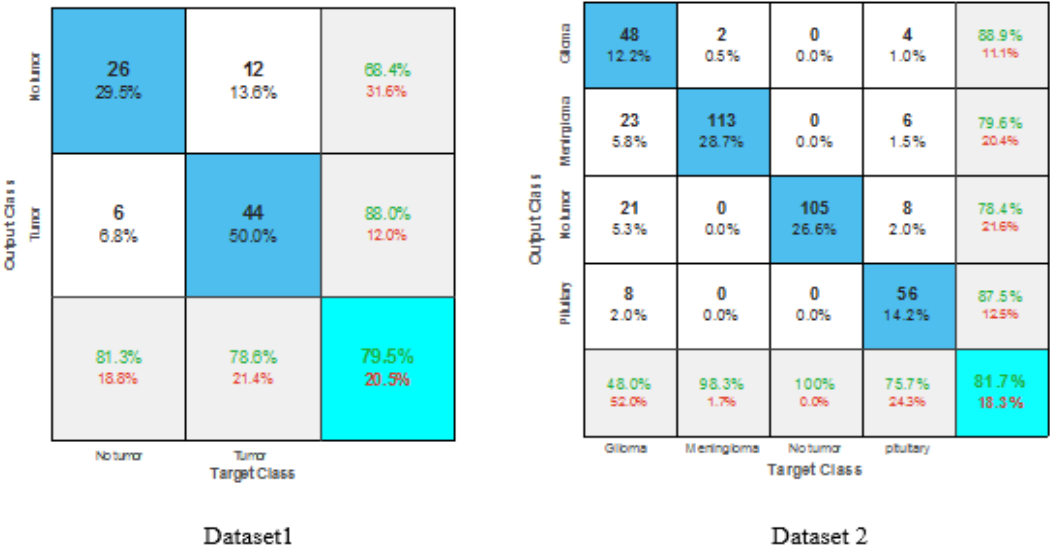


Figure V-7: Confusion matrix of DRB with data 1 and Data 2.

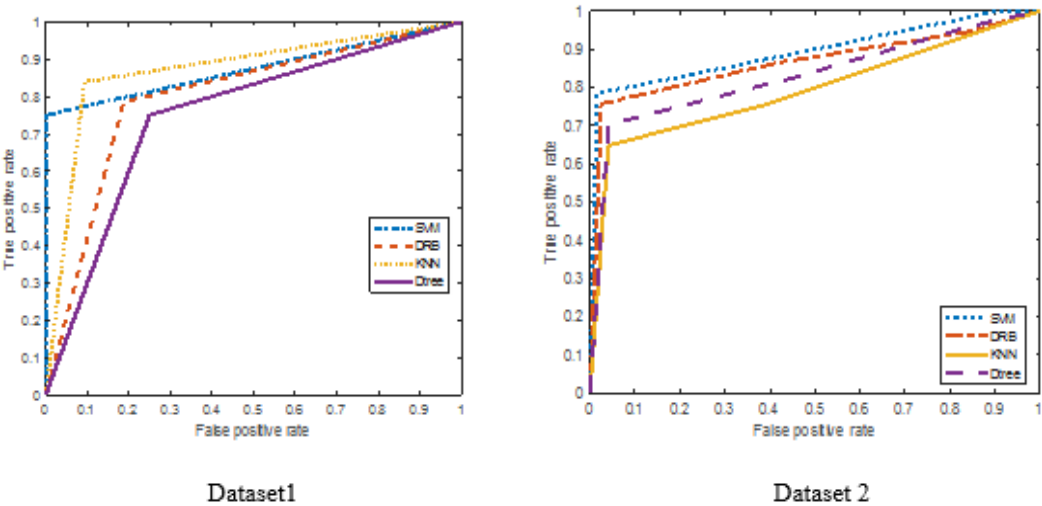


Figure V-8: ROC curves of dataset 1 and dataset

V.4.3 Experiment 3: ResNet-50 with 4 different classifiers

In **Experiment 3**, ResNet-50, a deep convolutional neural network, was used in conjunction with four different classifiers. ResNet-50 is designed to process RGB images of 224x224 pixels, so as part of the experimental setup, all grayscale images were resized and converted to RGB format to meet this requirement.

The architecture of ResNet-50, detailed in **Table V.7**, highlights the different layers of ResNet-50, including the feature maps, kernel sizes, strides, and padding. A key strength of ResNet-50 lies in its residual blocks, which facilitate the efficient training of deep networks by mitigating the vanishing gradient problem. By leveraging its ability to extract high-level features, ResNet-50 serves as a powerful feature extractor for training and evaluating four classifiers: SVM, KNN, Decision Tree, and DRB.

Table V.7: Architecture of ResNet-50

Layer	Feature map	stride	Padding	Size
Input	1			$[224 \times 224 \times 3]$
Conv1	$7 \times 7 \times 3$	2	3	$[112 \times 112 \times 96]$
Maxpool1	3×3	2	-	$[56 \times 56]$
	$[1 \times 1 \text{conv}, 64], [3 \times 3 \text{conv}, 64], 1 \times 1 \text{conv}, 256]$	2	-	
Conv2	$[1 \times 1 \text{conv}, 64], [3 \times 3 \text{conv}, 64], 1 \times 1 \text{conv}, 256]$	1	-	$[56 \times 56]$
	$[1 \times 1 \text{conv}, 64], [3 \times 3 \text{conv}, 64], 1 \times 1 \text{conv}, 256]$	1	-	
	$[1 \times 1 \text{conv}, 128], [3 \times 3 \text{conv}, 128], 1 \times 1 \text{conv}, 512]$	2	-	
Conv3	$[1 \times 1 \text{conv}, 128], [3 \times 3 \text{conv}, 128], 1 \times 1 \text{conv}, 512]$	1	-	$[28 \times 28]$
	$[1 \times 1 \text{conv}, 128], [3 \times 3 \text{conv}, 128], 1 \times 1 \text{conv}, 512]$	1	-	
	$[1 \times 1 \text{conv}, 128], [3 \times 3 \text{conv}, 128], 1 \times 1 \text{conv}, 512]$	1	-	
	$[1 \times 1 \text{conv}, 256], [3 \times 3 \text{conv}, 256], 1 \times 1 \text{conv}, 1024]$	2	-	
	$[1 \times 1 \text{conv}, 256], [3 \times 3 \text{conv}, 256], 1 \times 1 \text{conv}, 1024]$	1	-	
Conv4	$[1 \times 1 \text{conv}, 256], [3 \times 3 \text{conv}, 256], 1 \times 1 \text{conv}, 1024]$	1	-	$[14 \times 14]$
	$[1 \times 1 \text{conv}, 256], [3 \times 3 \text{conv}, 256], 1 \times 1 \text{conv}, 1024]$	1	-	
	$[1 \times 1 \text{conv}, 256], [3 \times 3 \text{conv}, 256], 1 \times 1 \text{conv}, 1024]$	1	-	
	$[1 \times 1 \text{conv}, 256], [3 \times 3 \text{conv}, 256], 1 \times 1 \text{conv}, 1024]$	1	-	
	$[1 \times 1 \text{conv}, 512], [3 \times 3 \text{conv}, 512], 1 \times 1 \text{conv}, 2048]$	2	-	
Conv5	$[1 \times 1 \text{conv}, 512], [3 \times 3 \text{conv}, 512], 1 \times 1 \text{conv}, 2048]$	1	-	$[7 \times 7]$
	$[1 \times 1 \text{conv}, 512], [3 \times 3 \text{conv}, 512], 1 \times 1 \text{conv}, 2048]$	1	-	
Average pool	7×7	7	-	$[1 \times 1]$
Fc1000				1000

V.4.3.1 Analysis of Results

The results in **Table V.8** compare the performance of ResNet-50 for feature extraction with four different classifiers (DRB, SVM, KNN, and Decision Tree) across two datasets. The performance is evaluated in terms of **accuracy**, **sensitivity**, **specificity**, **precision**, and **F-measure**.

Table V.8: Comparative performance of ResNet 50 with 4 different classifiers

ResNet-50 with 4 different classifiers						
Data set	Architecture	Accuracy	Sensitivity	Specificity	Precision	F-measure
Data set1	DRB	82.95%	0.8125	0.8393	0.7429	0.7761
	SVM	78.41%	0.8125	0.7679	0.6667	0.7324
	KNN	79.55%	0.8750	0.7500	0.6667	0.7568
	Decision Tree	72.73%	0.7188	0.7321	0.6053	0.6571
Data set2	DRB	78.17%	0.2900	0.9490	0.6591	0.4028
	SVM	77.16 %	0.3000	0.9320	0.6000	0.4000
	KNN	62.18 %	0.4100	0.6939	0.3130	0.3550
	Decision Tree	68.78 %	0.2800	0.8265	0.3544	0.3128

From this **Table V.8**, we can draw the following observations:

1- Performance on Dataset 1

- **DRB (82.95% accuracy)** provides the best overall performance, showcasing a balanced trade-off between precision (0.7429) and sensitivity (0.8125). The F-measure of 0.7761 reflects a good balance between precision and recall, making DRB the most effective classifier for this dataset.
- **SVM (78.41% accuracy)** follows DRB closely, performing well in terms of sensitivity (0.8125) but showing a lower precision (0.6667). The F-measure is lower than DRB at 0.7324, indicating that SVM struggles slightly in maintaining a balance between correct classifications and false positives.
- **KNN (79.55% accuracy)** performs reasonably well with decent sensitivity (0.8750) but has a lower precision (0.6667). Its F-measure of 0.7568 indicates a better balance compared to SVM.

- **Decision Tree** (72.73% accuracy) shows the lowest performance across all metrics for Dataset 1, with the lowest precision (0.6053) and F-measure (0.6571), indicating it is less reliable for this dataset.

2- Performance on Dataset 2

- **DRB** (78.17% accuracy) again performs the best in terms of accuracy but shows a significant drop in sensitivity (0.2900) compared to Dataset 1. The precision (0.6591) is relatively high, but the F-measure (0.4028) suggests a weak balance between precision and recall, indicating DRB's classification is less consistent in Dataset 2.
- **SVM** (77.16% accuracy) performs similarly to DRB, with a slightly higher sensitivity (0.3000) but comparable precision (0.6000). Its F-measure (0.4000) reflects that it also struggles with maintaining balance in this dataset.
- **KNN** (62.18% accuracy) exhibits the lowest accuracy in Dataset 2. With a lower sensitivity (0.4100) and precision (0.3130), KNN seems to perform poorly in extracting meaningful features from this dataset.
- **Decision Tree** (68.78% accuracy) performs slightly better than KNN but still lags in precision (0.3544) and F-measure (0.3128), making it less effective for this dataset as well.

V.4.3.2 Key Findings

The key findings from Experiment 3 provide critical insights into the effectiveness of the ResNet-50 architecture when paired with various classifiers (SVM, KNN, Decision Tree, and DRB) in the context of MRI brain tumor classification. This analysis highlights how these classifiers utilize the high-dimensional features extracted from ResNet-50, revealing their performance differences across two distinct datasets.

- DRB outperforms the other classifiers in terms of accuracy in both datasets, but its sensitivity drops significantly in Dataset 2, indicating a reduced ability to correctly classify positive samples in this dataset.
- SVM and KNN generally perform reasonably well, but their precision and F-measure fluctuate between datasets, showing they are less consistent than DRB.
- Decision Tree consistently underperforms compared to the other classifiers, particularly in Dataset 1, where it exhibits the lowest precision and F-measure.

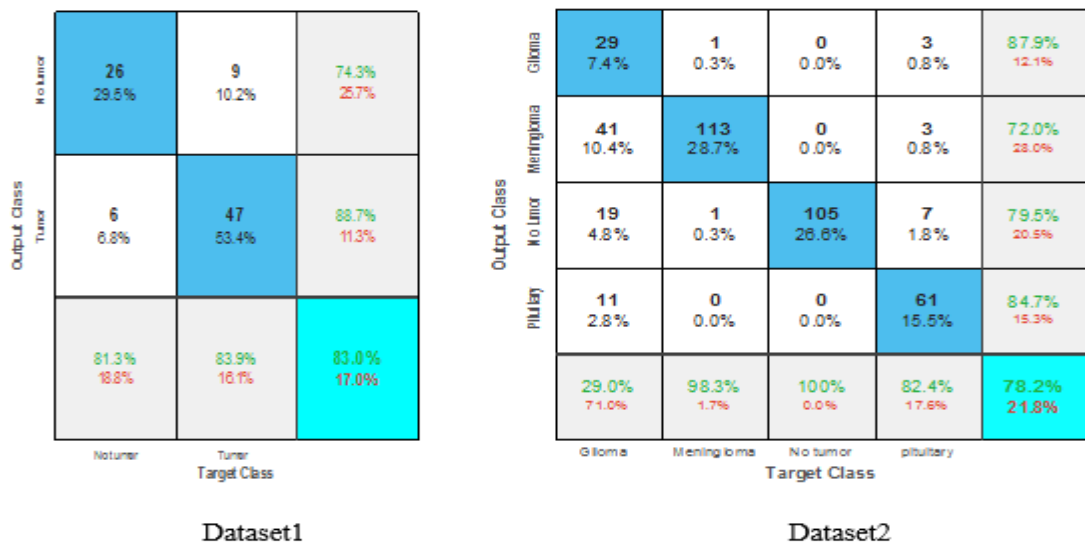


Figure V-9 : Confusion matrix of DRB with data 1 and Data 2.

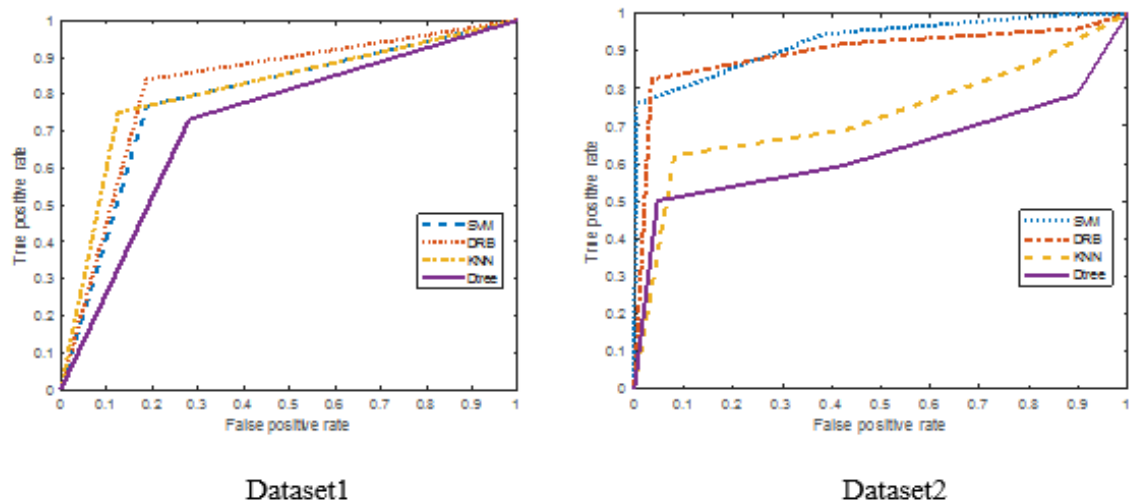


Figure V-10: ROC curves of dataset 1 and dataset 2

The results indicate that DRB consistently outperforms the other classifiers in terms of accuracy for both datasets, although it experiences a noticeable decline in sensitivity when transitioning from Dataset 1 to Dataset 2. This suggests that while DRB excels in overall classification performance, it may struggle to correctly identify positive samples in more complex scenarios. In contrast, SVM and KNN demonstrate reasonably competitive performance but exhibit variability in precision and F-measure across datasets, indicating a lack of consistency in their classification abilities. Meanwhile, the Decision Tree classifier consistently underperformed relative to the others, particularly in Dataset 1, where it recorded the lowest precision and F-measure.

V.4.4 Experiment 4: ResNet-18 with 4 different classifiers

In Experiment 4, the pre-trained ResNet-18 model is used to extract feature vectors from images for classification tasks. The features are taken from the "pool5" layer, the last layer before the classification head. Since ResNet-18 requires input images of size 224x224 pixels in RGB format, all images are resized and converted as needed. After extracting the features, four different classifiers are used to perform the classification, with each classifier fine-tuned for optimal performance. This approach leverages the power of deep feature extraction from ResNet-18 alongside traditional classifiers. a breakdown of the ResNet-18 layers is shown in **Table V.9**.

Table V.9: Details of ResNet-18 layers

Layer	Kernel size	Stride	Output size
Input		-	$[224 \times 224 \times 3]$
Conv1	$11 \times 11 \times 3$	2	$[112 \times 112 \times 64]$
Max-pool	3×3	2	$[56 \times 56 \times 64]$
Conv2	$3 \times 3 \times 64$	-	$[56 \times 56 \times 64]$
	$3 \times 3 \times 64$	-	$[56 \times 56 \times 64]$
Conv3	$3 \times 3 \times 128$	-	$[28 \times 28 \times 128]$
	$3 \times 3 \times 128$	-	$[28 \times 28 \times 128]$
Conv4	$3 \times 3 \times 256$	-	$[14 \times 14 \times 256]$
	$3 \times 3 \times 256$	-	$[14 \times 14 \times 256]$
Conv5	$3 \times 3 \times 512$	-	$[7 \times 7 \times 512]$
	$3 \times 3 \times 512$	-	$[7 \times 7 \times 512]$
Average pool	7×7	-	$[1 \times 1 \times 512]$
Fully connected			1000
Softmax			1000

Table V.10 compares the performance of the ResNet-18 feature extractor combined with four different classifiers SVM, KNN, Decision Tree, and DRB across two datasets, Dataset1 and Dataset2. The performance metrics include Accuracy, Sensitivity, Specificity, Precision, and F-measure.

V.4.4.1 Analysis of Results

The analysis is focused on key performance metrics such as accuracy, sensitivity, specificity, precision, and F-measure. These metrics provide insights into how well each classifier handles different aspects of classification, including the ability to correctly identify positive and negative instances and maintain a balance between precision and recall. By comparing the results across Dataset1 and Dataset2, this analysis aims to determine the

strengths and weaknesses of each classifier in handling the high-dimensional features extracted by ResNet-18.

Table V.10: Comparative performance of ResNet18 with 4 different classifiers

ResNet18 with 4 different classifiers						
Dataset	Architecture	Accuracy	Sensitivity	Specificity	Precision	F-measure
Dataset1	DRB	85.22%	0.9063	0.8214	0.7436	0.8169
	SVM	77.27%	0.6250	0.8571	0.7143	0.6667
	KNN	81.82%	0.7813	0.8393	0.7353	0.7576
	Decision Tree	69.32%	0.9063	0.7514	0.5472	0.6824
Dataset2	DRB	80.46%	0.3200	0.9694	0.7805	0.4539
	SVM	75.89%	0.2900	0.9184	0.5472	0.3791
	KNN	65.74%	0.3900	0.7483	0.3451	0.3662
	Decision Tree	73.35%	0.3200	0.8741	0.4638	0.3787

1. Dataset1 Performance :

- **Accuracy:** DRB achieves the highest accuracy at **85.22%**, followed by SVM at **77.27%**, KNN at **81.82%**, and Decision Tree at **69.32%**. This indicates that DRB is the most effective classifier for this dataset.
- **Sensitivity (Recall):** DRB has the highest sensitivity (**0.9063**), suggesting it is most effective at correctly identifying positive instances. The Decision Tree shows the lowest sensitivity (**0.6250**).
- **Specificity:** SVM performs best in terms of specificity (**0.8571**), which means it is most accurate at identifying negative instances, while Decision Tree has the lowest specificity (**0.5472**).
- **Precision:** DRB also leads in precision (**0.8169**), meaning it has the highest rate of correct positive predictions among the classifiers. Decision Tree has the lowest precision (**0.6824**).
- **F-measure:** DRB achieves the highest F-measure (**0.7576**), reflecting a good balance between precision and recall. The Decision Tree has the lowest F-measure (**0.6824**).

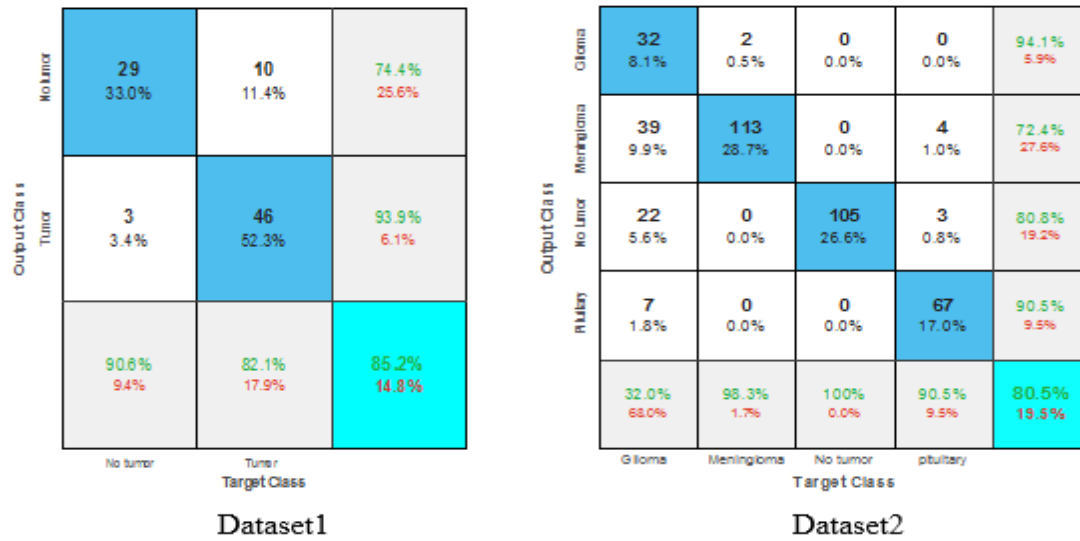


Figure V-11: Confusion matrix of DRB with data 1 and Data 2.

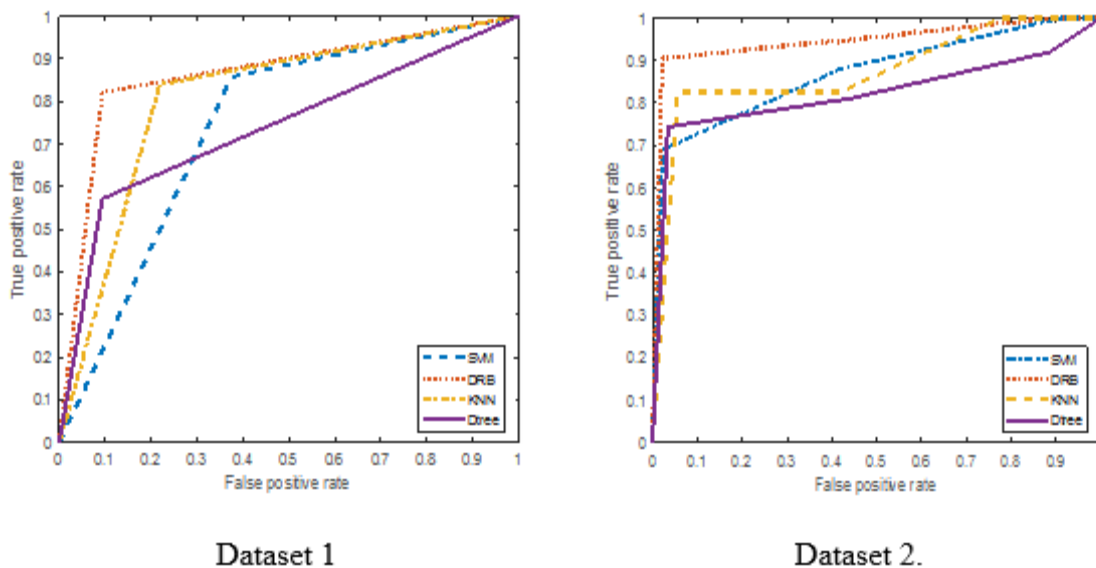


Figure V-12: ROC curves of dataset 1 and dataset 2.

Dataset2 Performance :

- **Accuracy:** DRB leads with **80.46%**, followed by Decision Tree (**73.35%**), SVM (**75.89%**), and KNN (**65.74%**). This indicates DRB is the most accurate classifier for Dataset2 as well.
- **Sensitivity (Recall):** All classifiers have relatively low sensitivity on Dataset2, with DRB and Decision Tree both at **0.3200**, which indicates a poorer ability to identify positive instances.

- **Specificity:** DRB shows the highest specificity (**0.9694**), indicating it is the most effective at identifying negative instances, while KNN has the lowest specificity (**0.7483**).
- **Precision:** DRB also leads in precision (**0.4539**), showing it is better at positive prediction accuracy compared to others. KNN has the lowest precision (**0.3662**).
- **F-measure:** DRB again performs best with an F-measure of **0.3787**, suggesting the most balanced performance. KNN has the lowest F-measure (**0.3662**).

V.4.4.2 Key findings

The key findings from Experiment 4 highlight the comparative performance of ResNet-18 features with different classifiers (DRB, SVM, KNN, and Decision Tree) on two MRI brain tumor datasets:

- **DRB consistently performs best** across both datasets, excelling in accuracy, sensitivity, precision, and F-measure. Its performance indicates that DRB is well-suited for utilizing ResNet-18 features effectively, making it the most robust classifier for this task.
- **SVM exhibits strong specificity** in Dataset1 but shows weaker performance in other metrics, suggesting that while it is reliable at identifying negative instances, it is less effective overall.
- **KNN generally underperforms** across both datasets, particularly in sensitivity and precision, indicating that it struggles with this classification task and may not be suitable for the problem at hand.
- **Decision Tree shows inconsistent performance**, with lower scores in various metrics, making it less reliable compared to DRB and SVM in these experiments.

DRB is generally the most reliable and robust classifier, although performance can vary depending on the dataset and classification task.

V.4.5 Comprehensive Analysis of Results

To comprehensively evaluate the classifiers (DRB, SVM, KNN, Decision Tree) and deep learning features (AlexNet, VGG-16, ResNet-50, ResNet-18) used in our experiments on MRI brain tumor classification, we compare their performance metrics, highlight their strengths and limitations, and provide insights into their behavior across various conditions.

This section discusses the results in terms of both the classifiers and the deep feature extractors to offer an in-depth interpretation.

V.4.5.1 Classifiers: Strengths and Challenges

Classifier selection is a critical step in any machine learning project, particularly in classification tasks. The choice of classifier can significantly impact the accuracy, efficiency, and interpretability of the model. A well-chosen classifier can lead to highly accurate predictions, while a poorly chosen one can result in suboptimal performance. **Table V.11** provides a comparative analysis of various machine learning classifiers (DRB, SVM, KNN and Decision tree) used in this research, highlighting their strengths and weaknesses.

By understanding the strengths and limitations of each classifier, we can make informed decisions when selecting the most suitable algorithm for a specific task.

- **Deep Rule-Based**

The DRB classifier excels with consistently high performance, demonstrating strong accuracy, sensitivity, specificity, and precision across various datasets and deep learning features. It effectively integrates the strengths of deep learning feature extraction with rule-based logic, enhancing its ability to classify complex patterns, such as those found in MRI brain tumor images. This combination also contributes to its robustness in detecting tumors while minimizing false positives and negatives. However, DRB's complexity can be a drawback, as its implementation and tuning require more effort due to the intricate integration of deep learning and rule-based components.

- **Support Vector Machine**

SVM offers strong sensitivity and specificity, effectively distinguishing between classes, especially with a clear margin, making it a reliable choice in some cases. It also demonstrates good generalization when a suitable kernel and parameters are selected, particularly in complex datasets. However, its performance is highly sensitive to the choice of kernel and parameter tuning, which can be challenging. Additionally, SVM may face scalability issues, performing less effectively with very large datasets or high-dimensional feature spaces unless properly optimized.

- **K-Nearest Neighbors**

KNN is a simple and intuitive algorithm that is easy to understand and implement, with no training phase required. Its flexibility allows it to handle various types of data and

feature distributions effectively. However, KNN struggles with high-dimensional data due to the curse of dimensionality, which can significantly degrade its performance. Additionally, its effectiveness is highly sensitive to the choice of K and the distance metric, requiring careful tuning for optimal results.

- **Decision Tree**

Decision Tree algorithms are highly interpretable, providing clear decision rules that are easy to understand. They can effectively model non-linear relationships and feature interactions. However, they are prone to overfitting, especially when dealing with complex datasets or deep trees. Additionally, Decision Trees can be unstable, as small changes in the data can significantly alter the structure of the tree, impacting its performance.

Table V.11: Comparison of different classifiers

<i>Classifier</i>	<i>Strengths</i>	<i>Weaknesses</i>
DRB	<ul style="list-style-type: none"> • High Performance • Combines the power of deep learning features with rule-based logic • Robustness in detecting tumors and avoiding false positives/negatives. 	<ul style="list-style-type: none"> • Complexity
SVM	<ul style="list-style-type: none"> • High Sensitivity and Specificity • Performs well with a well-chosen kernel and parameters 	<ul style="list-style-type: none"> • Parameter Sensitivity • less effective with very large datasets
KNN	<ul style="list-style-type: none"> • Simple and Intuitive • Flexibility: Can handle various types of data 	<ul style="list-style-type: none"> • Struggles with high-dimensions • Parameter Sensitivity
DecisionTree	<ul style="list-style-type: none"> • Interpretability • Handles Non-linearity 	<ul style="list-style-type: none"> • Overfitting • Less Stability

V.4.5.2 Deep Learning Features

Feature extraction is a fundamental step in many machine learning and computer vision tasks, including image classification. It involves transforming raw data into meaningful features that can be used to train a classifier. The choice of feature extractor can significantly impact the performance of a classification model.

Table V.13 provides a comparative analysis of several popular feature extraction architectures used in this research (AlexNet, VGG-16, ResNet-50, and ResNet-18). These architectures have been instrumental in advancing the field of computer vision, particularly in image classification tasks. The table delves into the strengths and weaknesses of each architecture, considering factors such as:

- **Architectural Depth:** The number of layers in the network.
- **Feature Extraction Capability:** The ability to extract relevant and discriminative features from images.
- **Computational Cost:** The computational resources required to train and deploy the model.
- **Overfitting Potential:** The tendency of the model to overfit the training data.

By understanding the trade-offs between these factors, we can make informed decisions when selecting the most suitable feature extractor.

- **AlexNet**

AlexNet is well-known for pioneering deep learning in image classification and provides effective feature extraction, making it a good choice for initial experiments and simpler datasets. Its relatively shallow architecture results in lower computational costs compared to deeper models. However, this limited depth also restricts its ability to extract complex features, which can be a disadvantage when working with more intricate or challenging datasets.

- **VGG-16**

VGG-16 features a deep architecture with more layers than AlexNet, enabling it to capture more complex features and generally achieve better feature representations and classification performance. However, this deeper architecture comes with higher computational costs due to the increased number of parameters. Additionally, VGG-16 is more prone to overfitting, particularly on smaller datasets, unless regularization techniques are applied effectively.

- **ResNet-50**

ResNet, through its use of residual learning, effectively addresses the problem of vanishing or exploding gradients, allowing for the successful training of very deep networks. This architecture excels at extracting complex features, resulting in strong performance

across a wide range of tasks. However, the depth and use of residual connections make ResNet more complex and computationally intensive compared to simpler models.

- **ResNet-18**

ResNet-18 leverages residual connections to enhance training and performance in deep networks, benefiting from residual learning. It strikes a good balance between depth and complexity, being shallower than ResNet-50, which makes it less computationally demanding while still maintaining the advantages of residual learning. However, its shallower architecture may limit its ability to capture as complex features as ResNet-50, though it remains effective for many applications.

The analysis highlights that deeper architectures like VGG-16 and ResNet generally perform better in extracting features compared to older, shallower models like AlexNet. ResNet-50, in particular, excels at feature extraction due to its deeper layers, though it can be computationally intensive. Classifiers like SVM perform well with deep features, offering high sensitivity, but models like KNN and Decision Trees can struggle with high-dimensional or complex data, leading to inconsistent results. Performance also varies depending on the dataset, with simpler datasets benefiting more from deeper models, while complex or imbalanced datasets present greater challenges. In conclusion, choosing the right combination of architecture and classifier is crucial for achieving optimal results.

Table V.12: Performance Comparison of DRB with Different Deep Features

DRB with 4 different deep features						
Dataset	Architecture	Accuracy	Sensitivity	Specificity	Precision	F-measure
Dataset1	AlexNet	85.23%	0.9375	0.8036	0.7317	0.8219
	VGG-16	79.55%	0.8125	0.7857	0.6842	0.7429
	ResNet50	82.95%	0.8125	0.8393	0.7429	0.7761
	ResNet18	85.22%	0.9063	0.8214	0.7436	0.8169
Dataset2	AlexNet	79.19%	0.3500	0.9422	0.6131	0.4605
	VGG-16	81.73%	0.4800	0.9422	0.7059	0.5714
	ResNet50	78.17%	0.2900	0.9490	0.6591	0.4028
	ResNet18	80.46%	0.3200	0.9694	0.7805	0.4539

Table V.13: Comparison of Feature Extractors

<i>Feature Extractor</i>	<i>Strenghts</i>	<i>Weaknesses</i>
<i>AlexNet</i>	<ul style="list-style-type: none"> • Effective Feature Extraction for simpler datasets. • Lower Computational Cost 	<ul style="list-style-type: none"> • Limited Depth, which limit its capabilities for complex datasets
<i>VGG-16</i>	<ul style="list-style-type: none"> • Deep Architecture • capture more complex features • Improved Performance 	<ul style="list-style-type: none"> • Computational Cost • Overfitting Risk
<i>ResNet-50</i>	<ul style="list-style-type: none"> • Residual Learning • Effective Feature Extraction 	<ul style="list-style-type: none"> • Complexity due to the depth and residual connections.
<i>ResNet-18</i>	<ul style="list-style-type: none"> • Residual Connections which improve training and performance • Balancing Depth and Complexity 	<ul style="list-style-type: none"> • Less Deep: Might not capture as complex features as ResNet-50

V.5 Comparison between the two contributions

Our contributions focus on improving brain tumor classification using the DRB classifier with two distinct approaches: texture-based descriptors (BSIF/B-BSIF) and deep feature extraction.

Contribution 1 (DRB with BSIF/B-BSIF) achieves strong classification performance, with accuracy reaching 84.30% and 84.73%, sensitivity at 86.44% and 87.57%, and specificity at 83.66% and 83.87%. These results demonstrate the effectiveness of BSIF/B-BSIF compared to traditional feature descriptors like LBP and LPQ. However, while impressive for texture-based methods, the accuracy and sensitivity are slightly lower than deep learning-based approaches, particularly with deeper architectures like ResNet.

Contribution 2 (DRB with deep features) leverages feature extraction from deep networks, resulting in improved classification performance. On Dataset 1, DRB with ResNet18 and AlexNet achieves accuracy of 85.22% and 85.23%, with significantly higher sensitivity (93.75% for AlexNet and 90.63% for ResNet18) and strong specificity (83.93% for ResNet50). On Dataset 2, while accuracy ranges from 79.19% to 81.73%, deep features maintain excellent specificity, especially with ResNet (up to 96.94%), highlighting their robustness in handling complex or imbalanced datasets. The higher sensitivity and precision of deep features make this approach more effective in detecting subtle tumor characteristics.

Based on the performance results achieved in the two contributions, Contribution 2 (DRB with deep features) appears to be more effective, especially when considering both datasets.

V.6 High Performance of the DRB Classifier

The high performance of the DRB classifier in our MRI brain tumor classification experiments can be explained and justified by several key factors related to its methodology and how it interacts with deep learning features. The following is a comprehensive analysis:

V.6.1 Characteristics of DRB Classifier

DRB classifier combines deep learning features with a rule-based system to enhance classification performance. It leverages both learned features from deep neural networks and predefined rules to make predictions. The key characteristics that contribute to its high performance include:

1. Feature Extraction from Deep Learning

DRB often integrates with deep learning models (like AlexNet, VGG-16, ResNet, etc.) to extract high-level features from MRI images. The deep learning component handles the complex feature extraction process, capturing intricate patterns and relationships within the images.

2. Rule-Based Classification

The DRB classifier utilizes learned rules tailored to the specific characteristics of brain tumors, which allows for more accurate classification. By incorporating rules that reflect domain knowledge and tumor-specific patterns, DRB enhances the discriminative power of the classification process.

3. Combining Strengths

The DRB classifier leverages robust feature representations from deep learning models and refines them with rule-based logic, resulting in improved performance. This combination effectively balances generalization from deep learning with precision from rule-based decisions, leading to robust classification outcomes.

V.6.2 Performance Metrics of the DRB Classifier

- **High Accuracy:** DRB's integration with deep learning models allows it to benefit from high-quality feature extraction, leading to accurate tumor classification. For example, in experiments with different datasets, DRB achieved high accuracy (e.g., 85.23% with AlexNet) due to its ability to leverage the deep features effectively.
- **High Sensitivity:** DRB's high sensitivity indicates its effectiveness in detecting tumors. This is crucial for medical diagnosis, where detecting all possible positive cases is essential. The rule-based component helps in refining the detection process by applying specific rules to the extracted features, thus enhancing sensitivity.
- **High Specificity:** DRB's high specificity reflects its capability to correctly identify non-tumor regions. The rule-based system contributes to this by applying logical rules that minimize false positives, ensuring accurate identification of non-tumor cases.
- **High Precision:** DRB's precision in classification indicates that when it predicts a tumor, it is usually correct. This is achieved through the combination of learned deep features and rule-based refinement, reducing the likelihood of false positives.

V.6.3 Comparison with Other Classifiers

- **SVM:** While SVM performs well, DRB's ability to incorporate domain-specific rules on top of deep features often results in better performance in complex scenarios like tumor detection.
- **KNN:** DRB outperforms KNN, especially in high-dimensional feature spaces, due to its rule-based approach that complements the feature extraction process.
- **Decision Trees:** DRB's performance is generally superior to decision trees because it avoids issues like overfitting and handles complex feature interactions more effectively through its rule-based system.

In summary, the high performance of the DRB classifier in MRI brain tumor classification can be attributed to its unique combination of deep learning feature extraction and rule-based logic. The deep learning models (e.g., AlexNet, VGG-16, ResNet) provide robust, high-level features from MRI images, capturing intricate patterns. The rule-based system then applies specific rules to these features, enhancing the discriminative power and precision of the classification. This synergy allows DRB to achieve high accuracy and sensitivity, crucial for detecting tumors, and high specificity, minimizing false positives by

accurately identifying non-tumor regions. Compared to classifiers like SVM, KNN, and Decision Trees, DRB excels by combining deep feature learning with domain-specific rules, offering superior performance in complex, high-dimensional data.

V.7 Conclusion

In this chapter, we introduced and validated our second contribution, which focused on leveraging the DRB classifier with deep feature extraction. Various deep learning architectures, including AlexNet, VGG-16, ResNet-50, and ResNet-18, were utilized to extract meaningful features, which were subsequently classified using the DRB approach. Experimental results demonstrated the superior performance of the DRB classifier when integrated with deep learning, achieving high accuracy, sensitivity, and specificity across multiple datasets.

In conclusion, both contributions presented innovative methodologies that significantly enhanced the accuracy and robustness of brain tumor classification. The findings confirm that integrating rule-based systems with deep learning features provides a powerful and effective approach for medical image analysis.

Conclusion and Perspectives

The central goal of this thesis was to improve the classification of brain tumors using MRI images by leveraging both hand-crafted feature extraction and deep feature-based approaches. The study began with an overview of MRI imaging and its crucial role in brain tumor diagnosis, followed by an extensive discussion of machine learning (ML) and deep learning (DL) paradigms. The fundamental principles of deep learning, its architectures, and its impact on medical image analysis were reviewed to establish the theoretical foundation of the research. The classification of brain tumors was examined in detail, highlighting the taxonomy of MRI classification algorithms, the classification process, and the importance of explainability in medical AI models.

The research introduced two key contributions aimed at improving MRI-based brain tumor classification. The first was the development and evaluation of the DRB-BSIF classifier, which integrates Binarized Statistical Image Features (BSIF) with the Deep Rule-Based (DRB) model. This hybrid approach enhanced interpretability, an essential aspect of medical AI models, ensuring transparency in decision-making. The experimental results demonstrated significant improvements in classification accuracy, but the performance remained somewhat constrained by the limitations of hand-crafted features, which may not fully capture high-level data representations.

To address this limitation, the second contribution extended the use of DRB classification with deep feature extraction. Deep learning architectures, such as AlexNet, VGG-16, ResNet-50, and ResNet-18, were explored to extract robust feature representations. A comparative analysis between the two approaches confirmed that deep features combined with DRB outperformed traditional hand-crafted feature-based methods, achieving a strong balance between interpretability, computational efficiency, and predictive performance.

Despite these advancements, certain challenges remain. The combination of deep learning and rule-based systems introduces increased computational complexity and implementation challenges. The risk of overfitting, especially on smaller datasets, necessitates the adoption of more effective regularization techniques. Additionally, the generalizability of the DRB classifier to larger and more diverse datasets requires further validation to ensure broader applicability in real-world clinical settings.

Future research directions include:

- **Enhancing Model Explainability:** Given the critical nature of medical diagnosis, integrating explainable AI (XAI) techniques into the DRB classifier could further improve trust and adoption in clinical environments.
- **Dataset Expansion and Augmentation:** Training the DRB classifier on larger and more diverse multi-modal datasets can improve its robustness and generalization.
- **Optimizing Computational Efficiency:** Reducing the computational cost of DRB-based classification while maintaining high accuracy remains an important challenge.
- **Optimized Feature Selection and Dimensionality Reduction:** Given the complexity of deep learning models, especially when dealing with high-dimensional deep features, selecting the most relevant features becomes crucial. Future work could explore feature selection or dimensionality reduction techniques to identify the most discriminative features for classification. This could reduce the computational burden and improve the efficiency of the system.
- **Hybrid and Transformer-Based Models:** Exploring hybrid models that combine DRB with transformer architectures or self-supervised learning techniques could further improve classification performance.
- **Clinical Deployment:** Developing a real-time, deployable system based on the DRB classifier will be essential for practical integration into healthcare workflows.

In conclusion, this thesis contributes to the advancement of AI-driven medical imaging, demonstrating that the combination of rule-based classification and deep learning offers a promising approach to MRI brain tumor classification. By bridging the gap between accuracy, interpretability, and clinical applicability, this research paves the way for future innovations in computer-aided diagnosis (CAD) systems and AI-assisted medical decision-making.

References

- [1] M. Lodge, "The role of the Commonwealth in the wider cancer control agenda," *Lancet Oncol.*, vol. 21, no. 7, pp. 879–881, 2020.
- [2] M. M. Badža and M. Č. Barjaktarović, "Classification of Brain Tumors from MRI Images Using a Convolutional Neural Network," *Appl. Sci.*, vol. 10, no. 6, p. 1999, 2020.
- [3] K. C. Burçak and H. Uğuz, "A new hybrid breast cancer diagnosis model using deep learning model and relieff," 2022.
- [4] I. U. Haq, "An overview of deep learning in medical imaging," *arXiv Prepr. arXiv2202.08546*, 2022.
- [5] J. Cheng *et al.*, "Enhanced performance of brain tumor classification via tumor region augmentation and partition," *PLoS One*, vol. 10, no. 10, p. e0140381, 2015.
- [6] X. Hu *et al.*, "Coarse-to-fine adversarial networks and zone-based uncertainty analysis for NK/T-cell lymphoma segmentation in CT/PET images," *IEEE J. Biomed. Heal. informatics*, vol. 24, no. 9, pp. 2599–2608, 2020.
- [7] X. Zhu, H.-I. Suk, Y. Zhu, K.-H. Thung, G. Wu, and D. Shen, "Multi-view classification for identification of Alzheimer's disease," in *Machine Learning in Medical Imaging: 6th International Workshop, MLMI 2015, Held in Conjunction with MICCAI 2015, Munich, Germany, October 5, 2015, Proceedings 6*, 2015, pp. 255–262.
- [8] T. Dhar, N. Dey, S. Borra, and R. S. Sherratt, "Challenges of deep learning in medical image analysis—improving explainability and trust," *IEEE Trans. Technol. Soc.*, vol. 4, no. 1, pp. 68–75, 2023.
- [9] H. Chellakh, A. Moussaoui, and A. Attia, "Improved Binarized Statistical Image Features for MRI Brain Tumor Identification and Classification," in *2024 International Conference on Information and Communication Technologies for Disaster Management (ICT-DM)*, 2024, pp. 1–7.
- [10] H. Chellakh, A. Moussaoui, A. Attia, and Z. Akhtar, "MRI Brain Tumor Identification and Classification Using Deep Learning Techniques.," *Ingénierie des Systèmes d'Information*, vol. 28, no. 1, 2023.
- [11] Wikipedia, "Brain tumor," 2002, February 25. .
- [12] C. C. Victoria, "Understanding brain tumours: types, symptoms, and treatment," 2024, June 25. [Online]. Available: https://www.cancervic.org.au/cancer-information/types-of-cancer/brain_tumour/brain-tumours-overview.html. [Accessed: 30-Jun-2024].
- [13] AANS, "Brain Tumors," 2024, June 25. [Online]. Available: <https://www.aans.org/patients/conditions-treatments/brain-tumors/>. [Accessed: 30-Jun-2024].
- [14] M. Clinic, "Brain tumor - Symptoms and causes. (n.d.)." [Online]. Available: <https://www.mayoclinic.org/diseases-conditions/brain-tumor/symptoms->

-
- causes/syc-20350084. [Accessed: 05-Sep-2024].
- [15] J. Hopkins, "Brain tumor types," 2021, November 8. [Online]. Available: <https://www.hopkinsmedicine.org/health/conditions-and-diseases/brain-tumor/brain-tumor-types>. [Accessed: 05-Sep-2024].
 - [16] P. Pillay, "Brain & Spine Tumors / Cancers," 2024, December 13. [Online]. Available: <https://singaporebrain.org/brain/brain-spine-tumors/>. [Accessed: 05-Sep-2024].
 - [17] P. G. Frija and B. Mazoyer, "L'imagerie médicale," *Fond. Rech. médicale*, 2002.
 - [18] P. J. Keller, J. P. Karis, E. K. Fram, J. E. Heiserman, and B. P. Drayer, "An alternative to GRASE: Toward spin-echo-like contrast with independent reconstruction of gradient-echo images," *Magn. Reson. Med.*, vol. 36, no. 5, pp. 804–808, 1996.
 - [19] K. V Dang, N., Tiwari, S., Khurana, M., & Arya, "Recent Advancements in Medical Imaging: a machine learning approach. In Studies in big data (pp. 189–212).," 2021.
 - [20] L. N. Tanenbaum, "Artificial intelligence and medical imaging: image acquisition and reconstruction," *Appl. Radiol.*, vol. 49, no. 3, pp. 34–35, 2020.
 - [21] S. E. Forshult, "Magnetic Resonance Imaging--MRI--An Overview," 2007.
 - [22] S. Currie, N. Hoggard, I. J. Craven, M. Hadjivassiliou, and I. D. Wilkinson, "Understanding MRI: basic MR physics for physicians," *Postgrad. Med. J.*, vol. 89, no. 1050, pp. 209–223, 2013.
 - [23] Uvaradweb, "Different imaging tests, explained. UVA Radiology and Medical Imaging Blog for Patients.," 2020, January 3. [Online]. Available: <https://blog.radiology.virginia.edu/different-imaging-tests-explained/>. [Accessed: 26-Jun-2024].
 - [24] M. Martucci *et al.*, "Magnetic resonance imaging of primary adult brain tumors: state of the art and future perspectives," *Biomedicines*, vol. 11, no. 2, p. 364, 2023.
 - [25] Triumri, "A Comprehensive Guide to Magnetic Resonance Imaging," 2024, June 27. [Online]. Available: <https://www.millenniummri.com/post/what-is-an-mri>. [Accessed: 30-Jun-2024].
 - [26] M. A. Brown and R. C. Semelka, *MRI: basic principles and applications*. John Wiley & Sons, 2011.
 - [27] V. P. B. Grover, J. M. Tognarelli, M. M. E. Crossey, I. J. Cox, S. D. Taylor-Robinson, and M. J. W. McPhail, "Magnetic resonance imaging: principles and techniques: lessons for clinicians," *J. Clin. Exp. Hepatol.*, vol. 5, no. 3, pp. 246–255, 2015.
 - [28] K. P. Andriole, "Image acquisition," in *PACS: A Guide to the Digital Revolution*, Springer, 2006, pp. 189–227.
 - [29] G. S. Tandel *et al.*, "A review on a deep learning perspective in brain cancer classification," *Cancers (Basel)*, vol. 11, no. 1, p. 111, 2019.
 - [30] A. Chahal and P. Gulia, "Machine learning and deep learning," *Int. J. Innov. Technol. Explor. Eng.*, vol. 8, no. 12, pp. 4910–4914, 2019.
 - [31] G. Zaharchuk, E. Gong, M. Wintermark, D. Rubin, and C. P. Langlotz, "Deep learning in neuroradiology," *Am. J. Neuroradiol.*, vol. 39, no. 10, pp. 1776–1784, 2018.
-

-
- [32] Y. LeCun, Y. Bengio, and G. Hinton, "Deep learning," *Nature*, vol. 521, no. 7553, pp. 436–444, 2015.
 - [33] B. Brenninkmeijer, A. De Vries, E. Marchiori, and Y. Hille, "On the generation and evaluation of tabular data using GANs," *PhD diss., Radboud Univ.*, 2019.
 - [34] P. P. Shinde and S. Shah, "A review of machine learning and deep learning applications," in *2018 Fourth international conference on computing communication control and automation (ICCUBEA)*, 2018, pp. 1–6.
 - [35] L. Deng, D. Yu, and others, "Deep learning: methods and applications," *Found. trends®in signal Process.*, vol. 7, no. 3--4, pp. 197–387, 2014.
 - [36] H. Wang and B. Raj, "On the origin of deep learning," *arXiv Prepr. arXiv1702.07800*, 2017.
 - [37] T. Hossain, F. S. Shishir, M. Ashraf, M. D. A. Al Nasim, and F. M. Shah, "Brain tumor detection using convolutional neural network," in *2019 1st international conference on advances in science, engineering and robotics technology (ICASERT)*, 2019, pp. 1–6.
 - [38] GeeksforGeeks, "Activation functions in Neural Networks," 2025, March 1. [Online]. Available: <https://www.geeksforgeeks.org/activation-functions-neural-networks/>. [Accessed: 04-Mar-2025].
 - [39] D. Lekkala, "Understanding different activation functions," 2023, August 15. [Online]. Available: <https://medium.com/@deepyachowdary/understanding-different-activation-functions-6aed5ed1c785>. [Accessed: 06-Mar-2025].
 - [40] D. B. Salvador, "A Guide into Activation Functions in Neural Networks.," 2024, May 3. [Online]. Available: <https://www.linkedin.com/pulse/guide-activation-functions-neural-networks-diego-bonilla-salvador-34lyc/>. [Accessed: 06-Mar-2025].
 - [41] Y. Pan, "Different Types of Neural Networks and Applications: Evidence from Feedforward, Convolutional and Recurrent Neural Networks."
 - [42] J.-G. Lee *et al.*, "Deep learning in medical imaging: general overview," *Korean J. Radiol.*, vol. 18, no. 4, pp. 570–584, 2017.
 - [43] A.-N. Sharkawy, "Principle of neural network and its main types," *J. Adv. Appl. & Comput. Math.*, vol. 7, pp. 8–19, 2020.
 - [44] M. Li, Y. Jiang, Y. Zhang, and H. Zhu, "Medical image analysis using deep learning algorithms," *Front. Public Heal.*, vol. 11, p. 1273253, 2023.
 - [45] D. Shen, G. Wu, and H.-I. Suk, "Deep learning in medical image analysis," *Annu. Rev. Biomed. Eng.*, vol. 19, pp. 221–248, 2017.
 - [46] G. Van Houdt, C. Mosquera, and G. Nápoles, "A review on the long short-term memory model," *Artif. Intell. Rev.*, vol. 53, no. 8, pp. 5929–5955, 2020.
 - [47] D. Saxena and J. Cao, "Generative adversarial networks (GANs) challenges, solutions, and future directions," *ACM Comput. Surv.*, vol. 54, no. 3, pp. 1–42, 2021.
 - [48] Y. Keneshloo, T. Shi, N. Ramakrishnan, and C. K. Reddy, "Deep reinforcement learning for sequence-to-sequence models," *IEEE Trans. neural networks Learn. Syst.*, vol. 31, no. 7, pp. 2469–2489, 2019.
-

-
- [49] R. Qamar and B. A. Zardari, "Artificial neural networks: An overview," *Mesopotamian J. Comput. Sci.*, vol. 2023, pp. 124–133, 2023.
 - [50] S. Ghosh, N. Das, I. Das, and U. Maulik, "Understanding deep learning techniques for image segmentation," *ACM Comput. Surv.*, vol. 52, no. 4, pp. 1–35, 2019.
 - [51] M. H. Hesamian, W. Jia, X. He, and P. Kennedy, "Deep learning techniques for medical image segmentation: achievements and challenges," *J. Digit. Imaging*, vol. 32, pp. 582–596, 2019.
 - [52] S. Saha, "A comprehensive guide to convolutional neural networks—the ELI5 way," *Toward. data Sci.*, vol. 15, p. 15, 2018.
 - [53] C. Shen, D. Nguyen, Z. Zhou, S. B. Jiang, B. Dong, and X. Jia, "An introduction to deep learning in medical physics: advantages, potential, and challenges," *Phys. Med. & Biol.*, vol. 65, no. 5, p. 05TR01, 2020.
 - [54] V. Maeda-Gutiérrez *et al.*, "Comparison of convolutional neural network architectures for classification of tomato plant diseases," *Appl. Sci.*, vol. 10, no. 4, p. 1245, 2020.
 - [55] S. Team, "The Ultimate Guide to Convolutional Neural Networks (CNN)," *SuperDataScience Team*, 2018.
 - [56] S. Port, "Development of object detection system to minimise tripping and slipping risk," Victoria University, 2022.
 - [57] J. Davis and M. Goadrich, "The relationship between Precision-Recall and ROC curves," in *Proceedings of the 23rd international conference on Machine learning*, 2006, pp. 233–240.
 - [58] V. Kampouraki, "Patch-level classification of brain tumor tissue in digital histopathology slides with deep learning." 2021.
 - [59] E. Chatzitheodoridou, "Brain tumor grade classification in mr images using deep learning." 2022.
 - [60] G. S. Handelman *et al.*, "Peering into the black box of artificial intelligence: evaluation metrics of machine learning methods," *Am. J. Roentgenol.*, vol. 212, no. 1, pp. 38–43, 2019.
 - [61] V. Jalali and D. Kaur, "A study of classification and feature extraction techniques for brain tumor detection," *Int. J. Multimed. Inf. Retr.*, vol. 9, no. 4, pp. 271–290, 2020.
 - [62] A. Hyvärinen, J. Hurri, and P. O. Hoyer, *Natural image statistics: A probabilistic approach to early computational vision.*, vol. 39. Springer Science & Business Media, 2009.
 - [63] J. Kannala and E. Rahtu, "Bsic: Binarized statistical image features," in *Proceedings of the 21st International Conference on Pattern Recognition (ICPR2012)*, 2012, pp. 1363–1366.
 - [64] N. Dalal and B. Triggs, "Histograms of oriented gradients for human detection," in *2005 IEEE computer society conference on computer vision and pattern recognition (CVPR'05)*, 2005, vol. 1, pp. 886–893.
 - [65] M. Douze, H. Jégou, H. Sandhawalia, L. Amsaleg, and C. Schmid, "Evaluation of gist
-

-
- descriptors for web-scale image search," in *Proceedings of the ACM international conference on image and video retrieval*, 2009, pp. 1–8.
- [66] A. Krizhevsky, I. Sutskever, and G. E. Hinton, "Imagenet classification with deep convolutional neural networks," *Adv. Neural Inf. Process. Syst.*, vol. 25, pp. 1097–1105, 2012.
 - [67] Y. Bengio, *Learning deep architectures for AI*. Now Publishers Inc, 2009.
 - [68] C. Szegedy *et al.*, "Going deeper with convolutions," in *Proceedings of the IEEE conference on computer vision and pattern recognition*, 2015, pp. 1–9.
 - [69] K. Simonyan and A. Zisserman, "Very deep convolutional networks for large-scale image recognition," *arXiv Prepr. arXiv1409.1556*, 2014.
 - [70] K. He, X. Zhang, S. Ren, and J. Sun, "Deep residual learning for image recognition," in *Proceedings of the IEEE conference on computer vision and pattern recognition*, 2016, pp. 770–778.
 - [71] H. Kataoka, K. Iwata, and Y. Satoh, "Feature evaluation of deep convolutional neural networks for object recognition and detection," *arXiv Prepr. arXiv1509.07627*, 2015.
 - [72] S. Xie, R. Girshick, P. Dollár, Z. Tu, and K. He, "Aggregated residual transformations for deep neural networks," in *Proceedings of the IEEE conference on computer vision and pattern recognition*, 2017, pp. 1492–1500.
 - [73] P. P. Angelov and X. Gu, "Deep rule-based classifier with human-level performance and characteristics," *Inf. Sci. (Ny)*, vol. 463, pp. 196–213, 2018.
 - [74] P. Domingos and M. Pazzani, "On the optimality of the simple Bayesian classifier under zero-one loss," *Mach. Learn.*, vol. 29, pp. 103–130, 1997.
 - [75] I. Rish and others, "An empirical study of the naive Bayes classifier," in *IJCAI 2001 workshop on empirical methods in artificial intelligence*, 2001, vol. 3, no. 22, pp. 41–46.
 - [76] K. Hechenbichler and K. Schliep, "Weighted k-nearest-neighbor techniques and ordinal classification," 2004.
 - [77] I. José, "KNN (K-Nearest Neighbors)," 2021, June 2. [Online]. Available: <https://medium.com/towards-data-science/knn-k-nearest-neighbors-1-a4707b24bd1d>. [Accessed: 26-Jun-2024].
 - [78] W. S. Noble, "What is a support vector machine?," *Nat. Biotechnol.*, vol. 24, no. 12, pp. 1565–1567, 2006.
 - [79] B. E. Boser, "Proceedings of the 5th annual ACM workshop on computational learning theory," (*No Title*), p. 144, 1992.
 - [80] S. Saxena, "Beginner's guide to support vector machine (svm)," *Anal. Vidhya*, vol. 8, p. 2021, 2021.
 - [81] C. Z. Janikow, "Fuzzy decision trees: issues and methods," *IEEE Trans. Syst. Man, Cybern. Part B*, vol. 28, no. 1, pp. 1–14, 1998.
 - [82] B. Charbuty and A. Abdulazeez, "Classification based on decision tree algorithm for machine learning," *J. Appl. Sci. Technol. Trends*, vol. 2, no. 01, pp. 20–28, 2021.
-

-
- [83] N. V. Shree and T. N. R. Kumar, "Identification and classification of brain tumor MRI images with feature extraction using DWT and probabilistic neural network," *Brain informatics*, vol. 5, no. 1, pp. 23–30, 2018.
 - [84] Y.-D. Zhang *et al.*, "Pathological brain detection in MRI scanning by wavelet packet Tsallis entropy and fuzzy support vector machine," *Springerplus*, vol. 4, no. 1, p. 716, 2015.
 - [85] N. B. Bahadure, A. K. Ray, and H. P. Thethi, "Image analysis for MRI based brain tumor detection and feature extraction using biologically inspired BWT and SVM," *Int. J. Biomed. Imaging*, vol. 2017, 2017.
 - [86] Y.-D. Zhang and L. Wu, "An MR brain images classifier via principal component analysis and kernel support vector machine," *Prog. Electromagn. Res.*, vol. 130, pp. 369–388, 2012.
 - [87] K. Usman and K. Rajpoot, "Brain tumor classification from multi-modality MRI using wavelets and machine learning," *Pattern Anal. Appl.*, vol. 20, no. 3, pp. 871–881, 2017.
 - [88] A. Ari and D. Hanbay, "Deep learning based brain tumor classification and detection system," *Turkish J. Electr. Eng. & Comput. Sci.*, vol. 26, no. 5, pp. 2275–2286, 2018.
 - [89] H. Byale, G. M. Lingaraju, and S. Sivasubramanian, "Automatic segmentation and classification of brain tumor using machine learning techniques," *Int. J. Appl. Eng. Res.*, vol. 13, no. 14, pp. 11686–11692, 2018.
 - [90] I. Goodfellow, Y. Bengio, and A. Courville, *Deep learning*. MIT press, 2016.
 - [91] D. C. Ciresan, U. Meier, L. M. Gambardella, and J. Schmidhuber, "Convolutional neural network committees for handwritten character classification," in *2011 International conference on document analysis and recognition*, 2011, pp. 1135–1139.
 - [92] K. Jarrett, K. Kavukcuoglu, M. Ranzato, and Y. LeCun, "What is the best multi-stage architecture for object recognition?," in *2009 IEEE 12th international conference on computer vision*, 2009, pp. 2146–2153.
 - [93] S. Gao, L. Duan, and I. W. Tsang, "DEFEATnet—A deep conventional image representation for image classification," *IEEE Trans. Circuits Syst. Video Technol.*, vol. 26, no. 3, pp. 494–505, 2015.
 - [94] P. Angelov, *Autonomous learning systems: from data streams to knowledge in real-time*. John Wiley & Sons, 2012.
 - [95] P. P. Angelov and X. Zhou, "Evolving fuzzy-rule-based classifiers from data streams," *IEEE Trans. Fuzzy Syst.*, vol. 16, no. 6, pp. 1462–1475, 2008.
 - [96] P. Angelov and R. Yager, "A new type of simplified fuzzy rule-based system," *Int. J. Gen. Syst.*, vol. 41, no. 2, pp. 163–185, 2012.
 - [97] P. P. Angelov, X. Gu, and J. C. Príncipe, "A generalized methodology for data analysis," *IEEE Trans. Cybern.*, vol. 48, no. 10, pp. 2981–2993, 2017.
 - [98] P. Angelov and X. Gu, "Autonomous learning multi-model classifier of 0-order (ALMMo-0)," in *2017 Evolving and Adaptive Intelligent Systems (EAIS)*, 2017, pp. 1–
-

-
- 7.
- [99] D. Selvaraj and R. Dhanasekaran, "A review on tissue segmentation and feature extraction of MRI brain images," *Int. J. Comput. Sci. Eng. Technol.*, vol. 4, no. 10, pp. 1313–1332, 2013.
- [100] S. Li, D. Gong, and Y. Yuan, "Face recognition using Weber local descriptors," *Neurocomputing*, vol. 122, pp. 272–283, 2013.
- [101] S. Liu, Y. Zhang, and K. Liu, "Facial expression recognition under partial occlusion based on Weber Local Descriptor histogram and decision fusion," in *Proceedings of the 33rd Chinese Control Conference*, 2014, pp. 4664–4668.
- [102] A. Bosch, A. Zisserman, and X. Munoz, "Representing shape with a spatial pyramid kernel," in *Proceedings of the 6th ACM international conference on Image and video retrieval*, 2007, pp. 401–408.
- [103] T. Ojala, M. Pietikäinen, and T. Mäenpää, "Multiresolution gray-scale and rotation invariant texture classification with local binary patterns," *IEEE Trans. Pattern Anal. Mach. Intell.*, no. 7, pp. 971–987, 2002.
- [104] A. Dhall, A. Asthana, R. Goecke, and T. Gedeon, "Emotion recognition using PHOG and LPQ features," in *Face and Gesture 2011*, 2011, pp. 878–883.
- [105] K. B. Raja, R. Raghavendra, and C. Busch, "Binarized statistical features for improved iris and periocular recognition in visible spectrum," in *2nd International Workshop on Biometrics and Forensics*, 2014, pp. 1–6.
- [106] A. Attia, M. Chaa, Z. Akhtar, and Y. Chahir, "Finger kunckle patterns based person recognition via bank of multi-scale binarized statistical texture features," *Evol. Syst.*, pp. 1–11, 2018.